Quantum Optimal Control of Josephson Junction-Based Circuits

Tesi di Perfezionamento

Scuola Normale Superiore di Pisa

Academic Year 2009

Candidate
Shabnam Safaei

Advisor
Prof. Rosario Fazio

Contents

Introduction

In the last decade device fabrication and experimental control have progressed to such an extent that made it possible to exploit quantum mechanics in different areas such as computation, communication, metrology and data storage. The principle of superposition and entanglement can be used to implement quantum algorithms [1] that are much more efficient than classical ones. Whereas, quantization and tunnelling provide the possibility to fabricate physical quantum bits or to introduce new standards in metrology. So far, several strategies in different realms such as atomic, solid state, optical and ionic systems has been developed in order to engineer physical devices and systems that operate on quantum mechancs principles. Regardless the specific physical system under consideration, however, there exist always a tradeoff: On one hand, quantum devices must be well controlled and strongly coupled to each other in order to design and operate more complicated quantum circuits. On the other hand, they must be completely isolated from the unwanted effects of the environment. The protection from these influences, except during the essential manipulations, control and measurement steps is a challenge which does not exist in the case of classical circuits. For instance, quantum devices based on microscopic degrees of freedom, such as electron or nuclei spin and transition dipoles of atoms or ions, are very well isolated from the environmental effects but not easily coupled to each other. Solid-state quantum devices, on the contrary, are easily coupled to each other due to their large electromagnetic cross-section but they suffer much more from decoherence. The coupling can be made via capacitors, inductors, or other simple electrical elements.

Among different solid-state quantum systems, superconducting circuits [2, 3, 4] are advantegous for the following reasons. First reason is the lack of dissipation in superconducting materials bellow the gap. Moreover, Josephson effect [5, 6] allows to harness the tunnelling principle of quantum mechanics and make use of non-linear and non-dissipative electronic elements in the circuits. The third reason is the scalability and fabrication of quantum integrated circuits based on superconducting material. Superconducting quantum circuits typically consist of micron-size or sub-micron-size components such as tunnel junctions, capacitors and inductors which are connected together by wires or transmission lines. The conventional methods used to fabricate classical integrated circuits can be employed to make superconducting quantum integrated circuits as well. Regarding the size of the elements, optical or electron-beam lithography are used to fabricate them on silicon substrates. Therefore all recent equipments and technical improvements used to make conventional semiconductor circuits are already available to make these kinds of quantum circuits. In the case of solid-state quantum circuits, the problem of protection from noise and having enough control on the system needs to be further addressed.

In this thesis we focus on two important superconducting devices (Cooper pair pump and Josephson phase qubit) and aim at improving their operations by means of optimizing external parameters which control their dynamics. A Cooper pair pump, in the simplest design, is made of a series of superconducting islands which are connected to each other via Josephson junctions and are biased by gate volatges. By a

suitable modulation of gate voltages, it is possible to transfer Cooper pairs through the circuit even without a bias voltage accross the array. A Cooper pair pump can play a key role in metrology if the pumped charge, in each cycle of gating, achieves quantized values with high accuracy enough for setting a new standard of current. In adiabatic Cooper pair pumps, where the duration time of each cycle is much longer than the characteristic time of the system, the quantization of pumped charge during a cycle is limited due to the quantum coherence of the macroscopic superconducting wave function. Furthermore, adiabaticity limits the maximum frequency of pumping and consequently the maximum intensity of the pumped current. In this thesis (Chapter 3) we will study the possibility of obtaining very accurate pumps in nonadiabatic regime by a suitable choice of shape of gate voltage pulses. The other device that we study, Josephson phase qubit, is a simple but interesting quantum bit which has attracted the attention of experimentalists due to its advanteges with respect to other kinds of qubits. First of all, this kind of qubit does not use an optimal working point and therefore the coupling between several qubits is straightforward. Secondly, phase qubit is tunable such that the transition frequency of energy levels, used as computational states, can be adjusted up to 30%. Moreover, the measurement step in this kind of qubit is buit-in meaning that there is no need for other circuit to be used as measurement apparatus. In a Josephson phase qubit, an applied ac current in microwave range and with a certain modulation is used to coherently manipulate the computational states. Conventionally, pulses with Gaussian modulations are used in experiments. In this thesis (Chapter 4) we study the possibility of finding optimal modulations of bias current which result in high-fidelity fast quantum gates.

Quantum optimal control theory [7, 8, 9], originally used in NMR systems, has been applied to different classes of quantum systems [10, 11, 12, 13, 14, 15] and has shown considerable improvement in implementing specific operations and transitions. This motivates us to employ the theory and apply it on Cooper pair pump and Josephson phase qubit in order to obtain optimal gate voltage pulses for Cooper pair pumping and microwave current modulations for quantum gates.

The thesis is organized as follows. In the first chapter of this thesis, after a brief introduction to superconductivity and Josephson effect (Sec. 1.1), the physics of some important classical (Sec. 1.2) and quantum (Sec. 1.3) superconducting devices, will be reviewed. The subjects covered in the first chapter are mostly taken from Ref. [6] and Ref. [3] and more details can be found there. The second chapter is devoted to an introduction to quantum optimal control theory and the algorithm, which we have used for the rest of the thesis, is explained. In Chapter 3, after an introduction to Cooper pair pumping (Sec. 3.1) and a description of the physical model that we have considered (Sec. 3.2), numerical results of optimization of Cooper pair pumping are presented (Sec. 3.3) while the effect of possible imperfection in the shape of pulses (Sec. 3.3.2), effect of noise on gate voltages (Sec. 3.3.3) and possible imperfections in the pump itself (Sec. 3.3.4) are discussed. In Chapter 4, first the model Hamiltonian of a phase qubit and the way single-qubit gates are performed will be explained (Sec. 4.2). Then numerical results of optimized quantum NOT-gate in a phase qubit with an extra energy level will be presented (Sec. 4.3.1). After addressing the effect of possible imperfection in the shape of pulses (Sec. 4.3.2) and effect of ignored off-resonance elements of the Hamiltonian (Sec. 4.3.3), we will discuss the effect of possible interaction with another qubit present in experimental setup (Sec. 4.3.4). Finally we will present numerical results of optimized NOT-gate for a qubit with three extra energy levels (Sec. 4.3.5) to investigate the effect of leakage outside the computational Hilbert space.

The original work presented in this thesis is based on the following publications:

- *Optimized Cooper pair pumps*, Shabnam Safaei, Simone Montangero, Fabio Taddei, and Rosario Fazio, Phys. Rev. B **77**, 144522 (2008). Also available as arXiv:0801.1839v2.

- *Optimized single-qubit gates for Josephson phase qubits*, Shabnam Safaei, Simone Montangero, Fabio Taddei, and Rosario Fazio, to be published in Physical Review B. Also available as arXiv:0811.2174v2.

Chapter 1

Josephson junction based circuits

1.1 Superconductivity and Josephson Effect

Superconductivity was discovered in 1911 by H. Kamerlingh Onnes [16] in Leiden, just 3 years after he was able to liquify Helium. Liquid Helium provided technique required to reach temperatures of a few degrees Kelvin. For decades, a fundamental understanding of this phenomenon attracted the attention of many scientists. Then, in the 1950s and 1960s, a remarkably complete and satisfactory theoretical picture of the classic superconductors was developed. In 1986, when a new class of high-temperature superconductors was discovered by Bednorz and Müller [17], a new chapter in the subject began. These new superconductors seem to obey the same general phenomenology as the classic superconductors, by the basic microscopic mechanism is still an open question.

What Kamerlingh Onnes observed was that the electrical resistance of various metals such as mercury, lead, and tin disappeared completely, in a small temperature range, at a critical temperature T_c, which is of the characteristics of the material. The complete disappearance of resistance is most sensitively demonstrated by experiments with persistent current in superconducting rings. Once set up, such currents have been observed to flow without measurable decrease for a year, and a lower bound of some 10^5 years for their characteristic decay time has been established by the circulating current. In fact, under many circumstances one expects absolutely no change in field or current to occur in times less than $10^{10^{10}}$ years! Thus, *perfect conductivity* is the first traditional characteristic of superconductivity. It is also the prerequisite for most potential applications, such as high-current transmission lines or high-field magnets.

After perfect conductivity the *perfect diamagnetism* was discovered in 1933 by Meissner and Ochsenfeld [18]. They found that not only a magnetic field is *excluded* from entering a superconductor , as might appear to be explained by perfect conductivity, but also that a field in an originally normal sample is *expelled* as it is cooled through T_c. This certainly could not be explained by perfect conductivity, which would tend to trap flux in. The existence of such a reversible *Meissner effect* implies that superconductivity will be destroyed by a critical magnetic field H_c, which is related thermodynamically to the free-energy difference between the normal and superconducting state in zero field, the so called condensation energy of the superconducting state. More precisely this thermodynamic critical field H_c is determined by equating the energy $H^2/8\pi$ per unit volume, associated with holding the field out against the magnetic pressure, with the condensation energy. That is,

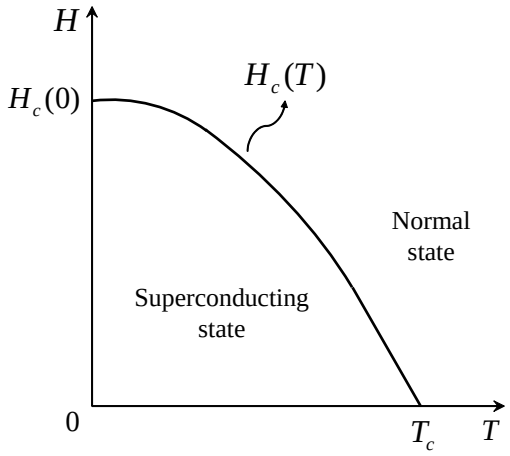

Figure 1: Temperature dependence of the critical field.

$$\frac{H_c^2(T)}{8\pi} = f_n(T) - f_s(T) \tag{1.1}$$

where f_n and f_s are the Helmholtz free energies per unit volume, respectively, in the normal and superconducting phase in zero field. It was found empirically that $H_c(T)$ is quite well approximated by a parabolic law

$$H_c(T) \approx H_c(0)[1 - (T/T_c)^2] \tag{1.2}$$

illustrated in fig.1. While the transition in zero field at T_c is of second order, the transition in presence of a field is of first order since there is a discontinuous change in the thermodynamic state of the system and an associated latent heat.

The two basic electrodynamic properties of superconductivity were well described in 1935 by the brothers F. and H. London, [19] who proposed two equations for microscopic electric and magnetic field (in 1953 a nonlocal generalization of the London equations was proposed by A. B. Pippard [20].):

$$\mathbf{E} = \frac{\partial}{\partial t}(\Lambda \mathbf{J}_s) \tag{1.3}$$

$$\mathbf{h} = -c\,\vec{\nabla} \times (\Lambda \mathbf{J}_s) \tag{1.4}$$

where

$$\Lambda = \frac{4\pi\lambda^2}{c^2} = \frac{m}{n_s e^2} \tag{1.5}$$

is a phenomenological parameter and $\mathbf{J}_s$ is the supercurrent density. The number density of superconducting electrons n_s was expected to vary from zero at T_c to a maximum value of the order of n (the number

density of conduction electrons) at very low temperatures $T \ll T_c$. In equations 1.3 and 1.4 $\mathbf{E}$ and $\mathbf{h}$ denote, respectively, the microscopic local value of electric field and the microscopic value of the flux density. Equation 1.3 describes perfect conductivity since any electric field accelerates the superconducting electrons instead of simply keeping constant their velocity against resistance as described in Ohm's law in a normal conductor. Substituting the Maxwell equation $\mathbf{h} = 4\pi\mathbf{J}/c$ in the second London equation leads to:

$$\nabla^2\mathbf{h} = \frac{\mathbf{h}}{\lambda^2} \tag{1.6}$$

This implies that a magnetic field is exponentially screened from the interior of a sample with penetration depth λ (Meissner effect). Therefore the parameter λ is defined as a penetration depth where temperature dependence is approximately given by

$$\lambda(T) \approx \lambda(0)[1 - (T/T_c)^4]^{-1/2} \tag{1.7}$$

The next step in the evolution of understanding of superconductors was the establishment of the existence of an energy gap Δ, of order kT_c, between the ground-state and the quasi-particle excitations of the system. In 1957, Bardeen, Cooper and Schrieffer [21] (BCS) formulated their pairing theory of superconductivity. In BCS theory, it was shown that even a weak attractive interaction between electrons, such as that caused in second order by the electron-phonon interaction, causes an instability of the ordinary Fermi-sea ground-state of the electron gas with respect to the formation of bound pairs of electrons occupying states with equal and opposite momentum and spin. These so-called *Cooper pairs* have a spatial extension of order ξ_0 which is the coherent length introduced by Pippard. Roughly speaking, Cooper pairs comprise the superconducting charge carriers anticipated in the phenomenological theories.

One of the key predictions of this theory was that a minimum energy $E_g = 2\Delta(T)$ should be required to break a pair, creating two quasi-particle excitations. This $\Delta(T)$ was predicted to increase from zero at T_c to a limiting value

$$E_g(0) = 2\Delta(0) = 3.528kT_c \tag{1.8}$$

for $T \ll T_c$. Not only did this result agree with the measured gap widths, but the BCS prediction for the shape of the absorption edge above $\hbar\omega_g = E_g$ was also in quantitative agreement with the data of the work done by Glover and Tinkham [22]. This agreement provided one of the most decisive early verifications of the microscopic theory.

Although a considerable body of work followed the appearance of the BCS theory, serving to substantiate its predictions for various processes such as nuclear relaxation and ultrasonic attenuation in which the energy gap and excitation spectrum play a key role, the most exciting developments of the following decade came in another direction. This direction was initiated by the Ginzburg-Landau (GL) theory of superconductivity, which concentrates entirely on the superconducting electrons rather than on excitations, and was actually proposed in 1950, seven years before BCS. Ginzburg and Landau [23] introduced a complex pseudowave-function ψ as an order parameter within Landau's general theory of second-order phase transitions. This ψ describes the superconducting electrons, and the local density of superconducting electrons (as defined in the London equations) was given by

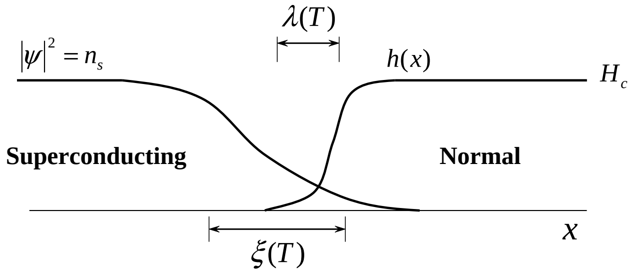

Figure 2: Interface between superconducting and normal domains in the intermediate state.

$$n_s = |\psi(x)|^2 \tag{1.9}$$

Then, using a variational principle and working from an assumed series expansion of the free energy in powers of ψ and $\Delta\psi$ with expansion coefficients $\alpha gy\alpha\psi\psi iyTJ$fεiltrd/

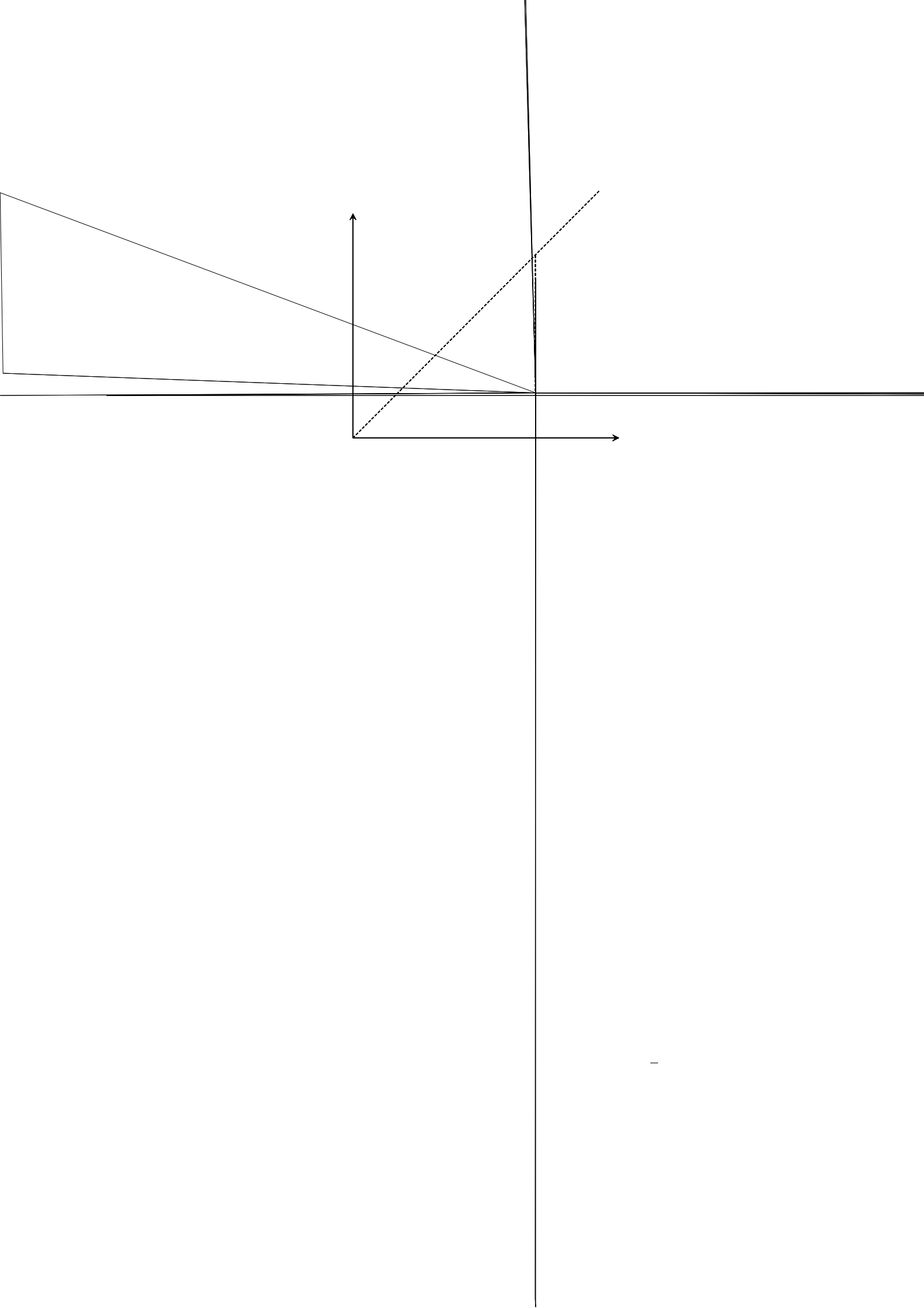

H_{c2}, the flux penetrates into the material in a regular array of flux tubes. Each of these tubes carries a quantum of flux

$$\Phi_0 = \frac{hc}{2e} = 2.07 \times 10^{-7}\ Gcm^2 \tag{1.14}$$

Within each unit cell of the array, there is a vortex of supercurrent concentrating the flux toward the vortex center. Although Abrikosov predicted a square array, it was later shown, upon correcting a numerical error, that a triangular array should have a slightly lower free energy. This vortex array was first demonstrated experimentally by a magnetic decoration technique coupled with electron microscopy [26]. Scanning tunneling microscope (STM) measurements [27] have also confirmed the existence of the vortex array. In addition it is possible to measure the details of the density of electronic states in the quasi-normal core at the center of each vortex by using STM. The random inhomogeneities in the underlying material lead to pinning of vortices at favorable locations which gives rise to glass-like patterns of flux tubes.

As it has been already noted, type II superconductors are not perfectly diamagnetic, and since $|\psi|^2$ turns out to go to zero in the centers of the vortices, it is not surprising to find that there is no energy gap in the cores. Thus, it is natural to ask whether the first characteristic of superconductors (perfect conductivity) is also lost in type II materials. In the presence of a transport current, the flux tubes experience *Lorentz force* $\mathbf{J} \times \Phi_0/c$ per unit length (analogous to the macroscopic force density $\mathbf{J} \times \mathbf{B}/c$) tending to make them move sideways, in which case a longitudinal resistive voltage is induced. In an ideal homogeneous material, Bardeen and Stephen [28] showed that this flux motion is resisted only by a viscous drag, and that the type II superconductors should show a resistance comparable to that in the normal state, only reduced by a factor $\sim\ B/H_{c2}$. In real materials, however, there is always some inhomogeneity to pin the flux, so that there is essentially no resistance until a finite current is reached, such that the Lorentz force exceeds the pinning force. In superconducting magnet wire, the pinning is deliberately made strong enough to give large critical currents.

Regarding the failure of the two characteristics of type I superconductors in type II materials, one might well ask what really is the essential universal characteristic of the superconducting state. The answer is the existence of the many-particle condensate wave function $\psi(\mathbf{r})$, which has amplitude and phase and which maintains phase coherence over macroscopic distances. This condensate is analogous to, but not identical to, the familiar Bose-Einstein condensate, which Cooper pairs of electrons replacing the single bosons which condense in superfluid helium, for example.

Since the phase and particle number are conjugate variables (see e.g. chapter 7 of [6]), reflecting complementary aspects of the wave-particle dualism, there is an uncertainty relation

$$\Delta N \Delta\varphi \geq 1 \tag{1.15}$$

which limits the precision with which N and φ can be simultaneously known. However, since $N \sim\ 10^{22}$ in a macroscopic sample, both N and φ can be known to within small fractional uncertainties, and the phase may be treated as a semiclassical variable. However, this is not the case in very small mesoscopic structures.

The physical significance of the phase degree of freedom was first emphasized in 1962 in the work of Josephson,[29] who predicted that pairs should be able to tunnel between superconductors even at *zero* voltage difference. He predicted that a zero voltage supercurrent

$$I_s = I_c \sin\Delta\varphi \tag{1.16}$$

should flow between two superconducting electrodes separated by a thin insulating barrier. Here $\Delta\varphi$ is the difference in the phase of the Ginzburg-Landau wave function in the two electrodes, and the *critical current* I_c is the maximum supercurrent that the junction can support. He further predicted that if a voltage difference V were maintained across the junction, the phase difference $\Delta\varphi$ would evolve according to

$$d(\Delta\varphi)/dt = 2eV/\hbar \tag{1.17}$$

so that the current would be an alternating current of amplitude I_c and frequency $\nu = 2eV/h$. Thus, the quantum energy $h\nu$ equals the energy change of a Cooper pair transferred across the junction. These predicted effects, known as the dc and ac Josephson effects, respectively, have been fully confirmed by many experiments.

Although Josephson's prediction was based on a microscopic theoretical analysis of the quantum mechanical tunneling of electrons through the barrier layer, it is now clear that the effects are much more general, and occur whenever two strongly superconducting electrodes are connected by a weak link. As illustrated in fig.4 the weak link can be an insulating layer as Josephson originally proposed, or a normal metal layer made weakly superconductive by the *proximity effect* (in which Cooper pairs from a superconducting metal in close proximity diffuse into the normal metal), or simply a short, narrow constriction in otherwise continuous superconducting material. These three typical cases are often referred to as $S-I-S$, $S-N-S$, or $S-c-S$ junctions, respectively, where the S, I, N, and c denote superconductor, insulator, normal metal, and constriction, respectively.

Given the two relations (1.16) and (1.17), one can derive the coupling free energy F stored in the junction by integrating the electrical work $\int I_s V dt = \int I_s(\hbar/2e)d(\Delta\varphi)$ done by a current source in changing the phase:

$$F = const. - E_J \cos\Delta\varphi \quad ; \quad E_J \equiv (\hbar I_c/2e). \tag{1.18}$$

Clearly, the energy is a minimum when the two phases are equal, so that $\Delta\varphi = 0$. This corresponds to the energy minimum in the absence of phase *gradients* in a bulk superconductor. The critical current is a measure of how strongly the phases of the two superconducting electrodes are coupled through the weak link. This depends on how thin and of what material the barrier is, or, in the case of constriction weak links, on the cross-sectional area and length of the neck.

In most applications I_c lies in the range of a microampere to a few milliamperes. The lower limit stems from the requirement that the coupling energy E_J exceed the thermal energy kT, i.e., $I_c > 2ekT/\hbar$; otherwise thermal fluctuations in $\Delta\varphi$ will wash out the phase-dependent supercurrent. Although the numerical factor $2ek/\hbar$ is only $\sim 0.04\ \mu AK^{-1}$, I_c must be sufficient to overcome an effective noise temperature which may approach room temperature rather than the temperature of the superconductor, unless the electrical leads are very well screened. At the other extreme are the weak links which couple together the strongly superconducting grains in a granular bulk superconductor such as the ceramic oxide high-temperature superconductors. Here one needs a critical current of ~ 1 mA between adjacent $1-\mu$m diameter grains to obtain a useful bulk critical current density of the order of 10^5 Acm^{-2}.

To finish the discussion about Josephson effect it is necessary to notice that the phase difference $\Delta\varphi$ is not a gauge-invariant quantity and does not have a unique value for a given physical situation; hence, it cannot in general determine the current I_s, which is a well-defined gauge-invariant physical quantity. This problem is overcome by replacing $\Delta\varphi$ throughout by the *gauge-invariant phase difference* δ, defined by

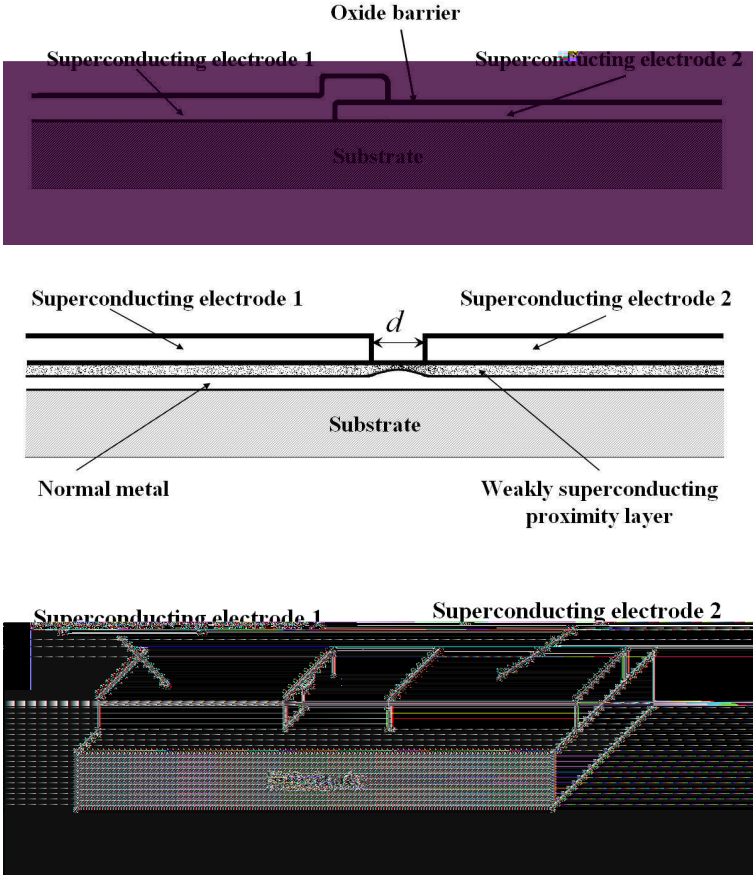

Figure 4: Three different types of Josephson junction. Up to down, respectively, $S-I-S$, $S-N-S$ and $S-c-S$.

$$\delta \equiv \Delta\varphi - (2\pi/\Phi_0) \int \mathbf{A}.d\mathbf{s} \tag{1.19}$$

where the integration is from one electrode of the weak link to the other. In terms of δ, the general expression for the supercurrent in an ideal Josephson junction is

$$I_s = I_c \sin\delta. \tag{1.20}$$

This is the result which one would have obtained by using the full gauge-invariant gradient expression $[(\hbar\nabla/i) - e^*\mathbf{A}/c]$ throughout the preceding discussion instead of using only its first term. In addition to curing a conceptual problem, the introduction of the gauge-invariant phase difference is the key to working out the effects of a magnetic field, which cannot be treated without introducing the vector potential $\mathbf{A}$. In other hand, as long as no magnetic field is present, $\mathbf{A}$ can be taken to be zero and δ and $\Delta\varphi$ can be used interchangeably. After this we will refer to the gauge-invariant phase with φ.

1.2 Classical superconducting devices

In this section some basic but important superconducting devices, based on Josephson effect, will be introduced and the way of finding the Hamiltonian which governs these kinds of systems will be presented [3]. In order to characterize the properties of the Josephson junction devices, in presence of a bias voltage (ac Josephson effect), we use the RCSJ (Resistively and Capacitively Shunted Junction) model (see chapter 6 of Ref. [6] for more details). In this model the physical Josephson junction is replaced with an ideal one described by (1.20), which is also shunted by a resistance R and capacitance C. The resistance R is responsible for dissipation in the finite voltage regime, without affecting the lossless dc regime and C represents the shunting capacitance between the two electrodes of the junction.

1.2.1 Current Biased Josephson Junction

The simplest circuit made of superconducting devices which one can imagine is a current-biased Josephson junction. Figure 5 shows a schematic drawing of such a circuit, its equivalent electrical circuit and the potential energy of this system as a function of phase φ. To derive the Hamiltonian of this circuit we use the well known Kirchhoff's law and write it for this system as follows

$$C\dot{V} + \frac{V}{R} + I_c Sin(\varphi) = I_e \tag{1.21}$$

where C and R are capacitance and resistance of the junction, V and φ are the voltage and superconducting phase difference across the junction. I_c stands for critical current and I_e is the external current which biases the junction. The junction resistance showed here is different from the normal junction resistance R_N and strongly depends on the applied voltage, temperature and the Josephson element associated with the tunneling through the junction. Three terms in the left side of the equation (1.21) correspond respectively to current through capacitance, resistance and tunneling branches of the equivalent circuit.

Following the equation (1.17) one gets

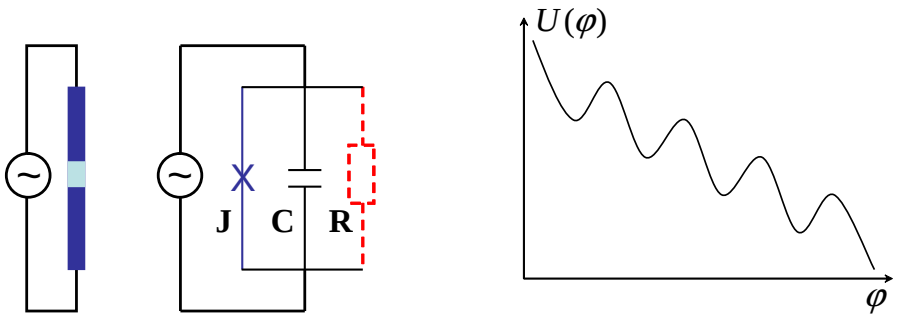

Figure 5: Left to right: Schematic drawing of current biased Josephson junction, its equivalent circuit and its potential energy $U(\varphi)$ (tilted washboard potential) as a function of superconducting phase φ across the junction.

$$V = \frac{\hbar}{2e}\dot{\varphi} \tag{1.22}$$

Substituting this in equation (1.21) leads to

$$\frac{\hbar}{2e}C\ddot{\varphi} + \frac{\hbar}{2eR}\dot{\varphi} + I_c Sin(\varphi) - I_e = 0 \tag{1.23}$$

This equation describes the dynamics of the superconducting phase and has the form of a damped non-linear oscillator where the Josephson part plays the role of non-linear inductance. Using the relation between critical current and Josephson energy $E_\mathrm{J} = \hbar I_c/2e$ and introducing the charging energy

$$E_C \equiv \frac{(2e)^2}{2C} \tag{1.24}$$

equation (1.23) leads to

$$\frac{\hbar^2}{2E_C}\ddot{\varphi} + \frac{\hbar^2}{2E_C}\frac{1}{RC}\dot{\varphi} + E_\mathrm{J} Sin(\varphi) - \frac{\hbar I_e}{2e} = 0 \tag{1.25}$$

If φ stands for position, this equation is analogous to the equation of motion of one particle with mass $\hbar^2/2E_C$ moving in a potential $U(\varphi)$ in presence of a dissipative force $(-\hbar^2/2E_C RC)\dot{\varphi}$ where $U(\varphi)$ is defined by

$$U(\varphi) = -E_\mathrm{J}\cos(\varphi) - \frac{\hbar I_e}{2e}\varphi \tag{1.26}$$

which is known as *tilted washboard potential* (see fig. 5).

If we assume that the dissipative part in equation (1.25) is very small and we can neglect it (by ignoring the resistive branch in the equivalent circuit) then the Hamiltonian which governs the dynamics of the system has the following form

$$H = \frac{\hbar^2}{4E_C}\dot{\varphi}^2 - E_{\mathrm{J}}\cos(\varphi) - \frac{\hbar I_e}{2e}\varphi \tag{1.27}$$

In the language of the mechanical particle the momentum of the particle $p = (\hbar^2/2E_C)\dot{\varphi} = (\hbar/2e)CV$ is related to the charge $q = CV$ on the junction capacitor, or the number n of Cooper pairs on the junction capacitor via

$$p = \frac{\hbar}{2e}q = \hbar n \tag{1.28}$$

therefore the kinetic term in the Hamiltonian (1.27) can be written in terms of the number of Cooper pairs on the junction capacitor

$$H = E_C n^2 - E_{\mathrm{J}}\cos(\varphi) - \frac{\hbar I_e}{2e}\varphi. \tag{1.29}$$

There is an important point which one must be careful about. To be allowed to neglect the dissipative part in the dynamics of current biased Josephson junction the temperature must be much lower than the energy gap of the superconductor, $kT \ll \Delta$. Moreover the time evolution of the superconducting phase must be done slowly such that the energy associated with the characteristic frequency ω be always smaller than the gap of the superconductor, $\hbar\omega \ll \Delta$. If these conditions are not fulfilled the amount of quasiparticle excitations would be so high that the gap of the superconductor will not have any significant effect. Because of high amount of dissipation the normal conducting state becomes more important than the superconducting state. But if kT, $\hbar\omega \ll \Delta$ then equilibrium and non-equilibrium excitations are exponentially suppressed and superconducting state plays the dominant role.

1.2.2 rf-SQUID

SQUID (Superconducting QUantum Interference Device) is an important simple device which has wide applications in superconducting circuits used for quantum computation purposes. SQUID simply is a superconducting loop interrupted by one or more Josephson junctions. Fig. 6 shows the schematic drawing of a one-junction SQUID, which is biased with an external magnetic flux Φ_e, and the equivalent circuit as well.

The corresponding Kirchhoff's law has the following form

$$C\dot{V} + \frac{V}{R} + I_c Sin(\varphi) + \frac{1}{L}\Phi = \frac{1}{L}\Phi_e. \tag{1.30}$$

Since the superconducting phase difference and magnetic flux are connected together via equation (1.19), one obtains

$$\varphi = 2\pi\frac{\Phi}{\Phi_0} \quad \text{or} \quad \varphi = \frac{2e}{\hbar}\Phi \tag{1.31}$$

so that all terms in the equation (1.30) can be written in terms of phase:

$$\frac{\hbar}{2e}C\ddot{\varphi} + \frac{\hbar}{2eR}\dot{\varphi} + I_c Sin(\varphi) + \frac{\Phi_0}{2\pi L}(\varphi - \varphi_e) = 0 \tag{1.32}$$

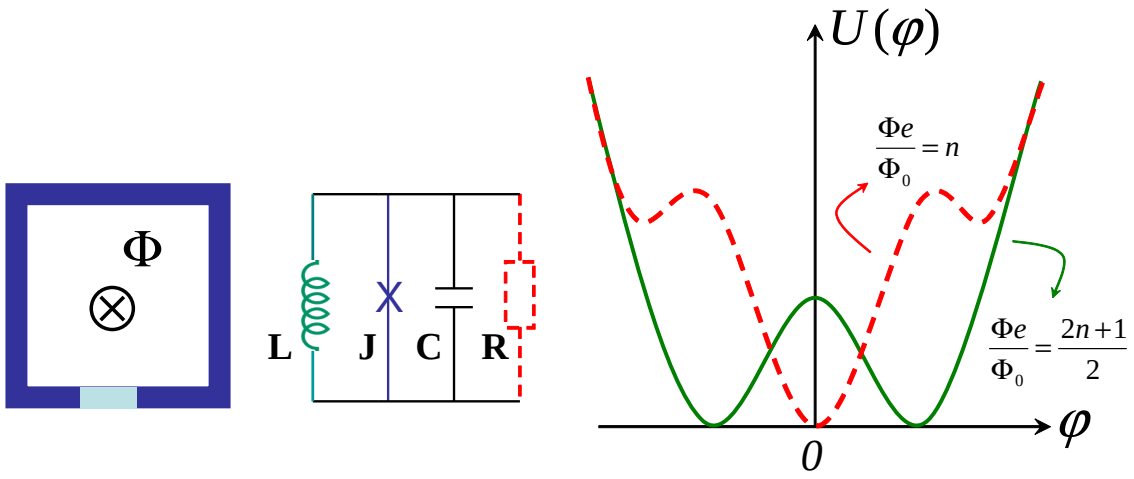

Figure 6: Left to right: Schematic drawing of an rf-SQUID, its equivalent circuit and its potential $U(\varphi)$ as a function of superconducting phase φ across the junction for two special values of applied external magnetic flux Φ_e.

In absence of tunneling ($I_c \approx 0$) this equation describes a linear damped oscillator with resonant frequency $1/\sqrt{LC}$ and damping factor $1/(RC)$. By using the definitions of E_C and E_J and introducing

$$E_L \equiv \frac{\Phi_0^2}{4\pi^2 L} \tag{1.33}$$

one obtains:

$$\frac{\hbar^2}{2E_C}\ddot{\varphi} + \frac{\hbar^2}{2E_C}\frac{1}{RC}\dot{\varphi} + E_\mathrm{J} Sin(\varphi) + E_L(\varphi - \varphi_e) = 0 \tag{1.34}$$

Which is similar to the equation (1.25) for current biased Josephson junction except the potential which here has a form of a double well shown in Fig. 6 and is described by

$$U(\varphi) = -E_\mathrm{J}\cos(\varphi) - \frac{E_L}{2}(\varphi - \varphi_e)^2 \tag{1.35}$$

and so (by neglecting the dissipative term) the Hamiltonian of this system simply is

$$H = \frac{\hbar^2}{4E_C}\dot{\varphi}^2 - E_\mathrm{J}\cos(\varphi) + \frac{E_L}{2}(\varphi - \varphi_e)^2 \tag{1.36}$$

and equivalently

$$H = E_C n^2 - E_\mathrm{J}\cos(\varphi) + \frac{E_L}{2}(\varphi - \varphi_e)^2 \tag{1.37}$$

The potential defined by (1.35) has one absolute minimum at $\varphi = \varphi_e$ if the external applied flux is equal to integer number of flux quanta ($\Phi_e = n\Phi_0$ or $\varphi_e = 2\pi n$). In the case that the bias flux is equal to half

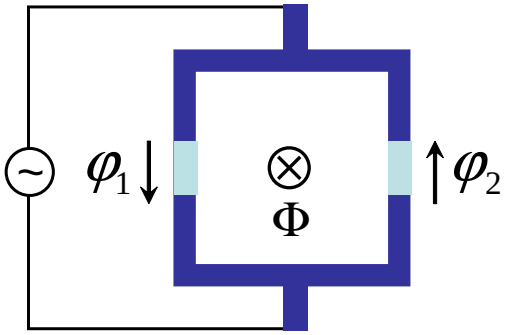

Figure 7: Schematic drawing of a dc-SQUID with two Josephson junctions. SQUID is biased with current and an external magnetic flux which is used to tune the effective Josephson energy of the device.

integer of flux quanta ($\Phi_e = (2n+1)\Phi_0/2$ or $\varphi_e = (2n+1)\pi$) there are two degenerate minima for this potential which correspond to two persistent current states, with equal amplitude and opposite directions, circulating in the SQUID.

1.2.3 dc-SQUID

A dc-SQUID is a SQUID with two or more junctions which has very low inductance and is biased with an external current and magnetic field. Fig. 7 shows a two-junction SQUID.

Since this device must have very weak inductance one can treat it as a current-biased Josephson junction with tunable effective Josephson energy and phase. In order to see how it is possible we assume that there is an effective Josephson current $I_{c_{eff}}$ and phase φ_{eff} associated with this device, then considering the phase differences φ_1 and φ_2 as defined in Fig. 7 one can write:

$$I_{c1}Sin(\varphi_1) - I_{c2}Sin(\varphi_2) = I_{c_{eff}}Sin(\varphi_{eff}) \tag{1.38}$$

On the other hand because of the low inductance the magnetic energy of circulating currents is supposed to be (approximately) zero and then the total gauge invariant phase difference $(\varphi_1 + \varphi_2 - \varphi_e)$ in the SQUID loop must be zero where φ_e is the phase associated with the external biasing magnetic flux. Therefore

$$\varphi_1 + \varphi_2 = \varphi_e \tag{1.39}$$

and by introducing new variables:

$$\varphi_\pm \equiv \frac{\varphi_1 \pm \varphi_2}{2} \tag{1.40}$$

and substituting these in the equation (1.38) one simply obtains following equations for effective current and effective phase:

$$I_{c_{eff}} = \sqrt{I_{c1}^2 + I_{c2}^2 + I_{c1}I_{c2}\cos(\varphi_e)} \tag{1.41}$$

$$\varphi_{eff} = \varphi_- + \vartheta \tag{1.42}$$

where

$$\vartheta = Arctan\left(\frac{I_{c1} - I_{c2}}{I_{c1} + I_{c2}} tan(\frac{\varphi_e}{2})\right) \tag{1.43}$$

From these last three equations it is clear that both $I_{c_{eff}}$ and φ_{eff} are tunable by the external biasing magnetic flux. If the SQUID is symmetric such that $I_{c1} = I_{c2} = I_c$ then ϑ will become zero and therefore:

$$I_{c_{eff}} = 2I_c \cos(\frac{\varphi_e}{2}) \tag{1.44}$$

$$\varphi_{eff} = \varphi_- \tag{1.45}$$

Since in Fig. 7 two junctions are coupled in parallel to a current source I_e, the effective capacitance of the device is simply sum of two capacitances C_1 and C_2. Now if we drop the $-$ subscript from φ_-, in analogy to the current biased Josephson junction described in section 1.3.1, the Hamiltonian of a two-junction dc-SQUID reads as:

$$H = \frac{\hbar^2}{4E_C}\dot{\varphi}^2 - 2E_{\mathrm{J}} \cos(\frac{\varphi_e}{2}) \cos(\varphi) - \frac{\hbar I_e}{2e}\varphi \tag{1.46}$$

while remembering that here $E_C \equiv (2e)^2/(2(C_1 + C_2))$ and $\varphi = (\varphi_1 - \varphi_2)/2$.

1.3 Quantum superconducting devices

So far we have treated the Josephson phase φ as a semiclassical variable in the sense that it is well defined and the phase-number uncertainty relation (1.15) puts no significant constraint on the precise specification of the phase in macroscopic superconductors connected to reservoirs. Since modern microfabrication techniques have provided the possibility of making very small devices, it is important to study the behavior of phase and number of particles in such small systems where the electronic charge of a single electron matters. In this field of research, in addition to uncertainty rule, other quantum conjugate properties of phase and number play an important role and quantum fluctuations remain important even at $T \approx 0$. In this section the conditions under which the quantum behavior of charge and phase could be observed will be explained and then some widely-used quantum superconducting devices, based on phase or charge degree of freedom, will be introduced.

In order to make the observation of quantum behavior of phase and number possible, one must consider some conditions and constraints. Mostly studied quantum superconducting devices consist of one or several small and isolated superconducting grains or islands which are connected to each other and reservoirs through small tunnel junctions. Knowing that the typical capacitance C of such islands is very small and tunneling junctions have very high resistance R, one can estimate the necessary constraints on these parameters.

First of all in order to keep the importance of the charging energy of a single electron $e^2/2C$, the thermal fluctuations must be suppressed which means that the thermal energy kT must be much smaller than the charging energy otherwise thermal fluctuations will average over the charge numbers. For example at $T \approx 1$ K the capacitance of the junction must be smaller than one fF and consequently the area of the junction must be smaller than one μm^2.

The second constraint which concerns the tunneling resistance R can be obtained from the fact that charging energy $e^2/2C$ is not observable unless it exceeds the energy uncertainty $\Delta E \geq \hbar/\Delta t$ associated with the finite lifetime $\Delta t \approx \hbar/RC$ of the charge on the capacitor. Therefore the tunneling resistance R must be bigger than the quantum resistance $R_Q = h/4e^2$ otherwise the effects will be washed out by quantum fluctuations of the number of particles. If this constraint is satisfied, tunneling of Cooper pairs through junctions can be controlled by the charging energy and this effect is referred to as *Coulomb blockade effect*[30].

Under above conditions one can not treat phase φ across the junction and number of cooper pairs N on the junction area as classical variables anymore and quantum consequences of small junctions with high tunneling resistance must be taken to account. In fact now the uncertainty relation (1.15) has its usual meaning in quantum physics and implies that there is a limit in the precision to which φ and N are known. As a simple example one can consider a single isolated junction at $T = 0$ with capacitance C and Josephson energy E_J and without any external biasing current. In classical approach the Hamiltonian of the system is

$$H = \frac{1}{2}CV^2 - E_J\cos(\varphi) = \frac{\hbar^2}{4E_C}\dot{\varphi}^2 - E_J\cos(\varphi), \tag{1.47}$$

where $E_C = (2e)^2/2C$ is the charging energy of a pair. Now treating the number of Cooper pairs $N = CV/2e$ and superconducting phase φ as quantum variables and replacing N with $i\partial/\partial\varphi$ leads to

$$\dot{\varphi} = \frac{2E_C}{\hbar}\left(i\frac{\partial}{\partial\varphi}\right). \tag{1.48}$$

Therefore in quantum mechanical approach the Hamiltonian (1.47) becomes

$$H = -E_C\frac{\partial^2}{\partial\varphi^2} - E_J\cos(\varphi). \tag{1.49}$$

The ratio $y \equiv E_C/E_J$ is a proper quantity to define the relative importance of charging or Josephson term in Hamiltonian (1.49). To intuitively understand how a very big charging energy can delocalize the phase φ we consider to extremes $y \ll 1$ and $y \gg 1$. Although it is possible to obtain the eigenstates of Hamiltonian (1.49) numerically, to have an intuitive understanding it is enough to find the ground-state of (1.49) approximately. If $\psi(\varphi)$ represents the ground-state of (1.49). In the limit $y \ll 1$, a gaussian function with a characteristic width d, which minimizes the eigenenergy associated with the ground-state, is a trial approximation for $\psi(\varphi)$:

$$\psi(\varphi) \approx e^{-\left(\frac{\varphi}{2d}\right)^2} \tag{1.50}$$

and consequently the minimum energy is

$$E \approx -E_J \left(1 - \sqrt{\frac{y}{2}}\right) \tag{1.51}$$

In the other case when $y \gg 1$ the proper approximation for ψ must be a periodic function of φ and satisfies the boundary condition of zero slope at the edge of each cell, therefore a cosinus can be a trial function:

$$\psi(\varphi) \approx (1 + a\cos(\varphi)), \tag{1.52}$$

where a is a constant and consequently the approximate energy of the ground-state is

$$E \approx -\frac{E_J}{2y} = -\frac{E_J^2}{2E_C}. \tag{1.53}$$

Comparing (1.51) and (1.53) one can clearly see that big charging energy ($y \ll 1$) leads to a ground-sate energy which is of second order in E_J while the opposite case gives a first-order energy. Moreover for $y \ll 1$ the ground-state is a narrowly peaked function of φ with a width of the order of $y^{1/4}$ which means that quantum fluctuations in the phase are small and φ can be specified with high precision while for $y > 1$ the wave function ψ is broaden in φ and therefore the probability density for phase φ is sufficiently delocalized so that it is not a good approximation to treat φ as a well-defined semiclassical variable and one should use ground-state in the N space instead of $\psi(\varphi)$. In a brief explanation, if $|\psi_\varphi\rangle$ is a state with indefinite number of Cooper pairs N but with a definite phase φ, the state with definite number of cooper pairs and an indefinite phase, which we refer to it by $|\psi_N\rangle$, is the Fourier transform of $\psi(\varphi)$:

$$|\psi_N\rangle = \int_0^{2\pi} d\varphi e^{-iN\varphi/2} |\psi_\varphi\rangle \tag{1.54}$$

and naturally are the proper choice of eigenbasis in such problems in which the charging energy is dominant and therefore number of Cooper pairs is the well-defined variable and not φ. In the rest of this thesis we will simplify the notation and use $|n\rangle$ instead of $|\psi_N\rangle$.

In following sections some superconducting devices based on Josephson junctions which work in quantum regime will be introduced. Despite their simple design, all of them play important roles in new areas of research specially to build a new generation of computers called quantum computers.

1.3.1 Single Cooper pair box

The simplest but important and fundamental superconducting device which works in regimes where charging energy is the dominant energy in the system is a Cooper pair box. A Cooper pair box consists of a small superconducting island connected to a superconducting reservoir via a Josephson junction and is capacitively biased by a gate voltage V_g (Fig. 8). If instead of superconducting materials normal materials are used this kind of device is called *single electron box*. The reason for this name is that in very low temperature and for very small islands the charging energy associated with adding one extra electron (or Cooper pair) into the island is significant and the tunneling into/out of the island is practically forbidden due to *Coulomb blockade effect* [30]. There are some specific gate voltages in which the energy of the island with n and $n+1$ electrons (or Cooper pairs) are degenerate and therefore charge can tunnel into and out of the island one by one and

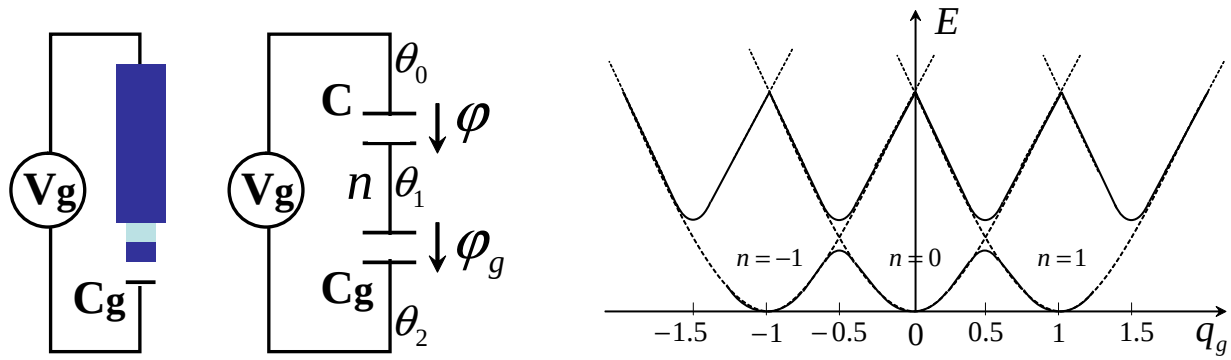

Figure 8: Left to right: Schematic drawing of a single Cooper pair box (SCB), its equivalent (electrostatic) circuit and its energy diagram as a function of normalized gate charge $q_g = -C_g V_g/(2e)$.

moreover the number of electrons (Cooper pairs) inside the island differs by one from one degenerate case to the next one.

In a Cooper pair box the number of pairs inside the island is the important variable and the superconducting phase in the island is its quantum conjugate and not the phase difference across the junction φ. Although in Coulomb blockade regime, due to uncertainty relation between number of Cooper pairs and superconducting phase (equation (1.15)), the phase on the island is not a well-defined variable, in order to write the Hamiltonian of a Cooper pair box in terms of the number of Cooper pairs inside the box, we have no way other than writing the Lagrangian L of the system in terms of the superconducting phase inside the island. The electrostatic energy consists of the energy associated with junction capacitance C with voltage V and the energy of the gate capacitor with capacitance C_g and voltage drop $V_g - V$. Since in language of mechanical particle the electrostatic energy always plays the role of kinetic energy the Lagrangian of the system will have following form:

$$L = \frac{1}{2}CV^2 + \frac{1}{2}C_g(V_g - V)^2 + E_{\mathrm{J}}\cos(\varphi) \tag{1.55}$$

As it is shown in figure 8 we use the phase differences across the junction capacitor φ and across the gate capacitor φ_g to rewrite the Lagrangian:

$$L = \frac{1}{2}\left(\frac{\hbar}{2e}\right)^2 (C\dot{\varphi}^2 + C_g\dot{\varphi}_g^2) + E_{\mathrm{J}}\cos(\varphi) \tag{1.56}$$

If θ_0, θ_1 and θ_2 denote the superconducting phase in three points as it is illustrated in Fig. 8, the voltage drop on junction and gate capacitor which are respectively proportional to $\dot{\varphi}$ and $\dot{\varphi}_g$, can be written in terms of $\dot{\theta}_0$, $\dot{\theta}_1$ and $\dot{\theta}_2$ using the following relations:

$$\begin{aligned} \dot{\varphi} &= \dot{\theta}_1 - \dot{\theta}_0 \\ \dot{\varphi}_g &= \dot{\theta}_2 - \dot{\theta}_1 \\ \dot{\varphi} + \dot{\varphi}_g &= \frac{2e}{\hbar}V_g, \end{aligned} \tag{1.57}$$

therefore by setting $\dot{\theta}_0 = 0$ one obtains:

$$\begin{aligned} \dot{\varphi} &= \dot{\theta}_1 \\ \dot{\varphi}_g &= \frac{2e}{\hbar} V_g - \dot{\theta}_1 \end{aligned} \tag{1.58}$$

which leads to

$$L = \frac{1}{2}\left(\frac{\hbar}{2e}\right)^2 \left[C_\Sigma \dot{\theta}_1^2 - 2\left(\frac{2e}{\hbar}\right) C_g V_g \dot{\theta}_1 + \left(\frac{2e}{\hbar}\right)^2 C_g V_g^2 \right] + E_\mathrm{J}\cos(\varphi) \tag{1.59}$$

where $C_\Sigma = C + C_g$. Since θ_1 is the superconducting phase inside the box, if p is its conjugate momentum then $p = \hbar n$ where n is the number of Cooper pairs inside the box. From equation (1.59) one obtains

$$p = \frac{\partial L}{\partial \dot{\theta}_1} = \left(\frac{\hbar}{2e}\right)^2 C_\Sigma \dot{\theta}_1 + \hbar q_g, \tag{1.60}$$

where $q_g = -C_g V_g / 2e$ is the normalized gate charge. Eventually (by omitting the term which does not depend on n or φ) the Hamiltonian of a Cooper pair box reads

$$H = p\dot{\theta}_1 - L = E_C (n - q_g)^2 - E_\mathrm{J}\cos(\varphi). \tag{1.61}$$

Here $E_C = (2e)^2 / 2C_\Sigma$. As we mentioned before, a Cooper pair box works in charging regime and it is appropriate to write the Hamiltonian (1.61) in the basis of eigenvectors of charging energy $|n\rangle$. Since the Josephson tunneling term is equivalent to adding/removing one pair to/from the box, in charge basis we can replace $\cos(\varphi)$ with $\frac{1}{2}\sum_n \left(|n+1\rangle\langle n| + |n\rangle\langle n+1|\right)$ which leads to

$$H = E_C \sum_n (n - q_g)^2 |n\rangle\langle n| - \frac{E_J}{2} \sum_n \left(|n+1\rangle\langle n| + |n\rangle\langle n+1|\right) \tag{1.62}$$

The energy diagram of a box is shown in figure 8. In absence of Josephson term (dashed curves) the diagram consists of several parabola corresponding to different ns and the tunneling between different states with different numbers of Cooper pairs inside the box is forbidden due to Coulomb blockade effect unless the gate voltage reaches some special values such that $q_g = (2n \pm 1)/2$. At these points two states with n and $n \pm 1$ Cooper pairs are degenerate and tunneling into and out of the box becomes possible. Josephson term mixes the eigenstates of the charging term of the Hamiltonian and introduces a gap in vicinity of degeneracy points (solid curves) but still far from the degeneracy points tunneling is forbidden due to Coulomb energy. Single Cooper pair Box (SCB) was first described theoretically by Büttiker [31] and was first realized experimentally by the Saclay group in 1997 [32]. Quantum dynamics in the time domain were first seen by the NEC group in 1999 [33].

1.3.2 Cooper pair pump

Before Explaining the structure of a Cooper pair pump and deriving its Hamiltonian, we start with a brief introduction to charge pumping.

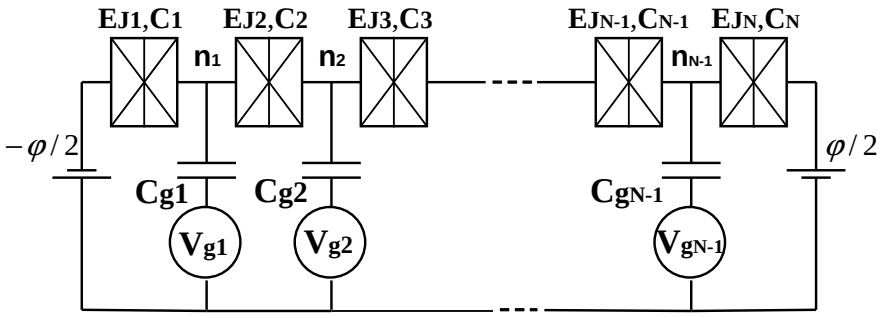

Figure 9: Schematic drawing of a Cooper pair pump consisting of N Josephson junctions and $N-1$ gated Cooper pair boxes. C_i and E_{Ji} are the capacitances and Josephson energies of the junctions. C_{gi} and V_{gi} are gate capacitances and voltages and φ is the overall phase difference through the pump. In a uniform pump $C_i \equiv C$ and $E_{Ji} \equiv E_J$.

In one sentence, charge pumping means transferring charge through a circuit or device without a bias voltage and just by means of changing some time-dependent parameters periodically [34] (gate voltages for example). If these parameters are changed so slowly that the time of each cycle is longer than typical time scale of the system, and therefore the system remains in a certain eigenstate of the Hamiltonian during the time evolution, pumping is adiabatic and in this case the pumped charge in each cycle does not depend on the details of the timing of the parameters but only on the geometrical properties of them.

There are many different kinds of mesoscopic systems in which charge pumping can be realized. For example if the system consists of some mesoscopic conductors which are connected to each other and to leads via highly transmissive barriers, periodic modulation of the phase of the scattering matrix can lead to parametric pumping (see references [35] to [43]). In the case that the system consists of quantum dots (boxes) connected together via tunnel junctions phase coherence is irrelevant and pumping is achieved by periodic modulation of Coulomb blockade [30] meaning that by changing time-dependent parameters one can make tunneling from one certain box to the next one possible while tunneling between all other boxes is forbidden due to Coulomb blockade effect. Since in the boxes with very high charging energy it is possible to control tunneling of a single electron by means of gate voltages, in the latter case of pumping the number of electrons transferred in each cycle is approximately quantized and generated current I is related to the frequency of cycle f via $I \sim (ne)f$, where n is the number of electrons transferred in each cycle and e is the charge of electron. Accurate single electron pumping has been demonstrated experimentally [44, 45, 46, 47, 48] and achieved very high accuracy (error of 10^{-8}) at frequency f of a few MHz.

In the case that the connected islands and leads are superconducting materials, at low temperatures, the unit of transferred charge is a Cooper pair instead of a single electron [49, 50]. In this case even if pumping is achieved by periodic lifting of the Coulomb blockade, the coherence of the superconducting phase is fundamental [51, 52]. Normally there is a phase bias between two electrodes of the circuit which leads to an additional contribution (super current) to total current. Therefore, even in adiabatic regime, in addition to the characteristics of the cycle, the pumped current depends also on the phase difference across the circuit. The geometric nature of the pumped charge in superconducting systems has been analyzed both in the Abelian [53, 54, 55, 56] and non-Abelian [57] cases and made it possible to detect the geometric phases in superconducting nano circuits in experiments [58]. An experimental detection of geometric phase by means of Cooper pair pumping has also been reported [59].

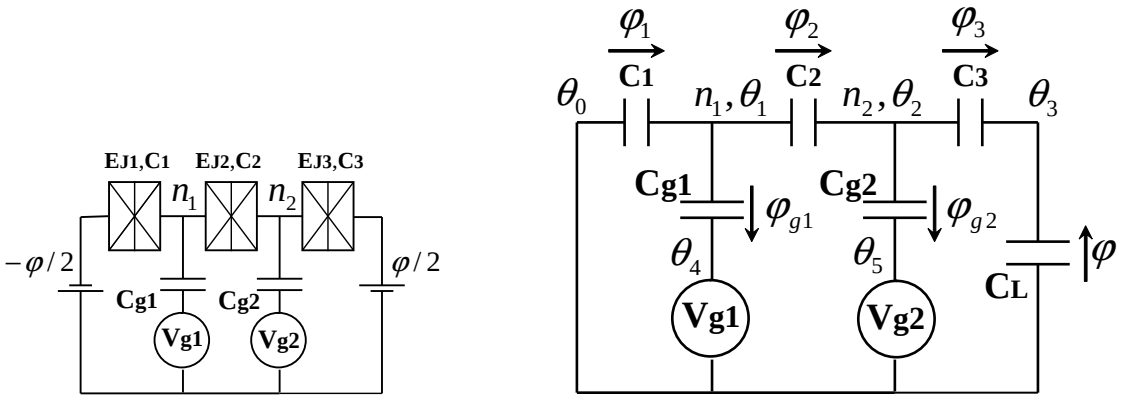

Figure 10: Schematic drawing of a three-junction pump and its equivalent (electrostatic) circuit used to derive the Hamiltonian of the system as a function of number of Cooper pairs inside boxes n_1 and n_2.

In the simplest form a Cooper pair pump can be realized by an array of Josephson junctions connected to two superconducting reservoirs (Fig. 9) with a biasing phase difference φ between two electrodes.As it was mentioned before, if this biasing phase is not zero, in addition to the pumped charge, there is another contribution to current due to Josephson effect. As it has been shown in figure 9, a pump with N Josephson junctions consists of $N-1$ Cooper pair boxes each one capacitively connected to a gate voltage. In this figure $E_{\mathrm{J}i}$ and C_i are Josephson energy and capacitance of the ith junction, n_i stands for the number of Cooper pairs inside the ith box and C_{gi} and V_{gi} are gate capacitance and gate voltage connected to this box. In a uniform pump $E_{\mathrm{J}i} = E_{\mathrm{J}}$ and $C_i = C$ and therefore if φ is the overall phase difference across the array, the phase difference across each junction will be φ/N.

In order to derive the charging part of the Hamiltonian of this system, for simplicity we consider a three-junction array (Fig. 10) which is a building block of a pump, and write the charging Lagrangian in terms of the superconducting phase inside the islands θ_1 and θ_2. Moreover we assume that $E_{\mathrm{J}i} = E_{\mathrm{J}}$, $C_i = C$ and $C_{gi} = C_g$, therefore the Lagrangian in the first step has the following form

$$L_C = \frac{C}{2}\left(\frac{\hbar}{2e}\right)^2(\dot{\varphi}_1^2+\dot{\varphi}_2^2+\dot{\varphi}_3^2) + \frac{C_g}{2}\left(\frac{\hbar}{2e}\right)^2(\dot{\varphi}_{g1}^2+\dot{\varphi}_{g2}^2) + \frac{C_L}{2}\left(\frac{\hbar}{2e}\right)^2\dot{\varphi}^2 \tag{1.63}$$

The last term in this equation is the work done by the external voltage source due to redistribution of charge in the array and C_L is *load capacitance*. Although we are interested in the case of charge pumping without a bias voltage ($\dot{\varphi}=0$) we keep the last term in the Lagrangian to show how the Hamiltonian looks in presence of bias voltage and at the end of calculation we will ignore it.

Following the same approach that we used in the case of single Cooper pair box, by setting $\dot{\theta}_0 = 0$, following relations between time derivative of phases $\dot{\theta}_i$ and phase differences $\dot{\varphi}_i$ can be easily obtained

$$\begin{aligned}
\dot{\varphi}_1 &= \dot{\theta}_1 \\
\dot{\varphi}_2 &= \dot{\theta}_2 - \dot{\theta}_1 \\
\dot{\varphi}_3 &= \dot{\theta}_3 - \dot{\theta}_2 \\
\dot{\varphi} &= \dot{\theta}_3
\end{aligned} \tag{1.64}$$

and from gate branches one finds

$$\begin{aligned}\dot{\varphi}_{g1} &= \frac{2e}{\hbar}V_{g1} - \dot{\theta}_1 \\ \dot{\varphi}_{g2} &= \frac{2e}{\hbar}V_{g2} - \dot{\theta}_2. \end{aligned} \tag{1.65}$$

Substituting these into the charging Lagrangian (1.63) results in

$$\begin{aligned}L_C &= \frac{C}{2}\left(\frac{\hbar}{2e}\right)^2\left[\left(2+\frac{C_g}{C}\right)\dot{\theta}_1^2 + \left(2+\frac{C_g}{C}\right)\dot{\theta}_2^2 + \left(2+\frac{C_L}{C}\right)\dot{\theta}_3^2 - 2\dot{\theta}_1\dot{\theta}_2 - 2\dot{\theta}_2\dot{\theta}_3\right] \\ &+ \hbar(q_1\dot{\theta}_1 + q_2\dot{\theta}_2) + \frac{C_g}{2}(V_{g1}^2 + V_{g2}^2) \end{aligned} \tag{1.66}$$

where $q_i = -C_{gi}V_{gi}/2e$ and we can omit the last constant term. The conjugate momentums are

$$\begin{aligned}p_1 &= \frac{\partial L_C}{\partial\dot{\theta}_1} = \left(\frac{\hbar}{2e}\right)^2 C\left[\left(2+\frac{C_g}{C}\right)\dot{\theta}_1 - \dot{\theta}_2\right] + \hbar q_1 \\ p_2 &= \frac{\partial L_C}{\partial\dot{\theta}_2} = \left(\frac{\hbar}{2e}\right)^2 C\left[\left(2+\frac{C_g}{C}\right)\dot{\theta}_2 - \dot{\theta}_3 - \dot{\theta}_1\right] + \hbar q_2 \\ p_3 &= \frac{\partial L_C}{\partial\dot{\theta}_1} = \left(\frac{\hbar}{2e}\right)^2 C\left[\left(1+\frac{C_L}{C}\right)\dot{\theta}_3 - \dot{\theta}_2\right]. \end{aligned} \tag{1.67}$$

Eventually one can derive the charging part3Td78648(o)0.43374fng

$$H_C = \frac{2}{3}E_C \sum_{n_1,n_2} \left[(n_1-q_1)^2 + (n_2-q_2)^2 + (n_1-q_1)(n_2-q_2)\right] |n_1,n_2\rangle\langle n_1,n_2| \tag{1.71}$$

The Josephson energy of a three-junction circuit is

$$H_{\mathrm{J}} = -E_{\mathrm{J}} \left(\cos(\varphi_1) + \cos(\varphi_2) + \cos(\varphi_3)\right). \tag{1.72}$$

If we choose $\varphi_1 = \theta_1 - \theta_0 + \frac{\varphi}{3}$, $\varphi_2 = \theta_2 - \theta_1 + \frac{\varphi}{3}$ and $\varphi_3 = -\theta_2 + \frac{\varphi}{3}$, considering that $\dot{\varphi} = 0$, both conditions on time derivatives of phases (equation (1.64)) and condition on sum over phases ($\varphi_1 + \varphi_2 + \varphi_3 = \varphi$) are satisfied if $\theta_0 = 0$. Now by writing $\cos(\theta_j)$ in terms of $e^{\pm i\theta_j}$, Josephson term of the Hamiltonian becomes:

$$H_{\mathrm{J}} = -\frac{E_{\mathrm{J}}}{2}\left(e^{i(\frac{\varphi}{3}+\theta_1)} + e^{i(\frac{\varphi}{3}+\theta_2-\theta_1)} + e^{i(\frac{\varphi}{3}-\theta_2)} + h.c.\right). \tag{1.73}$$

Since $e^{i\theta_j}$ is equivalent to adding one Cooper pair to the jth superconducting island with Josephson phase θ_j, we can substitute $e^{\pm i\theta_j}$ with $\sum_{n_j} |n_j \pm 1\rangle\langle n_j|$ which leads to:

$$H_{\mathrm{J}} = -\frac{E_J}{2}\sum_{n_1,n_2}\Big(e^{i\frac{\varphi}{3}}|n_1+1,n_2\rangle\langle n_1,n_2| + e^{i\frac{\varphi}{3}}|n_1-1,n_2+1\rangle\langle n_1,n_2| + e^{i\frac{\varphi}{3}}|n_1,n_2-1\rangle\langle n_1,n_2| + h.c.\Big) \tag{1.74}$$

It is possible to write this equation in a more compact form which is more suitable when a larger array is considered. First we introduce the vector $\vec{n}$ with elements n_1 and n_2 and use the index k to indicate the number of each junction. In a three-junction array $k = 1, 2, 3$. We also introduce a new set of vectors $\{\vec{\delta_k}\}$ which have the same dimension as $\vec{n}$ and we use them to show how the number of pairs inside each box changes when tunneling happens through kth junction. Tunneling of one Cooper pair through the kth junction changes the number of pairs on kth and $(k-1)$th island which means that, for example, if a Cooper pair tunnels from $(k-1)$th island to the kth island, n_{k-1} decreases by one while n_k will increase by one. Therefore the only non-zero components of $\vec{\delta_k}$ are $(\vec{\delta_k})_k = 1$ and $(\vec{\delta_k})_{k-1} = -1$. With this notation, the equation (1.74) becomes

$$H_{\mathrm{J}} = -\frac{E_J}{2}\sum_{n_1,n_2}\sum_{k=1}^{3}\left(e^{i\frac{\varphi}{3}}|\ \vec{n} + \vec{\delta_k}\rangle\langle\vec{n}\ | + h.c.\right). \tag{1.75}$$

It is straightforward to show that for a uniform pump with N Josephson junctions the full Hamiltonian, including charging and Josephson energy, has the following form [51]

$$\begin{aligned} H &= \frac{E_C}{N}\sum_{\vec{n}}\left[\sum_{k=1}^{N-1} k(N-k)(n_k-q_k)^2 + 2\sum_{l=2}^{N-1}\sum_{k=1}^{l-1} k(N-l)(n_k-q_k)(n_l-q_l)\right]|\ \vec{n}\rangle\langle\vec{n}\ | \\ &- \frac{E_J}{2}\sum_{\vec{n}}\sum_{k=1}^{N}\left(e^{i\frac{\varphi}{N}}|\ \vec{n} + \vec{\delta_k}\rangle\langle\vec{n}\ | + h.c.\right). \end{aligned} \tag{1.76}$$

The stability diagram of charging term of the Hamiltonian of a three-junction pump (equation (1.71)) is shown in figure 11. If $E_{\mathrm{J}} \ll E_C$ Josephson term of the Hamiltonian only makes some modifications close

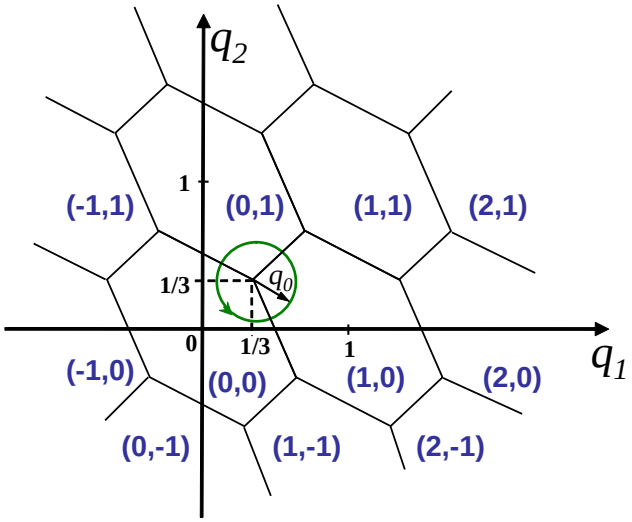

Figure 11: Stability diagram of charging term of the Hamiltonian of a three-junction pump and circular path as candidates for adiabatic Cooper pair pumping.

to degeneracy points. In this case, if gate voltages are changed in time slowly enough to keep the system in adiabatic regime, a circular path in (q_1, q_2) space around the degeneracy point of three charge states $|0,0\rangle$, $|1,0\rangle$ and $|0,1\rangle$ is expected to lead to pumping one Cooper pair after each cycle. This circular path is equivalent to two Sinusoidal gate voltages [51]

$$\begin{aligned} q_1 &= \frac{1}{3} + q_0 \cos(2\pi t/T + \vartheta_0) \\ q_2 &= \frac{1}{3} + q_0 \sin(2\pi t/T + \vartheta_0), \end{aligned} \tag{1.77}$$

where $q_1 = q_2 = 1/3$ is the degeneracy point and the center of path and q_0 is its radius. ϑ_0 defines the starting point of the cycle. T is the total time duration of one cycle and, in order to stay in adiabatic regime, the following inequality must be fulfilled

$$T \gg \frac{\hbar E_C}{E_J^2}. \tag{1.78}$$

Another option for gate voltages to lead the system from $|0,0\rangle$ to $|1,0\rangle$ then $|0,1\rangle$ and at the end again to $|0,0\rangle$ is a triangular path which directly connects these three points together and is equivalent to a sequence of sawtooth gate voltages. Although in experiments it is easier to prepare sinusoidal gates, for pumps with more than three junctions sinusoidal gates are not useful anymore and the only choice is sawtooth gates.

1.3.3 Quantum bits (Qubits)

The idea of quantum computation and consequently building computers which are based on quantum mechanics raised the question that which kind of devices are best candidates for quantum logic bits (qubits). As it has been explained in the introduction, superconducting devices, which are based on Josephson effect,

are promising devices to be used as building blocks of solid-state quantum computers [4, 2, 60, 61, 62]. Depending on which dynamical variable is most well defined and which basis are used as computational states $|0\rangle$ and $|1\rangle$, Josephson qubits can be categorized into three main classes, *charge*, *flux* and *phase* qubits. If the charging energy is the dominant energy in the system, the qubit is called charge qubit and two lowest eigenstates of the charging Hamiltonian are used as logical states. In the case that the superconducting phase or equivalently the magnetic flux is the important variable to define the two-level system, the qubit is known as phase qubit or flux qubit and normally the ground-state and first excited state play the role of computational states. There are also some mixed regimes where both charge and phase come in use to make more sophisticated qubits. In this section we review charge, flux and phase qubits and show that the simple devices, which are so far introduced in this thesis, can be used as quantum bits. We will show how one can practically separate two lowest states of the system from the rest of states and make transition between them by means of external applied physical parameters such as gate voltages, flux or current pulses.

Charge qubit

One can use a single Cooper pair box (SCB) as an elementary charge qubit if it operates in charge regime where $E_C \gg E_\mathrm{J}$. As it has been shown in section 1.3.1 the Hamiltonian of a SCB in the Hilbert space of charge states has following form

$$H = E_C \sum_n (n - q_g)^2 |n\rangle\langle n| - \frac{E_\mathrm{J}}{2} \sum_n (|n+1\rangle\langle n| + |n\rangle\langle n+1|) \tag{1.79}$$

The qubit Hamiltonian is derived by working with two parabolas associated with $n = 0$ and $n = 1$ in Fig. 8 and projecting the full Hamiltonian (1.79) onto two lowest charge states $|0\rangle$ and $|1\rangle$ which leads to

$$H = -\frac{1}{2}(\epsilon\sigma_z + \Delta\sigma_x) \tag{1.80}$$

where $\epsilon = E_C(1 - 2q_g)$ and $\Delta = E_\mathrm{J}$ and $\{\sigma_i\}$ are Pauli matrices. In analogy to spin $\frac{1}{2}$ problem we have shifted the zero-energy point to the middle of the energy difference between two charge states $|0\rangle$ and $|1\rangle$. One should notice that eigenstates of this Hamiltonian are not charge states $|n\rangle$ but they are superpositions of charge states with energies

$$E_0 = -\frac{1}{2}\sqrt{\epsilon^2 + \Delta^2} \quad ; \quad E_1 = +\frac{1}{2}\sqrt{\epsilon^2 + \Delta^2} \tag{1.81}$$

and transition frequency

$$\omega_{01} = \frac{1}{\hbar}\sqrt{\epsilon^2 + \Delta^2} \tag{1.82}$$

which is controllable by gate voltage. At degeneracy point of charge states, where $q_g = 1/2$, the energy levels of these two eigenstates are separated by $\Delta = E_\mathrm{J}$ (Fig. 12) and the qubit eigenstates correspond to the cat states $|E_0\rangle = |0\rangle + |1\rangle$ and $|E_1\rangle = |0\rangle - |1\rangle$. Far form the degeneracy point the eigenstates of the qubit are close to pure charge states $|0\rangle$ and $|1\rangle$.

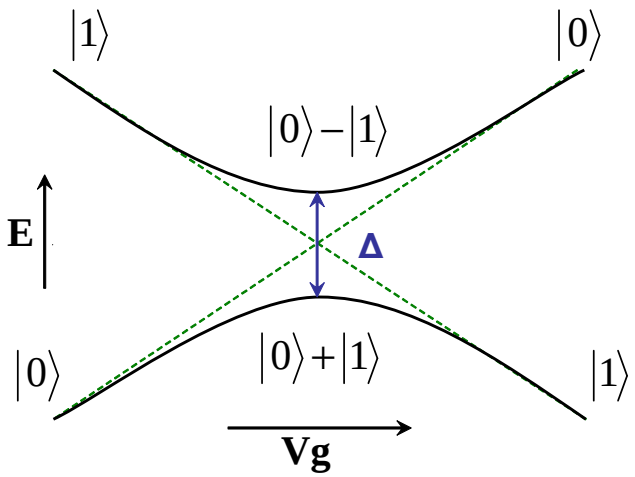

Figure 12: Energy spacing of two lowest states of a single Cooper pair box, used as states of charge qubit, as a function of gate voltage. At degeneracy point $q_g = -C_g V_g/(2e) = 1/2$ states correspond to cat states and their energy difference Δ is equal to E_J. Far from the degeneracy point qubit states approach pure charge states $|0\rangle$ and $|1\rangle$.

Flux qubit

An elementary flux qubit can be realized by an rf-SQUID operating in the phase regime, $E_\mathrm{J} \gg E_C$. As it has been explained in section 1.2.2 for external magnetic flux equal to half integer Φ_0 or equivalently $\varphi_e = \pi$, the potential of rf-squid (1.35) has two identical wells with equal energy levels if macroscopic quantum tunneling (MQT) between wells is neglected. Since it is not easy to find an exact analytical solution for eigenenergies and eigenstates of this potential let us address the problem in an intuitive way. First we assume that there is no MQT between two wells and therefore the state is totally localized in left or right well. These states correspond to the ground-state of the Hamiltonian (1.37) with potential U_l or U_r (see Fig. 13(a)) and we refer to them by the $|l\rangle$ and $|r\rangle$ and their energies are E_l and E_r so

$$H_l|l\rangle = E_l|l\rangle, \qquad H_r|r\rangle = E_r|r\rangle \tag{1.83}$$

We call these two states *flux states*. If the external biasing magnetic flux is exactly half integer then $E_l = E_r$ and flux states are degenerate and correspond to circulating currents in SQUID loop with opposite directions. When MQT is switched on the two lowest states of the system are not purely $|l\rangle$ or $|r\rangle$ but two superpositions of them. At degeneracy point, $\varphi_e = \pi$, these superpositions correspond to cat states $|l\rangle \pm |r\rangle$ and their energy splitting Δ depends on the rate of MQT which itself depends on the height of the potential barrier which is determined by the ratio E_J/E_L. For small MQT rate the level spacing between these cat states is much smaller than those between these and higher levels and thus a tight two-level system is formed (see Fig. 13(b)). By varying the external flux such that it deviates slightly from the half integer value, $\varphi_e = \pi + \delta\varphi_e$, the ground-states of two wells (in absence of MQT) are not equal anymore but still are close to each other, $E_l \approx E_r$. Now by switching the MQT on, levels become hybridized again but this time their energy splitting depend both on the rate of MQT and the difference between E_l and E_r.

The qubit Hamiltonian is derived by projecting the whole Hilbert space of the full Hamiltonian (1.37)

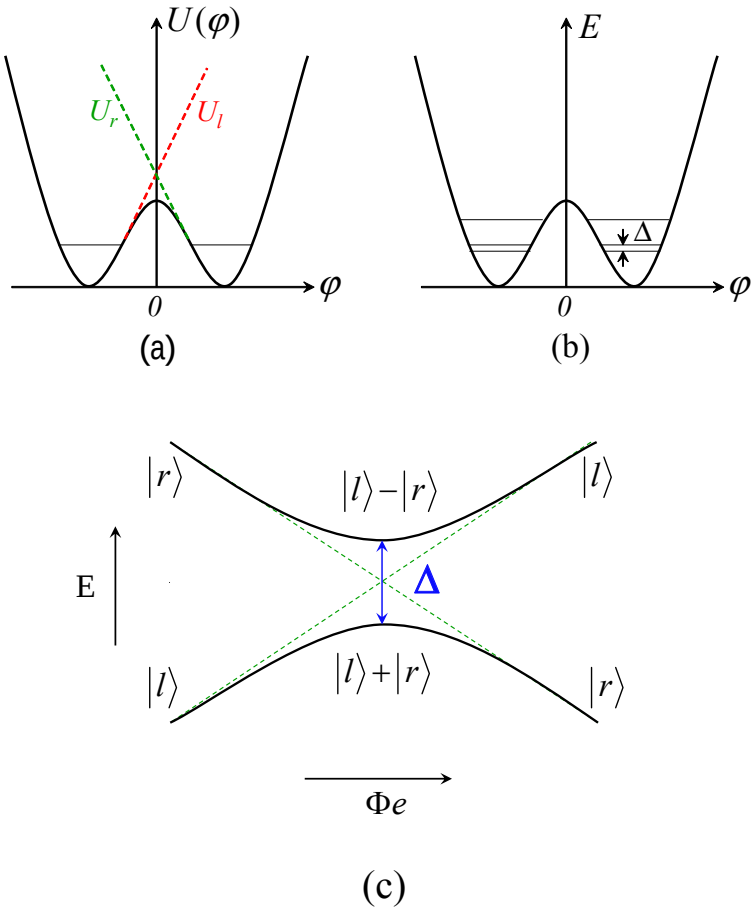

Figure 13: Schematic drawing of a flux qubit (a)approximated potentials in absence of MQT, (b)energy diagram inside wells while taking into account MQT which leads to a tight two-level system with energy spacing Δ and (c)the energy spacing of qubit states as a function of external magnetic flux Φ_e. At degeneracy point $\Phi_e = n\Phi_0$ level spacing Δ depends on the rate of MQT.

on the subspace of $|l\rangle$ and $|r\rangle$. The true eigenstate $|E\rangle$ of whole Hamiltonian H now can approximately be written as a superposition:

$$|E\rangle = a|l\rangle + b|r\rangle \tag{1.84}$$

and the qubit Hamiltonian is given by its elements with respect to the states $|l\rangle$ and $|r\rangle$:

$$\begin{aligned} H_{ll} &= E_l + \langle l|U - U_l|l\rangle \\ H_{rr} &= E_r + \langle r|U - U_r|r\rangle \\ H_{rl} &= E_l\langle r|l\rangle + \langle r|U - U_l|l\rangle \end{aligned} \tag{1.85}$$

Since the difference $U - U_{l,r}$ is appreciable only in vicinity of the potential barrier and the wave functions are exponentially small in that region, the second terms in diagonal elements of the full Hamiltonian are small. Moreover the off-diagonal element is exponentially small because of small overlap $\langle r|l\rangle$ of the ground-state wave functions in the left and right wells, and also here the main contribution comes from the first term. One can choose real wave functions to make the truncated Hamiltonian symmetric, $H_{lr} = H_{rl}$. Eventually the Hamiltonian of the flux qubit will have the following form

$$H = -\frac{1}{2}(\epsilon\sigma_z + \Delta\sigma_x) \tag{1.86}$$

where $\epsilon = E_r - E_l$, $\Delta = 2H_{rl}$ and again we have shifted the zero point energy to the middle of E_r and E_l. The Hamiltonian of the flux qubit is formally equivalent to the Hamiltonian of the charge qubit (equation (1.80)). The difference is that here Hamiltonian is written in terms of flux basis while in the case of charge qubit the charge states were chosen as basis. The eigenstates of the Hamiltonian (1.86) have energies and transition frequency which are the same as (1.81) and (1.82). While in a charge qubit the energy splitting and consequently the transition frequency between states of the qubit are controlled by means of a gate voltage, in a flux qubit the external biasing magnetic flux controls the energy spectrum (Fig. 13(c)). As we mentioned before, at the flux degeneracy point, $\varphi_e = \pi$, the level splitting Δ is determined by the small rate of the quantum tunneling through the macroscopic potential barrier and the wave functions correspond to the cat states which are equally-weighted superpositions of the flux states $|l\rangle$ and $|r\rangle$. Far from the degeneracy point, the qubit states are almost pure flux states.

The possibility of achieving quantum coherence of macroscopic current states in an rf-SQUID with a small-capacitance Josephson junction was first pointed out theoretically by Leggett in 1984 [63] and first successful experiment has been done in 2000 by Friedman et al. [64].

Phase qubit

Phase qubits, which are based on the Josephson phase degree of freedom, have significant importance because of their tunability and also their insensitivity to charge and flux noises which are the main sources of error in charge and flux qubits. In the simplest implementation a phase qubit can be realized by a current-biased Josephson junction and its energy spectrum and dynamics are controlled by biasing currents. As it has been explained in section 1.2.1, the Hamiltonian of a single junction biased by a dc current I_{dc} has the following form:

$$H_{dc} = E_C n^2 - E_{\mathrm{J}} \cos(\varphi) - \frac{\hbar I_{dc}}{2e}\varphi. \tag{1.87}$$

In the regime where superconducting phase φ is the appropriate quantum variable ($E_J \gg E_C$), by using the relation between n and φ and substituting $h/2e$ with Φ_0 one obtains:

$$H_{dc} = -E_C \frac{\partial^2}{\partial\varphi^2} - E_{\mathrm{J}} \cos(\varphi) - \frac{I_{dc}\Phi_0}{2\pi}\varphi. \tag{1.88}$$

As we mentioned before, the potential energy of this Hamiltonian, as a function of φ, has the form of tilted washboard potential. The wells of this potential have a depth ΔU which is related to I_{dc} via

$$\Delta U = \frac{2\sqrt{2}}{3\pi} I_c \Phi_0 \left(1 - \frac{I_{dc}}{I_c}\right)^{\frac{3}{2}}, \tag{1.89}$$

and the frequency of the classical oscillation ω_p in the bottom of the well is

$$\omega_p = \sqrt{\frac{2\pi I_c}{C\Phi_0}} \left[1 - \left(\frac{I_{dc}}{I_c}\right)^2\right]^{\frac{1}{4}}. \tag{1.90}$$

The ratio $\Delta U/\hbar\omega_p$ gives an estimate of the number of states in the well, therefore by changing the bias current I_{dc} one can change the depth of the potential wells of the tilted washboard potential and consequently sets the specific number of energy levels to be allowed inside each well. This system is normally biased by a dc current slightly smaller than critical current I_c. In an ideal case when only two lowest energy levels, E_0 and E_1, are inside the well (Fig. 14), their corresponding eigenstates, $|0\rangle$ and $|1\rangle$, can be used as computational states. In the basis of the two lowest eigenstates $|0\rangle$ and $|1\rangle$, the Hamiltonian of the phase qubit (1.88) takes the following form

$$H_{dc} = -\frac{1}{2}\epsilon\sigma_z, \tag{1.91}$$

where $\epsilon = E_1 - E_0 = \hbar\omega_{01}$ and ω_{01} is the transition frequency and is given by

$$\omega_{01} \approx \omega_p \left(1 - \frac{5}{36}\frac{\hbar\omega_p}{\Delta U}\right). \tag{1.92}$$

Although the Hamiltonian of the phase qubit biased with dc current I_{dc} has only one term proportional to σ_z, an additional term with σ_x or σ_y operation can be added to the Hamiltonian (1.91) if a microwave current $I_{\mu w} = I(t)\cos(\omega t + \theta)$ which oscillates with frequency $\omega = \omega_{01}$ is applied to the junction. In this case the phase of microwave current θ defines the axis of rotation in the xy plane of the Bloch sphere, while the amplitude and duration time of the current $I(t)$ define the angle of rotation. For example, $\theta = 0$ leads to rotations around x-axis and therefore the total Hamiltonian of the qubit $H = H_{dc} + H_{\mu w}$ takes the following form:

$$H \approx -\frac{1}{2}\epsilon\sigma_z + \Delta\sigma_x, \tag{1.93}$$

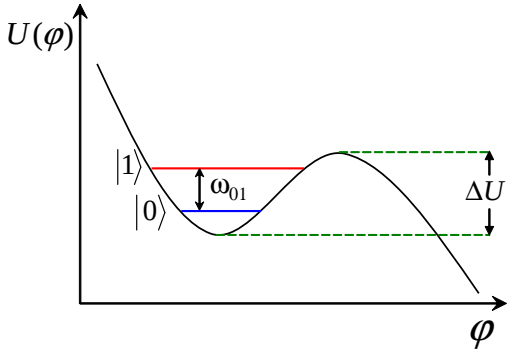

Figure 14: Schematic drawing of the potential energy U of a current biased Josephson junction as a function of Josephson phase φ across the junction. When the junction is biased with $I_{dc} \lesssim I_c$, two lowest states $|0\rangle$ and $|1\rangle$ inside the potential well with transition frequency $\omega_{01} = (E_1 - E_0)/\hbar$ can be used as computational states and the qubit is called Josephson phase qubit. Transition between these states can be done by means of a microwave current with frequency $\omega = \omega_{01}$.

where $\Delta = I(t)\sqrt{\hbar/2C\omega_{01}}$. Since the single-junction phase qubit and specially the effect of this microwave current is one of the main topics of the work done for this thesis, the physics of this system will be discussed in details in chapter 4 where a junction with three and five levels inside its potential has been studied.

Chapter 2

Quantum optimal control theory

Optimal control theory [65, 66] and some variational methods [67, 68, 69], similar to those used in optimal control, have been used to achieve selective excitations in NMR [70]. The first attempt to employ a specific quantum optimal control theory to achieve, or come close to, a specific state at a given time was done by A. P. Peirce and M. A. Dahleh [7] in 1987. In this problem the evolution of the state of the quantum system is governed by Schrödinger equation. Before the work done by Peirce and Dahleh for a specific problem, a general formalism for the control of quantum systems that applies to a variety of contexts was published by Butkovskii and Samoilenko [71]. The controllability of quantum systems [72, 73] , required conditions for global controllability, and a general theory of quantum-dynamical systems with observation, control, and feedback [74, 75] had been developed.

Since for works done in this thesis the optimal control theory for leading a quantum system to a desired final state, in a certain time, is of interest, a brief review of the theory introduced by Peirce and Dahleh will be presented in this chapter. More recent and generalized versions of the theory can be found in Refs. [8, 9].

2.1 An introduction to the theory

Before starting to formulate the Schrödinger optimal control problem, let us introduce a notation for Hilbert spaces which will be used later. Let $\Omega \subset \mathbf{R}^n$ be the spatial domain, and $[0, T]$ be the finite time interval under consideration. Then:

$X := L_2(\Omega), \quad X_t := L_2(\Omega, [0, T])$,

$X' := L_2(\Omega \times \Omega), \quad X'_t := L_2(\Omega \times \Omega, [0, T])$,

where L_2 is the space of 2-power integrable functions and sequence space of vectors with Euclidean norm.

Considering a quantum system with wavefunction $\psi(x, t)$, the aim is to drive this system from an initial state $\psi_{ini}(x)$ to a final desired state $\psi_{fin}(x)$, in a given time T, while the dynamics of the system is under control via a control parameter u. In the standard way [65, 66], the optimal control theory is posed by minimization of a cost functional, which is a measure of accuracy of achieving the target state, and can be defined as

$$J[u] = \langle \psi(x,T) - \psi_{fin}(x), \psi(x,T) - \psi_{fin}(x) \rangle_X + \alpha \langle u, u \rangle_{X'_t}; \tag{2.1}$$

subject to

$$i\hbar\frac{\partial\psi(x,t)}{\partial t} = (H_0 + U)\psi(x,t) \quad \text{for all} \quad x \in \Omega \quad \text{and} \quad t \in [0,T] \tag{2.2}$$

and $\psi(x,0) = \psi_{ini}(x)$ for all $x \in \Omega$.Here $\psi_{fin}(x)$ and $\psi_{ini}(x) \in X$, and $H_0 := [-(\hbar^2/2m)(d^2/dx^2) + V_0(x)]$ is the Hamiltonian of the quantum system to be controlled. The operator U is defined by

$$U\psi(x,t) := \int_\Omega u(x,x',t)\psi(x',t)dx' \tag{2.3}$$

where $u(x,x',t) \in X'$ for each t so that U is a Hilbert-Schmidt operator. Since all linear Hilbert-Schmidt operators on X' can be represented in this form [76], a large class of operators can be covered by this optimal control theory. Physically this optimization problem can be interpreted as finding the optimal external forcing, represented by the operator U, such that the state ψ becomes as close as possible in the required X norm to the target state ψ_{fin} in a given time T, while $\|u\|_{X'_t}$ remains finite. The parameter α is a positive real constant which can be used to balance the relative importance of two terms in the cost functional $J[u]$. First term is the error in achieving the target state ψ_{fin} and the second term is the magnitude of the external applied forcing. For example, if the external forcing is due to an applied optical field then the term $\langle u,u\rangle_{X'_t}$ represents the radiative energy and its presence in the cost functional poses the condition of minimal radiative energy deposition while reaching the target state ψ_{fin} as close as possible. As mentioned before, by means of parameter α one can change the importance of this condition compared with the importance of the fidelity of achieving the desired state.

The proof of existence of such an optimal solution to the Schrödinger control problem is beyond the subject of this thesis and we do not present it here but interested readers can refer to Ref. [7].

One physically interesting form of the operator U is when U corresponds to multiplication by some function. In this case the operator U would represent an external applied potential defined by $u(x,x',t) = \delta(x-x')u(x',t)$ in equation (2.3). Although in this case $u \notin X'$, by replacing the δ function by a δ-sequence function δ_ϵ such that $u_\epsilon(x,x',t) = \delta_\epsilon(x-x')u(x',t)$, it can be proved that there exists a solution to the optimization problem for each $\epsilon > 0$. Thus by choosing the δ_ϵ to be much narrower than the physical length scale of the problem one can replace the operator U by a multiplicative function $u(x,t)$ and consider it as an approximate solution.

Before deriving the necessary conditions for minimization of the cost functional, let us reformulate the optimization problem using the Lagrange-multiplier function in order to include the Schrödinger equation as a constraint in the minimization. From now on we assume that the operator U is an external applied potential and acts as a multiplication operator. Let $\chi(x,t) \in X_t$ be the Lagrange multiplier and consider the minimization problem: Find $\tilde{u}(x,t)$, $\tilde{\psi}(x,t)$, and $\tilde{\chi}(x,t)$ such that:

$$L[\tilde{u}(x,t),\tilde{\psi}(x,t),\tilde{\chi}(x,t)] = \inf L[u(x,t),\psi(x,t),\chi(x,t)] \tag{2.4}$$

where

$$L[u(x,t),\psi(x,t),\chi(x,t)] := J[u(x,t)] + \Re\int_0^T\int_\Omega \chi(x,t)\left[\dot{\psi}(x,t) + \frac{i}{\hbar}(H_0 + u(x,t))\psi(x,t)\right]^* dx\ dt. \tag{2.5}$$

In this way, when the functional is in a minimum, Schrödinger equation is satisfied too. The necessary conditions for minimizing the functional can be obtained by setting its Fréchet derivatives with respect to the argument functions u, ψ, and χ equal to zero:

$$\frac{\delta L}{\delta \chi}\delta\chi = 0 \quad \Rightarrow \quad \dot{\tilde{\psi}}(x,t) = -\frac{i}{\hbar}(H_0 + u(x,t))\tilde{\psi}(x,t) \quad ; \quad \tilde{\psi}(x,0) = \psi_{ini}(x) \tag{2.6}$$

$$\frac{\delta L}{\delta \psi}\delta\psi = 0 \quad \Rightarrow \quad \dot{\tilde{\chi}}(x,t) = -\frac{i}{\hbar}(H_0 + u(x,t))\tilde{\chi}(x,t) \quad ; \quad \tilde{\chi}(x,T) = 2[\psi_{fin}(x) - \tilde{\psi}(x,T)] \tag{2.7}$$

$$\frac{\delta L}{\delta u}\delta u = 0 \quad \Rightarrow \quad \int_0^T \int_\Omega \left[2\alpha\tilde{u}(x,t) - \Re\left[\tilde{\chi}(x,t)\frac{i}{\hbar}\tilde{\psi}^*(x,t)\right]\right]\delta u \; dx \; dt = 0 \tag{2.8}$$

These last three conditions form the basis for an iterative procedure: starting from an initial guess for the applied potential $u^{(0)}$ one can find the corresponding solutions $\psi^{(0)}(x,t)$ and $\chi^{(0)}$ from equations (2.6) and (2.7). These functions then can be used to compute the gradient $\delta L/\delta u$. Then the gradient is used to find a new applied potential $u^{(1)}$ for which the value of L is lower and using this new potential all steps are repeated until one optimize applied potential is found. For practical purposes we replace the infinite-dimensional Hilbert spaces X, X_t, and X_t^0 by finite-dimensional subspaces on which the optimization problem is considered. In the finite-dimensional subspaces the computed gradient $\delta L/\delta u$ can be used to search for an optimal applied potential by the method of steepest descents or by a conjugate direction procedure [77].

For the first work done in this thesis it is more convenient to consider another cost functional. Assume that instead of (2.5) we aim at minimizing the cost functional defined as [78]:

$$L = 1 - \left|\int \psi_{fin}(x)\psi^*(x,T)\; dx\right|^2 + 2\Re\int_0^T \int \chi(x,t)\left[\dot{\psi}(x,t) + \frac{i}{\hbar}H\psi(x,t)\right]^* dx \; dt \tag{2.9}$$

where

$$H = -\frac{\hbar^2}{2m}\frac{d^2}{dx^2} + V_0(x) + U(x,\{u_j(t)\}) \tag{2.10}$$

here U is a function of x and a set of time dependent external control parameters $\{u_j(t)\}$. Equating the partial derivatives of L, with respect to the arguments, to zero we obtain three necessary conditions for optimization:

$$\frac{\delta L}{\delta \chi}\delta\chi = 0 \quad \Rightarrow \quad \dot{\psi}(x,t) = -\frac{i}{\hbar}H\psi(x,t) \quad ; \quad \psi(x,0) = \psi_{ini}(x) \tag{2.11}$$

$$\frac{\delta L}{\delta \psi}\delta\psi = 0 \quad \Rightarrow \quad \dot{\chi}(x,t) = -\frac{i}{\hbar}H\chi(x,t) \quad ; \quad \chi(x,T) \equiv \psi_{fin}(x)\int \psi_{fin}(x)\psi^*(x,T)\; dx \tag{2.12}$$

$$\frac{\delta L}{\delta u_j}\delta u_j = 0 \quad \Rightarrow \quad -\frac{2}{\hbar}\Im\int_0^T \int \chi^*(x,t)\frac{\partial U(x,\{u_j(t)\})}{\partial u_j(t)}\psi(x,t)\; dx \; dt = 0 \tag{2.13}$$

which are the basis needed for iterative procedure.

Considering the fact that the second term in (2.1) is an optional constraint on the power of control parameter, the only term which differs from (2.5) to (2.9) is the first term which measures the error of achieving the target state. After this, for simplicity, we refer to cost functional (2.5) without the constraint, and (2.9) by their first term, keeping in mind that the term containing the Lagrange multiplier is indeed included. Since the Bra-Ket notation is more convenient for the works done in this thesis, we rewrite the two cost functionals as follows:

$$\begin{aligned} e_1 &= 1 - |\langle\psi(T)|\psi_{fin}\rangle|^2 \\ e_2 &= \||\psi(T)\rangle - |\psi_{fin}\rangle\|^2 . \end{aligned} \tag{2.14}$$

It is worthwhile noticing that, although the minimization of both e_1 and e_2 maximizes the population of the target state, the overall phase of target state is not forced to be preserved by minimizing e_1.

By using the set of equations obtained before, the *immediate feedback control* algorithm, which is guaranteed to reduce the cost functional at each iteration [78] can be summarized as follows. Assume that the Hamiltonian of the system depends on a set of controllable parameters $\{u_j(t)\}$. Starting from a proper initial guess $\{u_j^{(0)}(t)\}$ for control parameters, first the state of the system $|\psi(t)\rangle$ is evolved in time with the initial condition $|\psi(0)\rangle = |\psi_{ini}\rangle$ giving rise to $|\psi(T)\rangle$ after time T. At this point the iterative algorithm starts, aiming at decreasing the cost functional by adding a correction to control parameters in each step. In the nth step of this iterative algorithm

- the Lagrange multiplier $|\chi(t)\rangle$ is evolved backward in time starting from $|\chi(T)\rangle$ reaching $|\chi(0)\rangle$.

  In the case of minimizing e_1, $|\chi(T)\rangle = |\psi_{fin}\rangle\langle\psi_{fin}|\psi(T)\rangle$ and for minimizing e_2, $|\chi(T)\rangle = 2(|\psi(T)\rangle - |\psi_{fin}\rangle)$.

- The states $|\chi(0)\rangle$ and $|\psi(0)\rangle$ are evolved forward in time, respectively, with control parameters $\{u_j^{(n)}(t)\}$ and $\{u_j^{(n+1)}(t)\}$. Where,

  $$u_j^{(n+1)}(t) = u_j^{(n)}(t) + \frac{2}{\lambda(t)}\Im\left[\langle\chi(t)|\frac{\partial H}{\partial u_j(t)}|\psi(t)\rangle\right] \tag{2.15}$$

  are updated control parameters. $\lambda(t)$ is a weight function used to fix initial and final conditions on the control parameters in order to avoid major changes at the beginning and end of time evolution.

These two steps are repeated until the desired value of e_1 or e_2 is obtained.

In the numerical procedure, suggested in Ref. [7], the time evolution is done by means of the implicit Crank-Nicholson [79] scheme and descritizing the duration time of the evolution T with time steps Δt. The reason for choosing this method in preference to an explicit scheme such as *leapfrog* [80] method is that for explicit schemes the bound on the time step Δt depends on the unknown external applied potential U. Thus it is impossible to determine *a priori* the magnitude of the time step Δt in explicit methods while the Crank-Nicholson scheme is unconditionally stable. For the works done in this thesis, forward and backward evolutions in time are done by discretizing the time evolution propegator [8].

2.2 Applications

There have been many problems in physics and chemistry which are addressed within the framework of the quantum optimal control theory. For example it has been applied to the selective excitation problem in

NMR [70] and to the design of selective excitation strategies for achieving dissociation in chains of molecules treated classically [81], semiclassically [82] and quantum-mechanically [7]. Later on the idea of controlling quantum phenomena in a variety of nanoscale systems [83] attracted the interest of the society and starting from the very early work by Heberle *et al.* [84], coherent-carrier control in semiconductors and semiconductor nanostructures has also been established as a mature field of research.

When the idea of quantum information and quantum communication was proposed [1], because of the need for high precision one-bit and multi-bit gates, the quantum optimal control theory received new attention. The high-fidelity quantum state engineering calls for strategies that allow an optimal suppression of environment losses during the gating and data processing. Recently the optimal control theory has been applied in quantum computations, both with atoms in optical lattices [10] to operate quantum gates between physically distant qubits and with Josephson charge qubits [11, 12] to design high-fidelity two-qubit gates in the presence of leakage and noise. These last two works are the main motivations for the subject of this thesis, to examine the applicability of the optimal control theory in achieving faster and more accurate gating and transferring data, needed for realistic quantum computers.

Chapter 3

Optimized Cooper pair pumping

3.1 Introduction

As it was explained in Sec. 1.3.2 one can generate a dc current in a mesoscopic circuit, for example an array of Josephson junctions, by means of changing some external time-dependent parameters such as gate voltages periodically. It was also mentioned that in a three-junction array, applying a set of sinusoidal gate voltages (1.77), equivalent to a circular path in (q_1, q_2) plane (Fig. 11 of Chapter 1), is a way to drive the system from charging state $(0, 0)$ to $(1, 0)$ then $(0, 1)$ and at the end to $(0, 0)$ (where (n_1, n_2) refer to number of extra pairs on first and second island) and therefore pump one Cooper pair in each cycle. If the duration time of the cycle T is large enough to fulfill the adiabatic condition (1.78) then the pumped charge depends only on the geometrical properties of the path in (q_1, q_2) plane and not the detailed timing of the gate voltages. Due to the phase coherence in superconducting devices, in addition to the dependence of the pumped charge on the characteristics of the cycle, there is a dependence on the superconducting phase φ across the reservoirs which causes an uncertainty in the pumped charge proportional to $\cos(\varphi)$ and $(E_J/E_C)^{N-2}$ [51], where N is the number of junctions of a uniform array and E_J and E_C are Josephson and charging energies of each junction. Moreover if this phase is not zero it leads to an additional contribution to the current due to Josephson effect.

In addition to the importance of addressing fundamental questions related to the quantum mechanical behavior of macroscopic systems, accurate charge pumping can be used for metrological purposes. In the case of single-electron pumps the transfered charge at frequency f of a few MHz has reached such accuracy (uncertainty of 10^{-8}) that makes a new metrological standard of capacitance possible [46, 47, 48]. By pumping a certain number of electrons onto a capacitor and measuring the resulting voltage one can measure capacities of the order of 1pF. On the contrary the frequencies and consequently the current intensities in single-electron pumps has not been sufficiently high for setting a standard of current. A superconducting Cooper pair pump, in principle, would allow for higher frequencies although several effects such as Landau-Zener tunneling, supercurrent leakage through the pump, and coherent corrections (which are of crucial importance to reveal geometric phases) would lead to all sort of inaccuracies in Cooper pair pumping. Some works have been done to achieve more accurate pumping in adiabatic regime by optimizing the design of the pump [52, 56, 85]. In this work we follow a different approach. We aim at designing very accurate Cooper pair pumps by optimizing the pulse shapes of the gate voltages during the cycle. Most importantly we are not bound to work in the adiabatic limit therefore we would be able to increase, at the same time, both the accuracy and the frequency of operation. The theoretical framework which will be applied to achieve

this goal is that of optimal control theory (see Chapter 2). This approach has been successfully applied to superconducting qubits to improve one- and two-qubit gates [11, 12] and it was shown that it can help in reducing the error in the gate operation by several orders of magnitude. As we will describe in this chapter, optimal control is also helpful in the case of Cooper pair pumping where, for the case we consider, the error is reduced up to five orders of magnitude.

This chapter is organized as follows. In the next section we will describe the model for the Cooper pair pump discussed in the rest of the chapter. In Sec. 3.3 we present the numerical results obtained for our non adiabatic optimal pump. After having discussed the achieved accuracy (Sec. 3.3.1),in order to test the robustness of the pump, we analyze in details the effect of possible imperfections in the pulse shapes (Sec. 3.3.2), the effect of noise (Sec. 3.3.3), and finally the effect of possible imperfections in the pump itself (Sec. 3.3.4). Sec. 3.4 is devoted to conclusions and comments.

3.2 Model

As it has been discussed in Sec. 1.3.2, a Cooper pair pump can be realized by a uniform array of N JJs with $N-1$ gated islands (Fig. 9 of Chapter 1) and with Hamiltonian (1.76). Since the building block of a Cooper pair pump consists of two islands connected to each other and to the leads via three Josephson junctions, we will focus on a three-junction array (Fig. 10 of Chapter 1) with Hamiltonian:

$$\begin{aligned} H &= \frac{2}{3}E_C \sum_{\vec{n}} [(n_1-q_1)^2+(n_2-q_2)^2+(n_1-q_1)(n_2-q_2)]|\ \vec{n}\rangle\langle\vec{n} \\ &- \frac{1}{2}E_J \sum_{\vec{n}}\sum_{k=1}^{3}\left(e^{i\frac{\varphi}{3}}|\ \vec{n}+\vec{\delta_k}\rangle\langle\vec{n}\ |+h.c.\right) \end{aligned} \tag{3.1}$$

As it has been explained in Chapter 2, quantum optimal control algorithms are designed to lead a quantum system from an initial state to a target state by minimizing a defined cost functional by means of updating some control parameters. Notice that in order to use the quantum optimal control, one needs to have a desired final state differing from the initial state and at least one parameter as a control in the Hamiltonian of the system. Since pumping must be cyclic the initial and final states of the system, apart from a phase, are the same so we introduce a new quantum number which we refer to as the *counter*. This *counter* acts just as a witness for transferring Cooper pairs through the last junction in the array, and so if one pair passes this junction from left (right) to right (left) this quantity will change by 1 (-1). If one denotes the state of the JJs array by $|\Phi(t)\rangle$ and the state of the counter by $|m\rangle$, where $m=0,\pm1,\pm2...$, the state of the system will be $|\Psi(t)\rangle \equiv |\Phi(t)\rangle \otimes |m\rangle$, and therefore the initial and final states will be different due to different number of pairs passed through the array. In the Hilbert space of charge states plus the counter index the Hamiltonian of a three-junction uniform pump has the following form:

$$\begin{aligned} \mathcal{H} &= \frac{2}{3}E_C \sum_{m,\vec{n}} \left[(n_1-q_1)^2+(n_2-q_2)^2+(n_1-q_1)(n_2-q_2)\right]\left|\vec{n},m\right\rangle\left\langle\vec{n},m\right| \\ &- \frac{1}{2}E_J \sum_{m,\vec{n}} \Big[e^{i\frac{\varphi}{3}}\left(|n_1+1,n_2,m\rangle+|n_1-1,n_2+1,m\rangle+|n_1,n_2-1,m+1\rangle\right)\langle n_1,n_2,m|+h.c.\Big] \end{aligned} \tag{3.2}$$

As it is clear in the Hamiltonian (3.2), one can change the state of the counter without changing the energy and so all states $|\Phi(t)\rangle \otimes |m\rangle$ with different ms are degenerate. We consider the instantaneous ground-state of Hamiltonian (3.1), $|G(t)\rangle$, at time $t = 0$ and $t = T$ as the initial and final conditions for the state of the array, and since these to states must be equal we will refer to both of them with $|G(0)\rangle$.

In this work we will use the described quantum optimal control algorithm to drive the system from initial state $|\Psi_{ini}\rangle \equiv |G(0)\rangle \otimes |0\rangle$ to $|\Psi_{fin}\rangle \equiv |G(0)\rangle \otimes |1\rangle$, q_1 and q_2 are the control parameters. To prepare the system in the desired initial state $|G(0)\rangle \otimes |0\rangle$ it is necessary to decouple the array from the rest of the circuit and so to prevent tunneling through the array. Then gating starts while the array is coupled to electrodes very quickly in comparison with the duration time of the gating.

If the overall phase is zero the supercurrent vanishes and the expectation value of the counter operator $\hat{m} \equiv \sum_m m\ |m\rangle\langle m|$ represents the pumped charge Q_p in unit of $2e$. An important measure of accuracy of the pump is given by the deviation of the pumped charge from the quantized value

$$\mathcal{E} = \left| 1 - \frac{Q_p}{2e} \right|. \tag{3.3}$$

In addition since Cooper pair pumping is a coherent process, it is also interesting to test the accuracy of optimization protocol by measuring the departure of the final quantum state from the desired one. To this end we also study the fidelity at the end of time evolution,

$$\mathcal{F} = |(\langle 1| \otimes \langle G(0))|\Psi(T)\rangle|^2 \tag{3.4}$$

which measures the overlap between the final state of the array and the ground state $|G(0)\rangle$. In all plots we show the infidelity which is defined as $\mathcal{I} = 1 - \mathcal{F}$.

3.3 Numerical results

In this section we will present the numerical results based on the optimization procedure described in Chapter 2. The cost functional e_1, which is equivalent to $\mathcal{I}$, is chosen to be minimized in this work. We will show how it is possible to achieve fast and accurate Cooper pair pumping through an array of Josephson junctions by optimizing the gate voltages applied on Cooper pair boxes.

3.3.1 Optimized pumping

Motivated by the adiabatic case [51], as initial guess for control parameters, we choose the circular path (see section 1.3.2) in (q_1, q_2) plane, around the degeneracy point $q_1 = q_2 = \frac{1}{3}$ with radius q_0 (described by sinusoidal gate voltages $q_1 = \frac{1}{3} + q_0 \cos(2\pi t/T + \vartheta_0)$ and $q_2 = \frac{1}{3} + q_0 \sin(2\pi t/T + \vartheta_0)$). Charge states which we have considered for each box are $n = 0, \pm 1$, which means that nine lowest charge states of the whole system contribute to this process. Since the initial paths with radii greater than $\frac{1}{2}$ might involve more states we take $q_0 \leq \frac{1}{2}$. For each given radius optimal control algorithm modifies the path such that the infidelity $\mathcal{I}$ after one cycle reaches the value 0, and as we mentioned before the Q_p is the expectation value of the counter operator $\hat{m}$ at the end of the time evolution. Since the uncertainty of the pumped charge scales with E_J/E_C, one expects more accurate pumping when E_C is much big $E_C/E_J = 100$ with very short duration times, we will show only few examples of the results of this case. Instead we will focus on the more

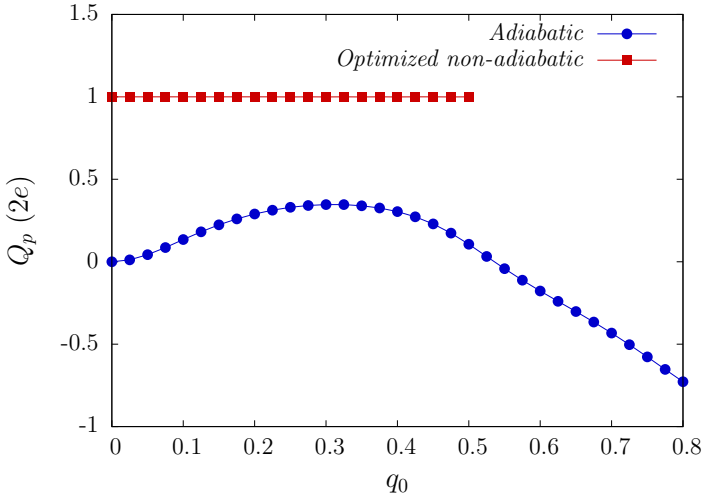

Figure 1: (Color on line) Pumped charge Q_p in one cycle as a function of radius of circular path q_0 in (q_1, q_2) plane, in both adiabatic and non-adiabatic regimes for $E_C/E_J = 10$. In adiabatic case results obtained from integration of instantaneous expectation value of current during the time evolution and the duration time of the cycle is $T = 200\pi \frac{\hbar}{E_J} = 20\pi \frac{\hbar E_C}{E_J^2}$. In non-adiabatic case results are the expectation value of the counter operator $\hat{m} \equiv \sum_m m|m\rangle\langle m|$ after using the quantum optimal control theory to modify the circular path with $T = 30\pi \frac{\hbar}{E_J} = 3\pi \frac{\hbar E_C}{E_J^2}$. In both cases $\varphi = 0$.

realistic case $E_C/E_J = 10$ which is the worst case in the adiabatic regime [51] and in which accuracy of the pumped charge is always less than 50%. For the case $E_C/E_J = 10$ we could achieve accurate pumping with $T = 30\pi \frac{\hbar}{E_J} = 3\pi \frac{\hbar E_C}{E_J^2}$.

In fig.1 we show the pumped charge Q_p as a function of radius of circular path q_0 for both adiabatic (blue circles) and optimized non-adiabatic (red squares) cases. Results for non-adiabatic case are obtained after 200 iterations and in both cases $\varphi = 0$. In the adiabatic case pumped charge is obtained by integrating the instantaneous expectation value of the current operator $I(t) = -\frac{2e}{\hbar}\frac{\partial H}{\partial \varphi}$ during the time evolution, we have chosen $T = 200\pi \frac{\hbar}{E_J} = 20\pi \frac{\hbar E_C}{E_J^2}$ to make sure that we are in adiabatic regime and results coincide with those in reference [51]. While in the adiabatic regime in the best case the pumped charge in units of $2e$ is less than 0.5, we have reached value 1 for all radii by using optimized gate voltages. Fig. 2 shows both the error $\mathcal{E}$ of pumped charge and the infidelity $\mathcal{I}$ as a function of the radius of initial circular path. Accurate pumped charge with high fidelity for final state of the array is clear in this figure. Both error and infidelity are always less than 10^{-4}. In both panels of fig.2 some results for $E_C/E_J = 100$ (triangles) are also shown, with error and infidelity less than 10^{-2}. The difference between the accuracy of these two cases is due to the stronger violation of adiabatic condition (1.78) in the case $E_C/E_J = 100$ compared to $E_C/E_J = 10$. Notice, moreover, that the optimization procedure allows us to directly control the fidelity but only indirectly the value of pumped charge so that the behavior of $\mathcal{I}$ and $\mathcal{E}$ as a function of q_0 are not expected to be equal.

3.3.2 Imperfection in the pulses shape

It is important to understand to which extent the pulses which optimize the pumping can be realized in experiments. Fig. 3 shows an example ($q_0 = 0.275$) of initial (red line) and optimized (blue dotted line)

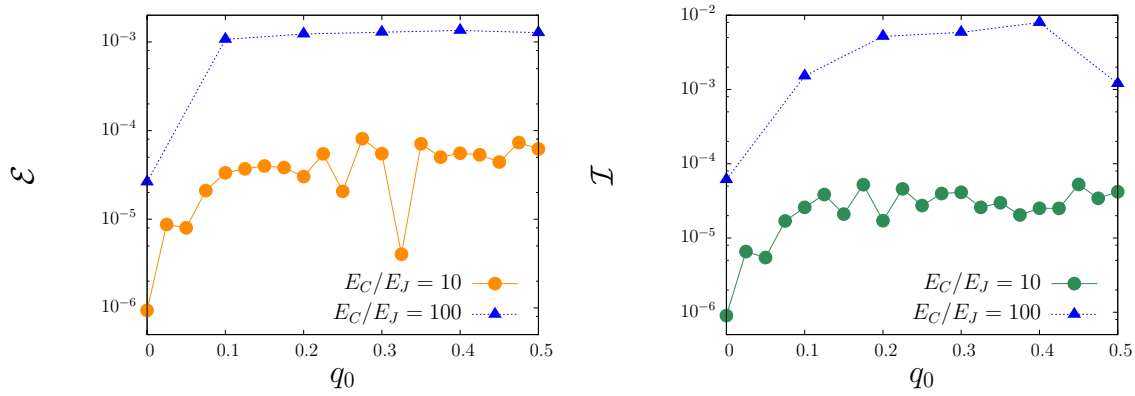

Figure 2: (Color on line) Left panel: Error in pumped charge $\mathcal{E}$ and Right panel: Infidelity $\mathcal{I}$ after one cycle as a function of radius of circular path q_0 in (q_1, q_2) plane, for $E_C/E_J = 10$ and 100. The vertical axis in both panels is in logarithmic scale. Results are obtained after using the quantum optimal control theory to modify the circular path. $T = 30\pi \frac{\hbar}{E_J}$ and $\varphi = 0$. The numerical error is at most of the order of 10^{-5}.

gate voltages q_1 (top panel) and q_2 (bottom panel) after 200 iterations. In the left panel of Fig. 4 we show the Fourier transform $q_1(\omega)$ of the optimized gate voltage $q_1(t)$ plotted in Fig. 3, while in the right panel the same curve is plotted on a smaller range of frequencies. Note that the largest contribution occurs for $\omega = \pm\frac{1}{15}\frac{E_J}{\hbar}$, which is the frequency of the initial sinusoidal gate voltages.

In a realistic situation, however, it is very difficult to imagine that all the details of the pulse, encoded in the high frequency components, can be reproduced faithfully. We accounted for imperfections in the pulse shape by introducing a bandwidth parametrized by a high frequency cutoff ω_{cutoff}. In Fig. 5 we show both the error and the infidelity as a function of the bandwidth for three different radii of initial circular path. No changes occur by decreasing ω_{cutoff} from 100 $\frac{E_J}{\hbar}$ until $\omega_{cutoff} \approx 15$ $\frac{E_J}{\hbar}$ is reached and at this point a dramatic increase in both error and infidelity occurs which demonstrates the importance of harmonics with frequencies close to this value. Another change in pumped charge and fidelity happens when $\omega_{cutoff} \approx 5$ $\frac{E_J}{\hbar}$ is reached. Therefore the most important harmonics for optimizing the gate voltages lie below $\omega = 20$ $\frac{E_J}{\hbar}$ and there is no need for higher frequencies in order to pump accurately.

3.3.3 Effect of noise

In this section we discuss the effect of external noise. Since Cooper pair pumping is a coherent process, the presence of an external environment may be disruptive. In general devices in which the dominant energy is the charging energy are sensitive to the effect of fluctuating background charges which produces $1/f$ noise. Therefore in Josephson nanocircuits in the charge regime the dominant mechanism of decoherence is $1/f$ noise (see e.g. Ref. [86]). It is important to know whether the pumped charge is stable while optimized gate voltages are affected by noise. Although its understanding is far from complete, $1/f$ noise is believed to originate from two-level fluctuators present in the substrate and/or in the insulation barrier. Several theoretical works have recently studied the effect of $1/f$ noise [87, 88, 89, 90, 91]. Following current approaches, we model the environment as a superposition of bistable classical fluctuators resulting in an additional random contribution $\delta q_k(t)$ to the gate charges $q_k(t)$ after optimization.

If γ represents the switching rate of fluctuators which lie in $[\gamma_{min} : \gamma_{max}]$ interval with a distribution

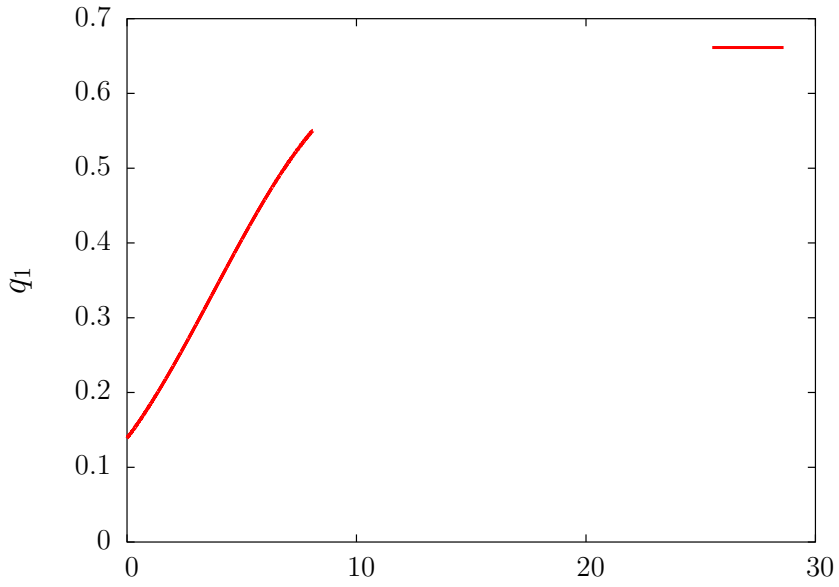
0.7
0.6
0.5
0.4
0.3
0.2
0.1
0
q_1
0
10
20
30

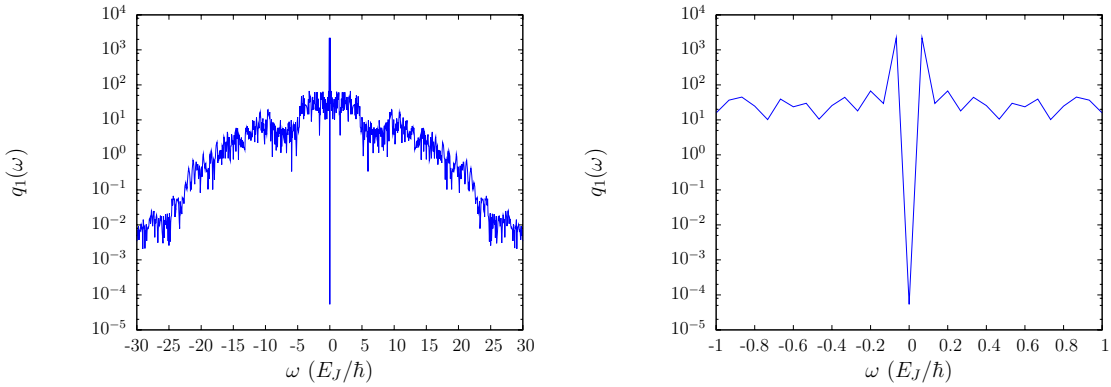

Figure 4: (Color on line) An example of Fourier transform of optimized gate voltage q_1 (blue dotted curve in the top panel of Fig.3). Left panel shows most important harmonics as a function of frequency and few first harmonics are shown in right panel. $q_0 = 0.275$, $T = 30\pi\ \frac{\hbar}{E_J}$, $E_C/E_J = 10$ and $\varphi = 0$.

function $P(\gamma) = c/\gamma$, where $c = \left(\ln \frac{\gamma_{max}}{\gamma_{min}}\right)^{-1}$, then sum over all these fluctuators results in a power spectrum of noise $\mathcal{S}_{q_k}(\omega) = \langle \delta q_k(t) \delta q_k(0) \rangle_\omega \approx \omega^{-1}$, if $\gamma_{min} \ll \omega \ll \gamma_{max}$. We chose the switching rates such that the $1/f$ part of the spectrum is centered around the typical frequency of the pump. Typically the $1/f$ region extends over two orders of magnitude in ω. We assume that fifty independent fluctuators are coupled weakly to the system and that the charge noise on the two separate gates are uncorrelated. Moreover we averaged the results over fifty different configurations of noise. In Fig. 6 we plot the error $\mathcal{E}$ (left panel) and infidelity $\mathcal{I}$ (right panel), as a function of q_0, for a strength of noise $\mathcal{A} = 10^{-5}$ ($\mathcal{S}(\omega) = \mathcal{A}/\omega$), which is a typical experimental value. Remarkably, the pumped charge is virtually unaffected by noise: for $E_C/E_J = 10$ the error in the pumped charge and infidelity are still less than 10^{-4}, which clearly shows the stability against noise. The case $E_C/E_J = 100$ is also stable. To complete the analysis, we plot in Fig. 7 the error in pumped charge (top panel) as well as the infidelity (bottom panel) as a function of $\mathcal{A}$ for a few different values of q_0 (note that both vertical and horizontal axes are in logarithmic scale). For all values of radius q_0 the accuracy of pumping and fidelity are larger than 90% even under the effect of noise with significant strength $\mathcal{A} = 10^{-3}$, which is a good improvement considering that the accuracy is less than fifty percent in adiabatic regime without noise. More importantly, both $\mathcal{E}$ and $\mathcal{I}$ are not increasing up to about $\mathcal{A} = 10^{-5}$.

3.3.4 Imperfections in the pump

Up to now we have assumed the ideal situation in which the parameters of the pump are known. In this section we address the effect of imperfections arising when such parameters are known only up to a given uncertainty from a uniform array. More precisely, we estimate how error in pumped charge and infidelity increase, as a function of the extent of the uncertainty, by evolving the system using the optimized pulse shapes calculated for the uniform array. To assess this issue we have implemented such an uncertainty on the parameters with two methods. In the first one we add to the nominal E_C and E_J, of a uniform array, a random fraction x taken in the range $[-x_0, x_0]$. In Fig. 8 we plot error and infidelity, averaged over 50 configurations as a function of x_0 for $E_C = 10E_J$, for $q_0 = 0.300$ and $q_0 = 0.475$. In the second method we perturb the uniform Hamiltonian by adding to it a weighted random matrix. In Fig. 9 we plot error and infidelity, as a function of the weight x_0 for $E_C = 10E_J$ and for two values of q_0. Both methods show that

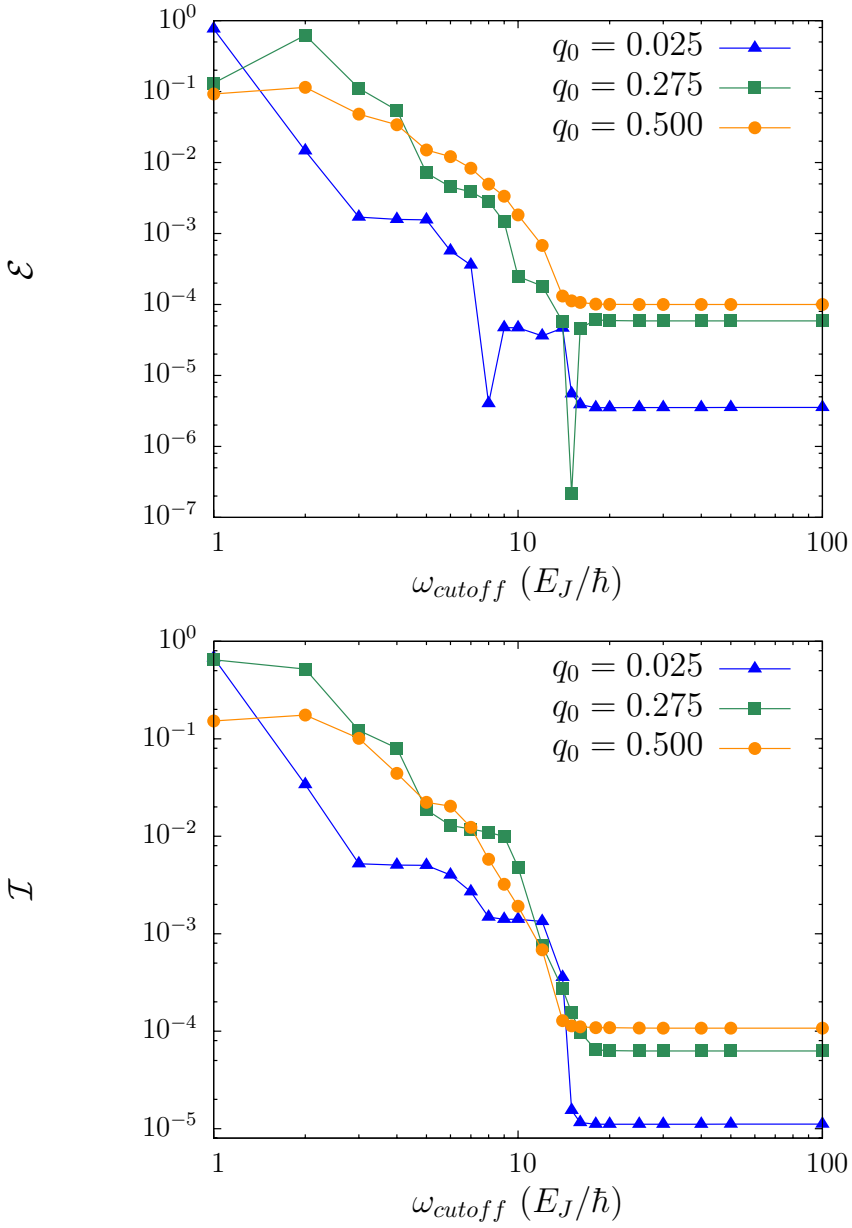

Figure 5: (Color on line) The error $\mathcal{E}$ of pumping one Cooper pair in each cycle (top panel) and the infidelity $\mathcal{I}$ of ending up to the ground state of the array at the end of cycle (bottom panel), in optimized non-adiabatic case, as a function of the cutoff frequency ω_{cutoff} of gate voltages. Different curves are related to different radii of circular path in (q_1, q_2) plane as the initial guess for control parameters in quantum optimal control theory. $E_C/E_J = 10$, $T = 30\pi\hbar/E_J$ and $\varphi = 0$. Numerical error is at most of the order of 10^{-5}.

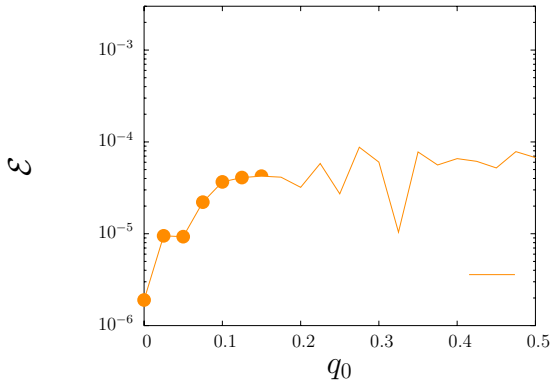

3

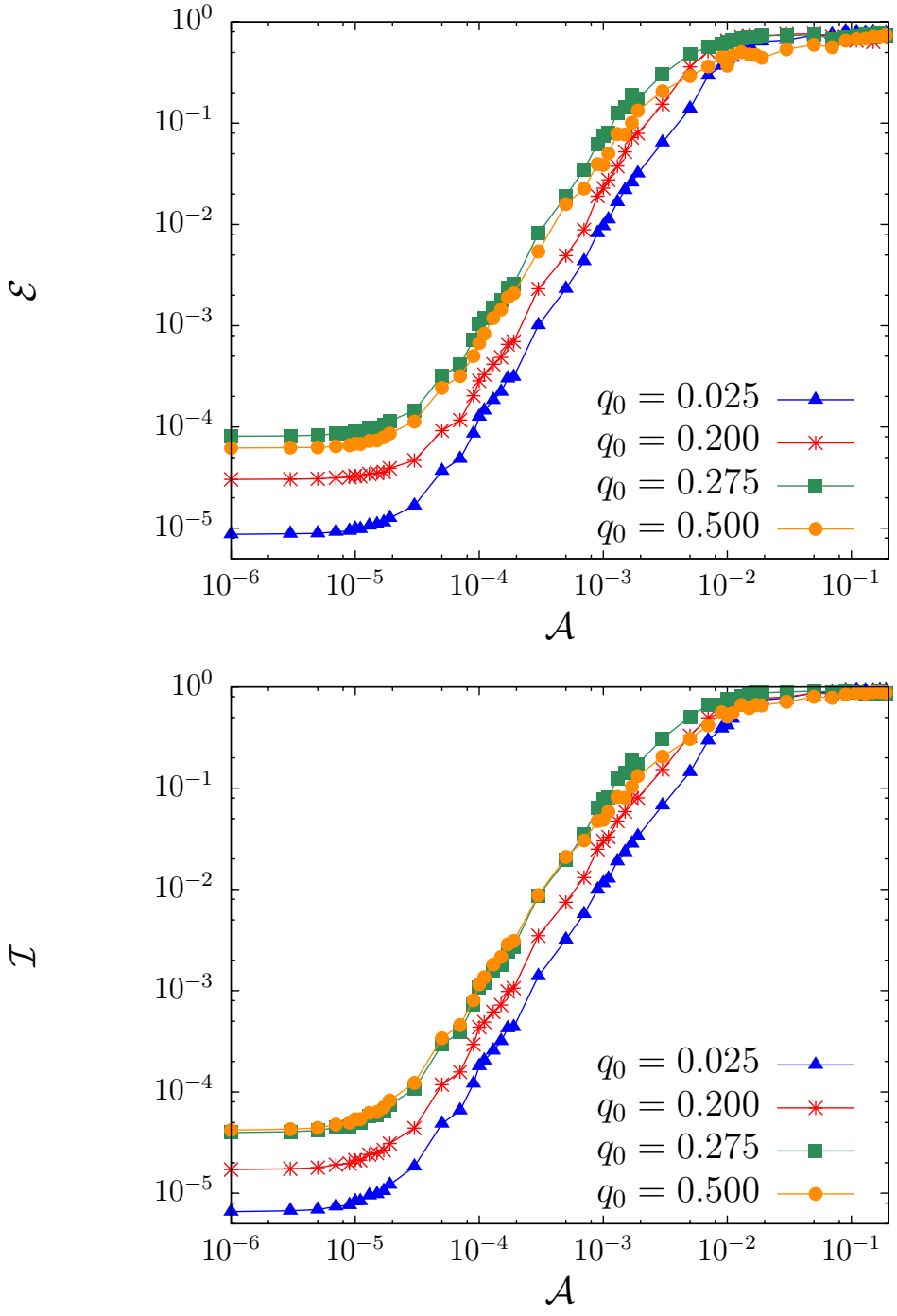

Figure 7: (Color on line) The error $\mathcal{E}$ in pumping one Cooper pair in each cycle (top panel) and the infidelity $\mathcal{I}$ of ending up to the ground state of the array at the end of cycle (bottom panel), in optimized non-adiabatic case, as a function of the strength of the $1/f$ noise $\mathcal{A}$ affecting gate voltages. Different curves are related to different radii of circular path in (q_1, q_2) plane as the initial guess for control parameters in quantum optimal control theory. $E_C/E_J = 10$, $T = 30\pi \frac{\hbar}{E_J}$ and $\varphi = 0$. Numerical error is at most of the order of 10^{-5}.

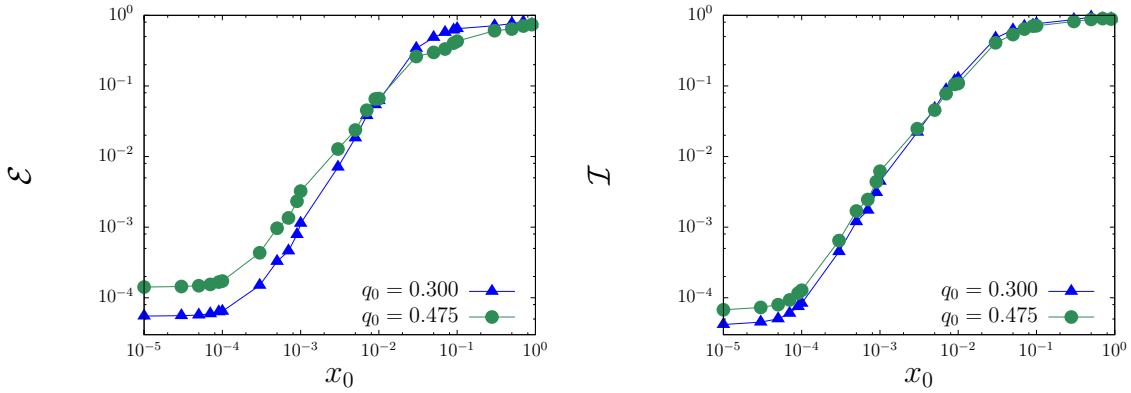

Figure 8: (Color on line) The error $\mathcal{E}$ (left panel) and the infidelity $\mathcal{I}$ (right panel), as a function of the random fraction x_0 added to the nominal E_C and E_J. Optimized pulses obtained for uniform array are used to calculate pumped charge and fidelity.$E_C/E_J = 10$, $T = 30\pi\ \frac{\hbar}{E_J}$ and $\varphi = 0$. Numerical error is at most of the order of 10^{-5}.

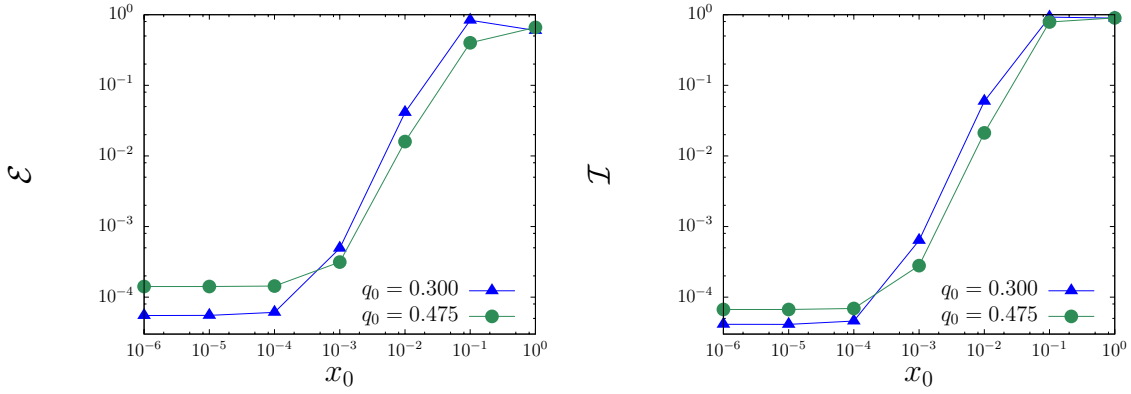

Figure 9: (Color on line) The error $\mathcal{E}$ (left panel) and the infidelity $\mathcal{I}$ (right panel), as a function of the weight x_0 of the random Hamiltonian added to the uniform Hamiltonian. Optimized pulses obtained from non-perturbed Hamiltonian are used to calculate pumped charge and fidelity. $E_C/E_J = 10$, $T = 30\pi\hbar/E_J$ and $\varphi = 0$. Numerical error is at most of the order of 10^{-5}.

Chapter 4

Optimized single-qubit gates for Josephson phase qubits

4.1 Introduction

Over the past decades, together with the development of the theory of quantum information [1] there has been an increasing effort to find those physical systems where quantum information processing could be implemented. Among the many different proposals, devices based on superconducting Josephson junctions are promising candidates in the solid state realm (see the reviews [2, 60, 61, 62]). As it was shown in Sec.1.3.3, Josephson qubits can be categorized into three main classes, charge, phase and flux qubits, depending on which dynamical variable is most well defined and consequently which basis states are used as computational states $|0\rangle$ and $|1\rangle$.

Phase qubits [92, 93, 94], subject of the present chapter, in their simplest configuration can be realized with a single current biased Josephson junction. For bias lower that the critical current, two lowest eigenstates of the system form the computational space. The application of a current pulse, with frequency which is in resonance with the transition frequency of the two logical states, typically in the microwave range allows to perform all the desired single bit operations. Recent experiments [95, 96] have realized both single-bit and two-bit gates in capacitive coupled phase qubits. In the experiments conducted so far, motivated by similar approach in NMR, the amplitude of the microwave current used to perform the qubit manipulation has a Gaussian shape [95, 97]. It turns out that Gaussian pulses perform better when their duration time is longer [97]. However, even for long pulses, the error of NOT-gate is always higher than 10^{-3}. The importance of achieving fast quantum gates with high fidelity raises the question whether there are modulations, other than Gaussian, which lead to higher fidelities even when the duration time of the pulse is short. Some theoretical work has already been done in this direction to examine the efficiency of different modulations [97, 98]. In the this work we follow a different approach and will show that by employing the quantum optimal control theory [7, 99, 100], we can further improve the (theoretical) bounds on the error of gate operations.

Quantum optimal control has been already applied to optimize quantum manipulation of Josephson nanocircuits in the charge limit [11, 12, 101, 13]. Here we want to test this method in the opposite regime of phase qubit (see also Ref. [14] and [15]) and see whether it is possible to find optimal modulations of microwave pulses, with different duration times, which give very good fidelity for single bit operations.

This chapter is organized as follows: in Sec. 4.2 we will describe the model for the single phase qubit

(Sec. 4.2.1) and the NOT quantum gate (Sec. 4.2.2), which has been chosen to be optimized for this work. In Sec. 4.2.3 the model of a two-interacting-qubit setup will be introduced. The numerical results for a phase qubit will be presented in Sec. 4.3. The achieved accuracy for desired operation, discussed in Sec. 4.3.1, is further tested against possible imperfections in the pulses shape (Sec. 4.3.2), presence of off-resonance elements in the Hamiltonian (Sec. 4.3.3) and possible presence of the inter-qubit capacitive interaction in multi-qubit systems (Sec. 4.3.4). The specific question of the leakage out of the qubit manifold is addressed in Sec. 4.3.5, where the numerical results obtained for a junction with five levels inside its potential are provided. A summary of the results obtained and possible perspectives of this work will be presented in the concluding remarks in Sec. 4.4.

4.2 Model

In this section, in addition to the detailed explanation of the Hamiltonians of a single-qubit and two-qubit setup, the single-qubit NOT-gate will also be introduced. In this chapter, for the sake of definitness, the symbol δ will be used to refer to the superconducting phase and φ represents another variable.

4.2.1 Single-qubit Hamiltonian

As it has been explained in Sec. 1.3.3, a phase qubit in its simplest form can be realized by a single Josephson junction biased with a dc current (Fig. 1). The Hamiltonian of this system is given by equation (1.88), where the resistive branch is neglected. Although the two lowest energy levels $|0\rangle$ and $|1\rangle$ can be used as computational states, the physical system may contain more states in each well (Fig. 1(b)). Since the level-spacing in such a system is inhomogeneous, a microwave current with frequency $\omega = \omega_{01} = (E_1 - E_0)/\hbar$ is used to make transition between these two levels.

To be effectively used as a two-level quantum system, the junction is biased with a dc current slightly smaller than the critical current $I_{dc} \lesssim I_c$. In this regime the potential energy of the system can be approximated by a cubic potential and the Hamiltonian (1.88) becomes:

$$H_{dc} \approx -E_C \frac{\partial^2}{\partial \delta^2} - \frac{\Phi_0}{2\pi}(I_c - I_{dc})(\delta - \frac{\pi}{2}) - \frac{I_c \Phi_0}{12\pi}(\delta - \frac{\pi}{2})^3. \tag{4.1}$$

It is a good approximation to use the eigenstates and eigenvalues of (4.1) instead of (1.88).

The microwave current $I_{\mu w} = I(t)\cos(\omega t + \varphi)$ is taken to account by adding the linear term $H_{\mu w} = \frac{\Phi_0}{2\pi} I_{\mu w} \delta$ to the Hamiltonian (4.1). Since the eigenstates of the junction biased with a dc current are used as computational states, it is appropriate to write the full Hamiltonian $H = H_{dc} + H_{\mu w}$ in this basis. Assuming that there are three levels inside the potential well, the Hamiltonian H takes the following form:

$$\begin{aligned} H &= \begin{pmatrix} E_0 & 0 & 0 \\ 0 & E_1 & 0 \\ 0 & 0 & E_2 \end{pmatrix} \\ &+ 2g(t)\cos(\omega t + \varphi) \begin{pmatrix} \Delta_{00} & \Delta_{01} & \Delta_{02} \\ \Delta_{10} & \Delta_{11} & \Delta_{12} \\ \Delta_{20} & \Delta_{21} & \Delta_{22} \end{pmatrix}, \end{aligned} \tag{4.2}$$

by introducing $g(t) = I(t)\sqrt{\hbar/2C\omega_{01}}$ and $\Delta_{mn} = \frac{1}{2}\sqrt{\hbar\omega_{01}}\langle m|\delta|n\rangle$ where $\{E_m\}$ and $\{|m\rangle\}$ are eigenenergies and eigenstates of the Hamiltonian (4.1). Moving to the rotating frame, in which the fast oscillations due

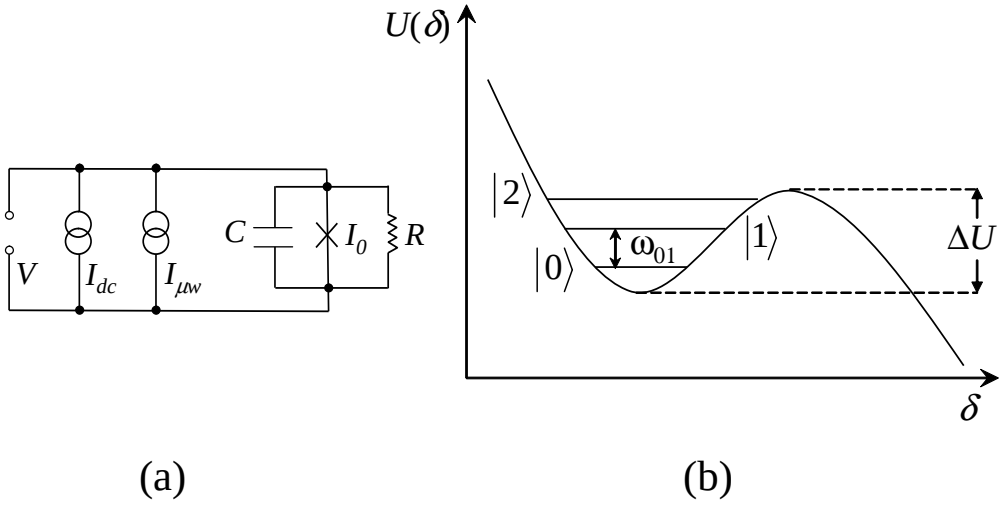

Figure 1: (a) Schematic drawing of a single-junction phase qubit with capacitance C, resistance R and critical current I_c which is biased by a dc current I_{dc}. A microwave pulse $I_{\mu w} = I(t)\cos(\omega t + \varphi)$, with frequency $\omega = \omega_{01}$, is applied to make transition between two lowest energy levels of the system $|0\rangle$ and $|1\rangle$. (b) By neglecting the resistive branch, the potential energy of the system U, as a function of the Josephson phase across the junction δ, has the form of a tilted washboard potential. This potential is defined by the height of the well ΔU and the frequency of the classical oscillations in the bottom of the well ω_p.

to $\cos(\omega t + \varphi)$ do not appear, the Hamiltonian $\tilde{H}$ in the rotating frame is related to the Hamiltonian in laboratory frame H via

$$\tilde{H} = VHV^{\dagger} - i\hbar V\frac{\partial}{\partial t}V^{\dagger} \tag{4.3}$$

where

$$V = \begin{pmatrix} 1 & 0 & 0 \\ 0 & e^{i\omega t} & 0 \\ 0 & 0 & e^{2i\omega t} \end{pmatrix}. \tag{4.4}$$

and the state of the system $|\tilde{\Psi}\rangle$ is related to the state in the laboratory frame $|\Psi\rangle$ by $|\tilde{\Psi}\rangle = V|\Psi\rangle$. In this frame the Hamiltonian (4.2) takes the following form

$$\tilde{H} \approx \begin{pmatrix} E_0 & g(t)\Delta_{01}e^{i\varphi} & 0 \\ g(t)\Delta_{10}e^{-i\varphi} & E_1 - \hbar\omega & g(t)\Delta_{12}e^{i\varphi} \\ 0 & g(t)\Delta_{21}e^{-i\varphi} & E_2 - 2\hbar\omega \end{pmatrix}, \tag{4.5}$$

where we have assumed that off-resonance terms have negligible effect and therefore we can ignore them in this step. Setting $E_0 = 0,\ \omega = \omega_{01}$ and introducing $\delta\omega \equiv \omega_{01} - \omega_{12}$ leads to

$$\tilde{H} \approx \begin{pmatrix} 0 & g(t)\Delta_{01}e^{i\varphi} & 0 \\ g(t)\Delta_{10}e^{-i\varphi} & 0 & g(t)\Delta_{12}e^{i\varphi} \\ 0 & g(t)\Delta_{21}e^{-i\varphi} & -\hbar\delta\omega \end{pmatrix}. \tag{4.6}$$

Therefore, if the elements of superconducting phase Δ_{ij} are known, by a proper choice of φ and microwave current modulation $g(t)$ it is possible to apply a certain operation on the computational states $|0\rangle$ and $|1\rangle$ in xy plane of the Bloch sphere.

To obtain the eigenvalues $\{E_m\}$ and eigenstates $\{|m\rangle\}$ of the Hamiltonian (4.1) we use perturbation theory while a harmonic oscillator with the same plasma frequency ω_p is considered as the unperturbed system. To the second order, perturbation theory leads to

$$\begin{aligned} \omega_{01} &\approx \left(1 - \frac{5}{36}\frac{\hbar\omega_p}{\Delta U}\right)\omega_p \\ \omega_{12} &\approx \left(1 - \frac{10}{36}\frac{\hbar\omega_p}{\Delta U}\right)\omega_p. \end{aligned} \tag{4.7}$$

4.2.2 Single-qubit gate

As one can see from the 2×2 top-left block of the Hamiltonian (4.6), the initial phase of the microwave pulse φ defines the axis of rotation, in xy-plane of the Bloch sphere, for a given state, while the pulse amplitude and duration time define the angle of rotation. For example, by setting $\varphi = 0$ ($\varphi = \pi/2$) such block is proportional to the Pauli matrix σ_x (σ_y), *i. e.* a rotation around the $x(y)$-axis. In a recent experiment [96] a π rotation around x has been implemented as a part of a sequence of operations to create entanglement between two phase qubits. This motivates us to set $\varphi = 0$ and focus this work on the single-qubit NOT-gate operation consisting of a π rotation around the x-axis.

In the typical experiment a shaped pulse with the following Gaussian modulation [97]

$$g(t) = \frac{a}{t_g}\, e^{-\frac{(t-\alpha t_g)^2}{2t_g^2}} \tag{4.8}$$

is used to induce flips between states $|0\rangle$ and $|1\rangle$. Here a, t_g and $T = 2\alpha t_g$ are, respectively, the amplitude, characteristic width and total width of the pulse, α being the cut-off of the pulse in time. The actual result of the operation can be quantified by the fidelity $|\langle\psi(T)|\psi_{fin}\rangle|^2$, where $|\psi_{fin}\rangle$ is the desired final state and $|\psi(T)\rangle$ is the state achieved at the end of time evolution starting from initial state $|\psi(t=0)\rangle = |\psi_{ini}\rangle$.

For a π rotation and with a typical cut-off value ($3 \le \alpha \le 5$) the amplitude $a \approx \sqrt{\pi/2}$ yields a pretty high fidelity of rotation. More precisely, Fig. 2 shows the error $1 - |\langle\psi(T)|\psi_{fin}\rangle|^2$ for a NOT-gate operation on an arbitrary superposition $|\psi_{ini}\rangle = b|0\rangle + c|1\rangle$, which would result in the state $|\psi_{fin}\rangle = b|1\rangle + c|0\rangle$, using a Gaussian pulse with cut-off $\alpha = 3$, amplitude $a = 1.25$ and duration time T. The leakage outside the qubit manifold, defined as $|\langle\psi(T)|2\rangle|^2$, is also shown in Fig. 3. It is worthwhile noting that although the leakage, for long enough pulses, can be of the order of 10^{-7}, the error in the NOT-gate operation is always higher than 10^{-3} [103].

In this work we use quantum optimal control theory in order to obtain microwave current modulations which give rise to a high-fidelity NOT-gate operation for a phase qubit. As it has been explained in chapter 2, quantum optimal control algorithms are designed to lead a quantum system with state $|\psi(t)\rangle$ from an initial state $|\psi(0)\rangle = |\psi_{ini}\rangle$ to a target final state $|\psi_{fin}\rangle$ at time T by minimizing a cost functional which is a measure of inaccuracy of reaching the desired final state. In order to implement the optimization of a NOT-gate for any arbitrary superposition of computational states, one must be able to flip $|0\rangle$ and $|1\rangle$ at the same time (*i. e.* with same pulse) making sure that the phase relation between them is preserved. This is

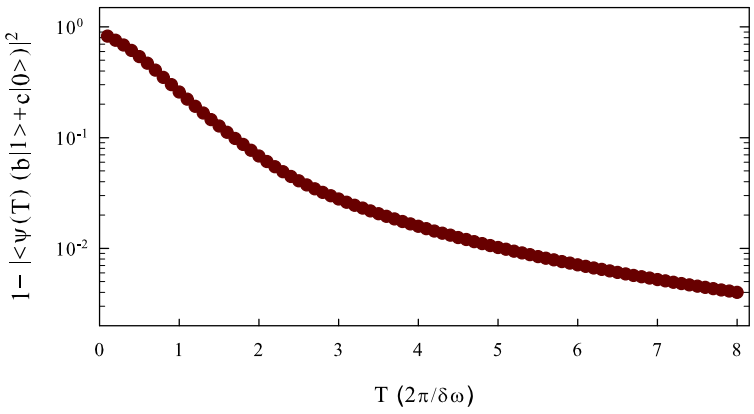

Figure 2: (Color on line) The error of a NOT-gate operation on an arbitrary superposition $b|0\rangle + c|1\rangle$, after applying a Gaussian pulse with amplitude $a = 1.25$ and cut-off $\alpha = 3$, as a function of the duration time T. $b|1\rangle + c|0\rangle$ is the expected final state and $\psi(T)$ is the final state achieved after applying the Gaussian pulse.

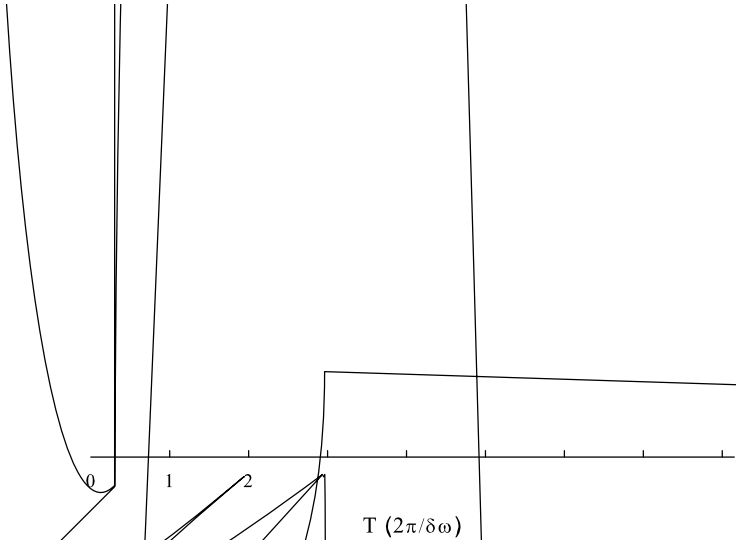

Fi e o t |

guaranteed by using the following definition of fidelity

$$\mathcal{F} \equiv \left| \frac{\langle \psi_0(T)|1\rangle + \langle \psi_1(T)|0\rangle}{2} \right|^2, \tag{4.9}$$

where $|\psi_0(T)\rangle$ and $|\psi_1(T)\rangle$ are final states achieved at time T after applying the same pulse on initial states $|0\rangle$ and $|1\rangle$. The minimization of the cost functional e_1 (see Chapter 2), for flipping at the same time the states $|0\rangle$ and $|1\rangle$, does not necessarily lead to maximization of the fidelity (4.9) due to possible changes in the phase relation between them. However if e_2 is minimized, the maximal fidelity is also guaranteed. Therefore in order to obtain a high-fidelity NOT-gate it seems more natural to minimize e_2 instead of e_1. However, in the following we will show that, although in the ideal case optimized pulses obtained from minimizing e_2 result in much higher fidelity, when more realistic cases are considered optimized pulses from minimizing e_1 lead to higher fidelities, specially for very short pulses. In this work we often use the error $\mathcal{E} = 1 - \mathcal{F}$ instead of fidelity.

4.2.3 Two-qubit Hamiltonian

Since in Sec. 4.3.4 the effect of the presence of a second qubit, which is capacitively coupled to the initial one, will be tested, here we derive the Hamiltonian of a two-interacting-qubit setup. The interaction capacitor, with capacitance C_x, leads to an additional term L_{int} in the Lagrangian of two non-interacting qubits which has the following form

$$L_{int} = \frac{1}{2} C_x V_x^2 = \frac{1}{2} C_x \left(\frac{\hbar}{2e}\right)^2 \left(\dot{\delta}_1 - \dot{\delta}_2\right)^2. \tag{4.10}$$

Here $V_x = \frac{\hbar}{2e}(\dot{\delta}_1 - \dot{\delta}_2)$ is the voltage drop across the capacitor and δ_1 and δ_2 are the Josephson phases across the junction 1 and 2. Therefore the interaction Hamiltonian H_{int} of a circuit with two identical phase qubits, which are coupled via a capacitor, has the following form:

$$\begin{aligned} H_{int} &= \frac{\partial L_{int}}{\partial \dot{\delta}_1}\dot{\delta}_1 + \frac{\partial L_{int}}{\partial \dot{\delta}_2}\dot{\delta}_2 - L_{int} \\ &= -\frac{E_C^2}{E_{C_x}} \left[\left(\frac{\partial^2}{\partial \delta_1^2} + \frac{\partial^2}{\partial \delta_2^2} \right) + 2 \left(i\frac{\partial}{\partial \delta_1} \otimes i\frac{\partial}{\partial \delta_2} \right) \right], \end{aligned} \tag{4.11}$$

where we have used the equation (1.48). Note that the term with second derivative in (4.11) can be included in the Hamiltonians of uncoupled qubits (4.1) by replacing the charging energy E_C with an effective one $E_{C_{eff}} = (2e)^2/(2C_{eff})$, where $C_{eff} \equiv C^2/C_\Sigma$ and $C_\Sigma = C + C_x$. Let $\{E_m\}$ and $\{|m>\}$ be the eigenenergies and eigenstates of the Hamiltonian (4.1) with $E_{C_{eff}}$. Therefore the total Hamiltonian of the system, when the microwave pulse is applied only to the first qubit, becomes

$$\begin{aligned} H &= \begin{pmatrix} E_0 & 0 & 0 \\ 0 & E_1 & 0 \\ 0 & 0 & E_2 \end{pmatrix} \otimes \mathbb{1} + \mathbb{1} \otimes \begin{pmatrix} E_0 & 0 & 0 \\ 0 & E_1 & 0 \\ 0 & 0 & E_2 \end{pmatrix} - \frac{C_x}{C_\Sigma}(\hbar\omega_{01}) \begin{pmatrix} \gamma_{00} & \gamma_{01} & \gamma_{02} \\ \gamma_{10} & \gamma_{11} & \gamma_{12} \\ \gamma_{20} & \gamma_{21} & \gamma_{22} \end{pmatrix} \otimes \begin{pmatrix} \gamma_{00} & \gamma_{01} & \gamma_{02} \\ \gamma_{10} & \gamma_{11} & \gamma_{12} \\ \gamma_{20} & \gamma_{21} & \gamma_{22} \end{pmatrix} \\ &+ 2g(t)\cos(\omega t + \varphi) \begin{pmatrix} \Delta_{00} & \Delta_{01} & \Delta_{02} \\ \Delta_{10} & \Delta_{11} & \Delta_{12} \\ \Delta_{20} & \Delta_{21} & \Delta_{22} \end{pmatrix} \otimes \mathbb{1} \end{aligned} \tag{4.12}$$

where $g(t) = I(t)\sqrt{\hbar/2C_{eff}\omega_{01}}$, $\Delta_{mn} = \frac{1}{2}\sqrt{\hbar\omega_{01}}\langle m|\hat{\delta}|n\rangle$ and $\gamma_{mn} = \sqrt{2E_{C_{eff}}/\hbar\omega_{01}}\langle m|i\frac{\partial}{\partial\delta}|n\rangle$. The proper rotating frame for this system is described by the operator

$$V = \begin{pmatrix} 1 & 0 & 0 \\ 0 & e^{i\omega t} & 0 \\ 0 & 0 & e^{2i\omega t} \end{pmatrix} \otimes \begin{pmatrix} 1 & 0 & 0 \\ 0 & e^{i\omega t} & 0 \\ 0 & 0 & e^{2i\omega t} \end{pmatrix}. \tag{4.13}$$

4.3 Numerical results

In this section we present the numerical results to show that the quantum optimal control theory allows to optimize the modulation of microwave pulses in order to implement a high-fidelity NOT-gate. The optimization is done in the rotating frame and the Hamiltonian (4.6) is used for time evolution while Δ_{ij} are calculated by means of perturbation theory.

4.3.1 Optimal NOT-gate

By employing the quantum optimal control algorithm described in the section 4.2.2 and using the modulation of the microwave pulse $g(t)$ as the control parameter, we start from Gaussian pulses (4.8) of given duration time T as the initial guess and optimize the two transitions $|0\rangle \rightarrow |1\rangle$ and $|1\rangle \rightarrow |0\rangle$ at the same time. We remind that the fidelity of NOT-gate is defined in equation (4.9) and $\mathcal{E} = 1 - \mathcal{F}$. We will show the results obtained from minimizing both e_1 and e_2 and refer to corresponding errors by $\mathcal{E}_1$ and $\mathcal{E}_2$ and corresponding optimized pulses by g_1 and g_2. The optimization has been stopped when either the cost functional reached the value 10^{-12} or 5000 iterations are done.

Figure 4 shows the error $\mathcal{E}$, as a function of duration time of the pulse T, for the Gaussian pulses used as initial guess (circles) and for the optimized pulses (unfilled triangles and squares). For most of points, the convergence is reached in much less than 5000 iterations. However for pulses with $T < 2\ \frac{2\pi}{\delta\omega}$, 5000 iterations has been completed. As we expected, minimizing e_2 results in high fidelity NOT-gate with $\mathcal{E} \approx 10^{-12}$ for all $T > 2\ \frac{2\pi}{\delta\omega} \approx 4$ ns, while for very short pulses it seems that, with same number of iterations, minimizing e_1 leads to better results.

In order to understand the reason for the oscillating behavior of $\mathcal{E}_1$ as a function of T, we plot the average value of e_1 for $|0\rangle \rightarrow |1\rangle$ and $|1\rangle \rightarrow |0\rangle$ transitions at the end of optimization (top panel of Fig. 5) which shows that the final value of e_1 for both of these transitions is of the order of 10^{-12}. As we explained in Sec.4.2.2, e_1 is insensitive to the phase of the final state and it turns out that while a given optimized pulse applied to initial state $|0\rangle$ leads to the final state $e^{i\theta_0}|1\rangle$, then the same pulse might transform the initial state $|1\rangle$ into $e^{i\theta_1}|0\rangle$, *i. e.* there is a phase difference between the two final states $\theta_{diff} \equiv \theta_1 - \theta_0$. The bottom panel of Fig. 5 shows this phase difference for optimized pulses with given duration time T which increases the error of NOT-gate $\mathcal{E}_1$ to what has been shown in Fig. 4.

Although this phase difference causes a major increase in the error while working with superpositions, the error $\mathcal{E}_1$ is at least one order of magnitude smaller than those from Gaussian pulses (Fig. 4). Moreover the final phase difference between $|0\rangle$ and $|1\rangle$ can be compensated by a following phase shift gate. In Fig. 4 results after applying a 0.01π (which is approximately the average of θ_{diff} in time) phase shift are also shown (filled triangles) which demonstrate a significant decrease of $\mathcal{E}_1$.

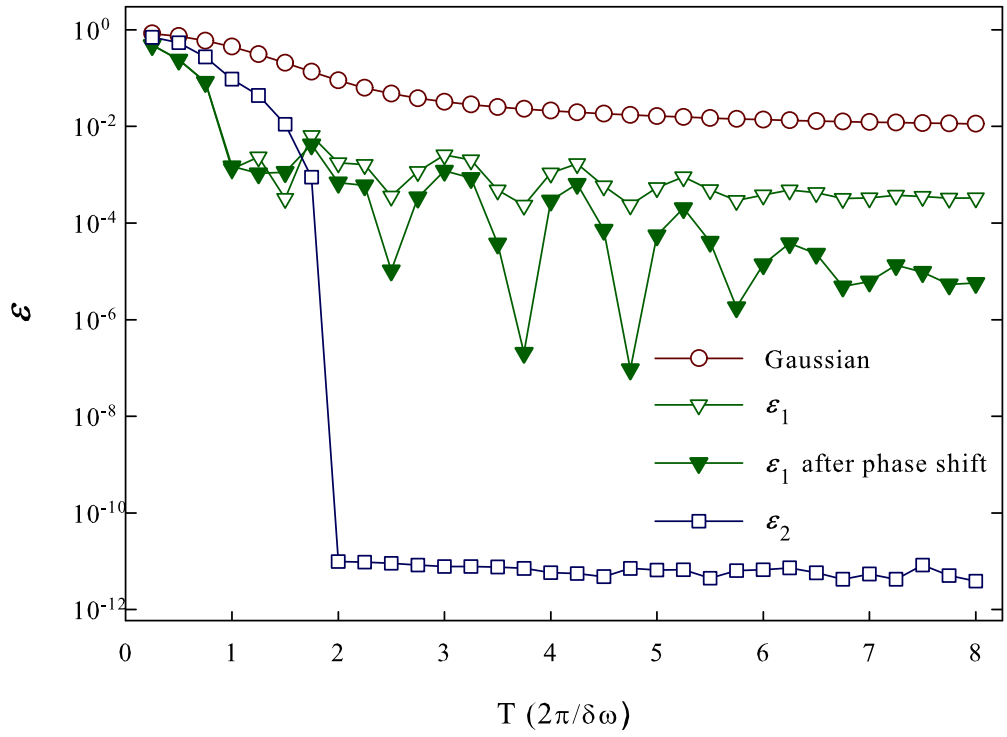

Figure 4: (Color on line) Error for a NOT-gate operation applied to any arbitrary superposition of states $|0\rangle$ and $|1\rangle$ made by pulses with Gaussian modulation (circles) and optimized modulation obtained from minimizing e_1 (unfilled triangles) and e_2 (squares) in a three-level system. Gaussian pulses have amplitude $a = 1.25$ and cut-off in time $\alpha = 3$. Optimized pulses are obtained after at most 5000 iterations and using Gaussian pulses as initial guess. Filled triangles are obtained by applying a 0.01π phase shift after optimized pulses obtained from minimizing e_1.

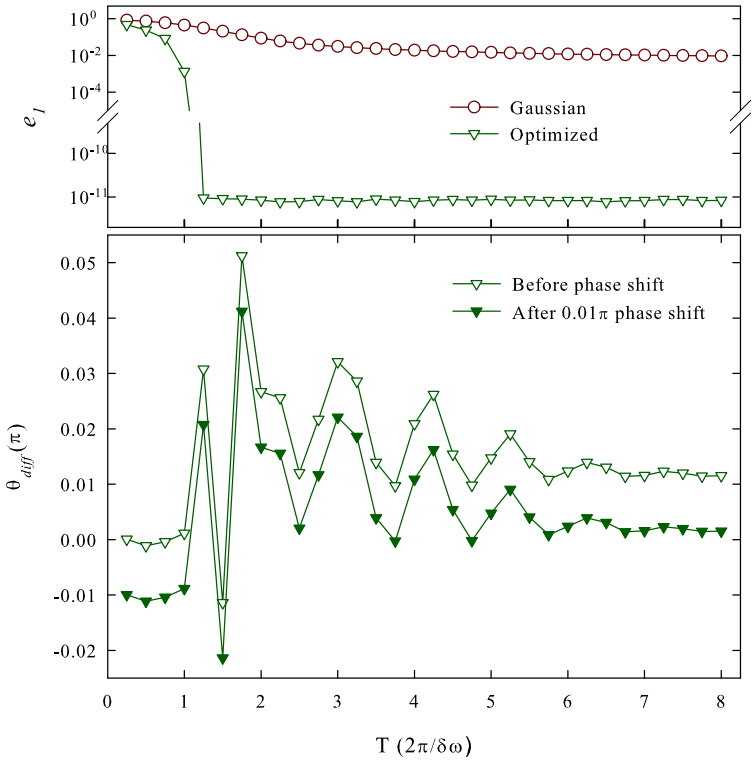

Figure 5: (Color on line) Top panel: the averaged value of e_1 for $|0\rangle \leftrightarrow |1\rangle$ transitions after applying pulses with Gaussian modulation (circles) and optimized modulation (triangles). Optimized pulses are obtained by minimizing e_1. Vertical axis is in logarithmic scale and T is the total width of the pulse. Bottom panel: the phase difference between final $|0\rangle$ and $|1\rangle$ states (after applying the optimized pulses) in units of π. This final phase difference increases the error of NOT-gate $\mathcal{E}_1$ to what has been shown in Fig. 4. In principle a proper phase shift gate can compensate this phase difference and decrease the error to 10^{-12}.

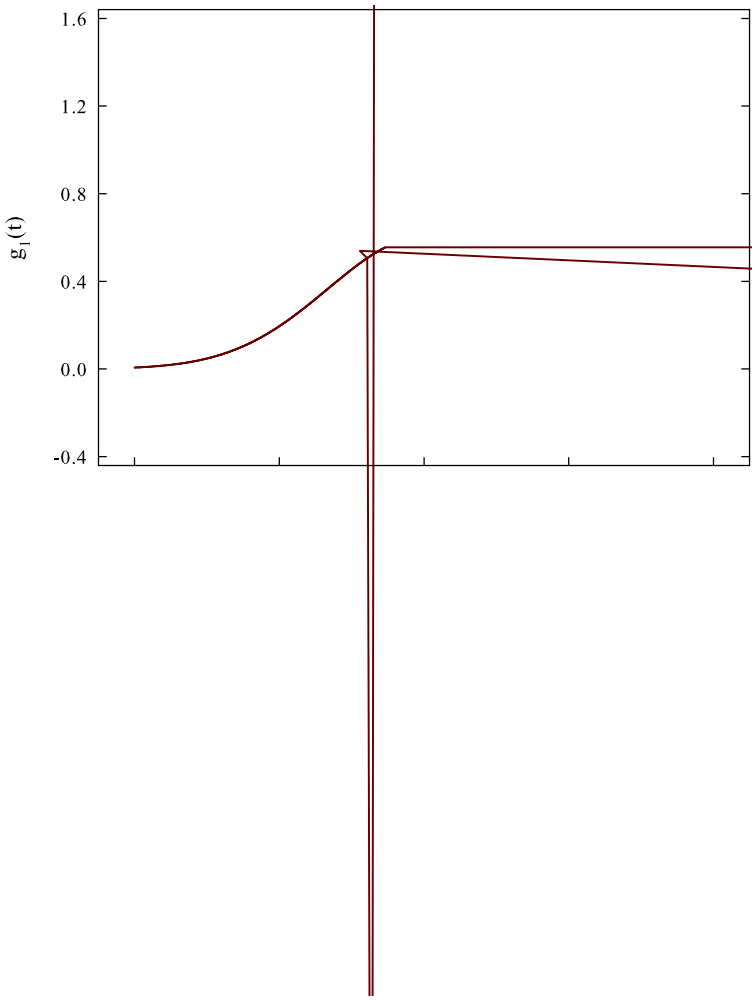
1.6
1.2
0.8
0.4
0.0
-0.4
g1(t)

4.3.2 Imperfections in the pulse shapes

In this section we study the Fourier transform of the optimized pulses, in order to see how practically they are realizable in the laboratory, and to examine the effect of high-frequency components. Two examples of the final optimized pulses (dashed lines) are shown in Fig. 6, both with duration time $T = 2\ \frac{2\pi}{\delta\omega} \approx 4$ ns. Optimized g_1 (top panel) and g_2 (bottom panel) are the results of minimizing, respectively, e_1 and e_2 which for $T = 2\ \frac{2\pi}{\delta\omega}$ both are of the order of 10^{-12}. The corresponding Gaussian pulse is also shown in both panels. g_1 is guaranteed to decrease the error of NOT-gate two orders of magnitude with respect to the Gaussian pulse while g_2 would reduce the error up to ten orders of magnitude.

Fig. 7 shows the Fourier transform of the two optimized pulses shown in Fig. 6. To filter out the high-frequency components of the optimized pulses we set a cut-off frequency ω_{cut} for Fourier components and apply the truncated pulse again and obtain the error. Fig. 8 shows the error for a NOT-gate for pulses with different duration times as functions of ω_{cut}. $\omega_{01}/2\pi$ is approximately 5 GHz and $\delta\omega$ is typically 10% of ω_{01}. In our calculation $\delta\omega = 0.1\ \omega_{01}$ which means that $\delta\omega/2\pi \approx$ 500 MHz.

In the case of $\mathcal{E}_1$, top panel of figure 8 makes clear that all important harmonics have frequencies smaller than $5\delta\omega$. Note that the number of harmonics included within the cutoff is equal to $T\omega_{cut}/2\pi$ so that, for $T = N\ \frac{2\pi}{\delta\omega}$, such number is equal to $N\ \frac{\omega_{cut}}{\delta\omega}$. As a result it seems that, for all values of T considered, about 20 harmonics should be sufficient to reach the smallest value of $\mathcal{E}_1$. $\mathcal{E}_2$, though, seems to be more sensitive to high-frequency components but still about four orders of magnitude smaller than $\mathcal{E}_1$ under the cutoff $\omega_{cut} = 10\delta\omega$.

4.3.3 Effect of off-resonance terms

As we mentioned before, we have assumed that off-resonance elements of the Hamiltonian (4.2) in the rotating frame are negligible and we have used Hamiltonian (4.6) for calculating the evolution. In this section we check this assumption by addressing the effect of off-resonance elements by evolving the complete Hamiltonian (4.2) using the optimized pulses obtained using Hamiltonian (4.6). Top panel of Fig. 9 shows the error for a NOT-gate operation implemented by Gaussian (circles) and optimized pulses from minimizing e_1 (triangles) and e_2 (squares). For $T > 2\ \frac{2\pi}{\delta\omega}$ the optimized pulses yield a much higher error, with respect to the case when off-resonance terms are neglected, still showing an improvement of two orders of magnitude if compared to Gaussian pulses. Bottom panel of Fig. 9 shows the absolute value of the error difference $\delta\mathcal{E}$ obtained by subtracting the error of the ideal case from the error with off-resonance terms. These figures makes clear that while for Gaussian pulses off-resonance terms can be neglected, for optimized pulses, specially those obtained from minimizing e_2, they are very important. Note that, contrary to the ideal case where $\mathcal{E}_2$ was about eight orders of magnitude smaller than $\mathcal{E}_1$, under the effect of off-resonance terms, $\mathcal{E}_2$ seems to be larger than $\mathcal{E}_1$ specially for very short puses with $T < 2\ \frac{2\pi}{\delta\omega}$. This means that the assumption of ignoring these terms is more accurate when e_1 is minimized. The simpler shape of the optimized pulses obtained from minimization of e_1 could be a reason for that.

4.3.4 Effect of capacitive interaction

So far we have considered a single qubit with three energy levels and obtained the modulation of the microwave pulses in order to optimize the NOT-gate operation for the two lowest energy states $|0\rangle$ and $|1\rangle$. It is now interesting to consider the setup [96] containing two qubits interacting via a capacitor. The question that we want to address is what happens if these optimized pulses are applied on the first qubit while the

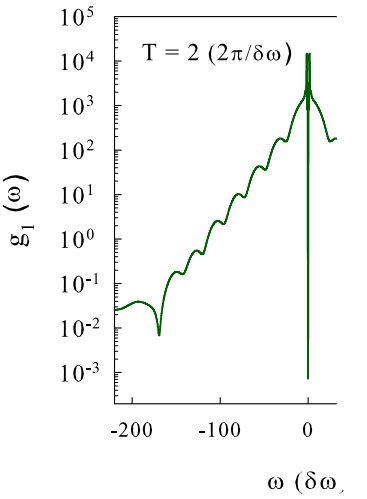
T = 2 (2π/δω)
g1 (ω)
ω (δω)

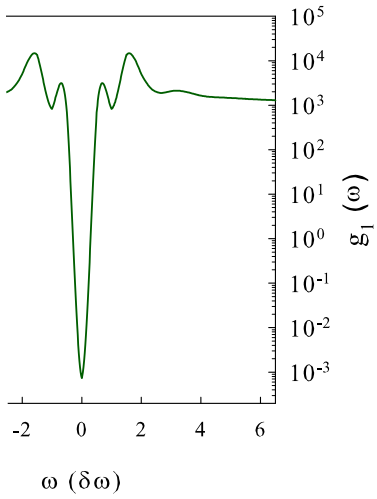
g1 (ω)
ω (δω)

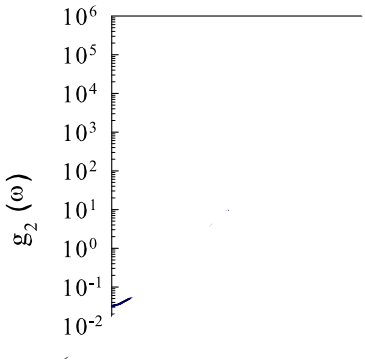
g2 (ω)

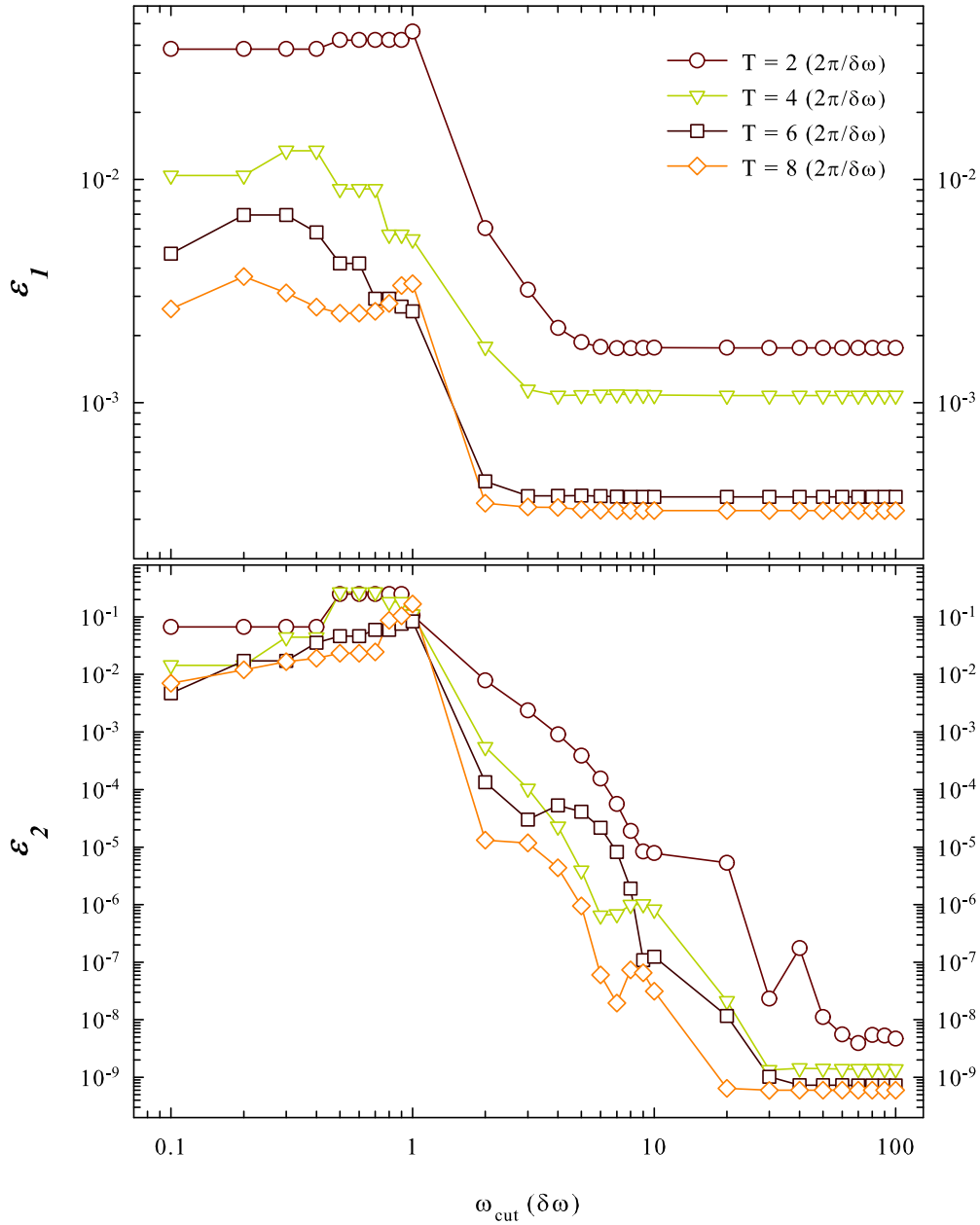

Figure 8: (Color on line) Error $\mathcal{E}$ for a NOT-gate with optimized pulses obtained by minimizing e_1 (top panel) and e_2 (bottom panel) as a function of the cutoff frequency ω_{cut}. Integer values of $T\omega_{cut}/2\pi$ correspond to the number of Fourier components included. $\delta\omega/2\pi$ is approximately 500 MHz.

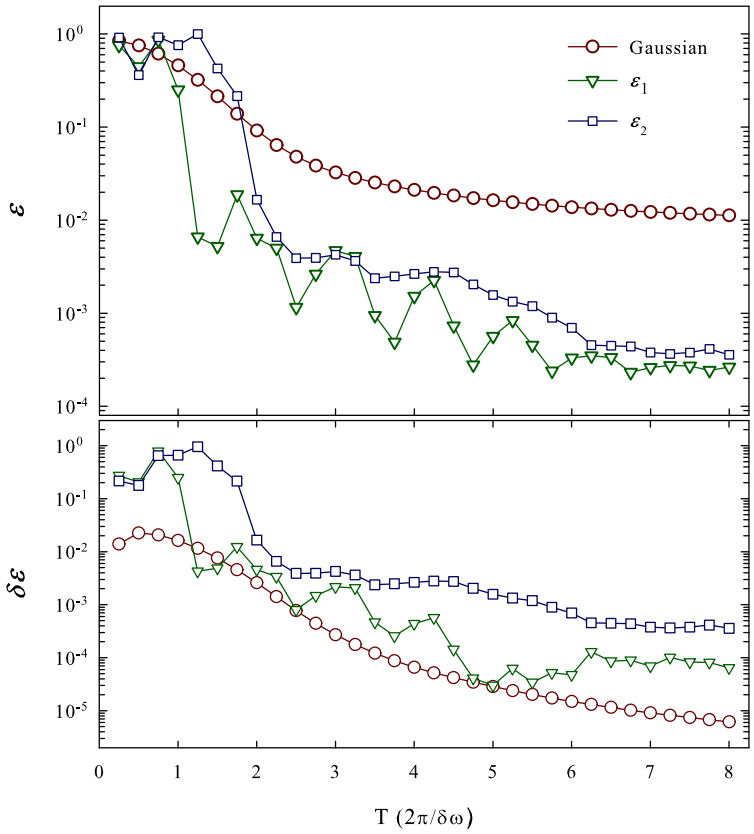

Figure 9: (Color on line) Top panel: the error $\mathcal{E}$ for a NOT-gate made by applying microwave pulses with Gaussian modulation (circles) and optimized modulation (triangles and squares) when off-resonance terms are kept. Note that optimized pulses are obtained by excluding off-resonance elements. Bottom panel: the absolute value of error difference $\delta\mathcal{E}$ obtained by subtracting the curves in the top panel from those in Fig. 4.

interaction with the second qubit is present.

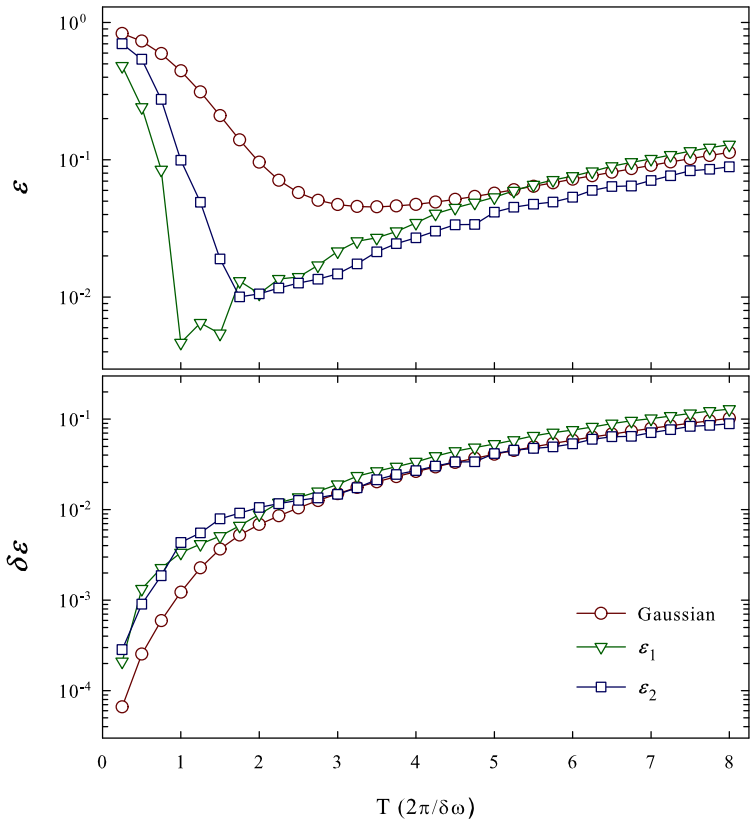

Figure 10: (Color on line) Error $\mathcal{E}$ for a NOT-gate on the first qubit implemented by applying Gaussian (circles) and optimized (triangles and squares) pulses on the first qubit of a two-qubit system in presence of capacitive interaction. Gaussian pulses have amplitude $a = 1.25$ and cutoff in time $\alpha = 3$ and are used as initial guess in the optimization procedure. Optimized pulses are obtained from the single-qubit setup. The strength of the interaction is $C_x/C_\Sigma = 2.3 \times 10^{-3}$. Bottom panel: the absolute value of error difference $\delta\mathcal{E}$ obtained by subtracting the curves in the top panel from those in Fig. 4.

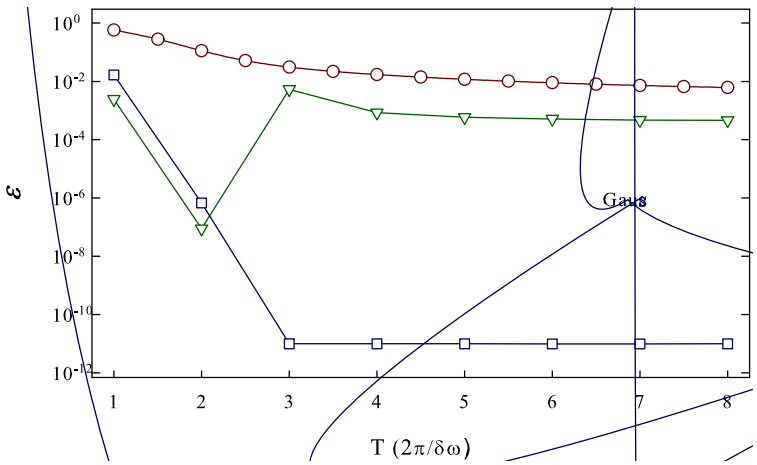
10^{0}
10^{-2}
10^{-4}
10^{-6}
10^{-8}
10^{-10}
10^{-12}
ε
1
2
3
4
5
6
7
8
T $(2\pi/\delta\omega)$
Gauss

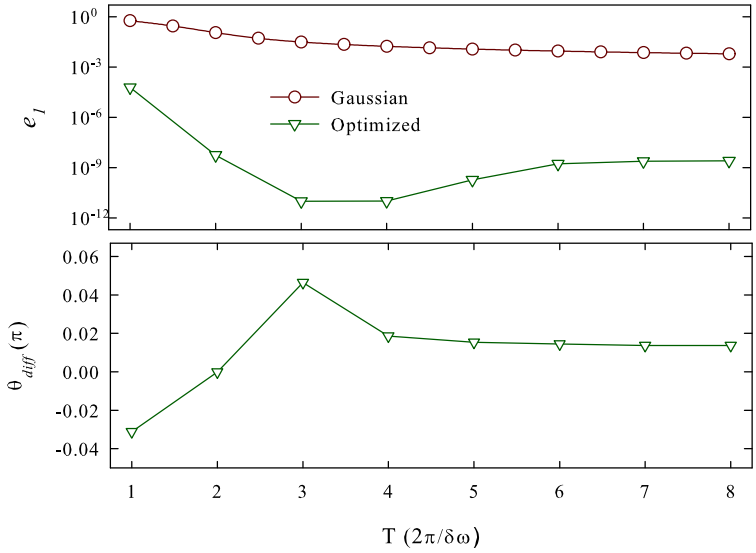

Figure 12: (Color on line) Top panel: the averaged value of e_1 for $|0\rangle \leftrightarrow |1\rangle$ transitions after applying the Gaussian pulses (circles) and optimized pulses (triangles) obtained from minimizing e_1. Vertical axis is in logarithmic scale. Bottom panel: the phase difference between final $|0\rangle$ and $|1\rangle$ states in units of π.

a very high fidelity.

Two examples of pulses with $T = 2\ \frac{2\pi}{\delta\omega}$ are shown in figure 13. g_1 is obtained from minimizing e_1 and gives rise to $\mathcal{E}_1 \approx 10^{-8}$ while g_2 is supposed to minimize e_2 with $\mathcal{E}_2 \approx 10^{-7}$. It seems that, compared to three-level system, higher frequencies and amplitudes are needed to reach high fidelity of NOT-gate. In three level system the iterative optimization algorithm is applied at most 5000 times to reach such fidelities while with five levels 15000 iterations were needed to obtain the results shown in figures 1

duration times, due to the very high fidelity reached. We have also addressed the effect of the presence of a capacitively-coupled second qubit and showed that, even though the optimized pulses are obtained for a single qubit, they still lead to a high fidelity for a NOT-gate (up to two orders of magnitude improvement) especially for very short pulses. Finally, we were able to obtain optimized pulses for a system with 5 energy levels in which the leakage outside qubit manifold is more severe.

In conclusion, the two-interacting-qubit system deserves for sure further attention. On the one hand, in order to improve the fidelity of a single-qubit operation, in the presence of capacitive coupling, it seems that a way to switch the interaction on and off should be found even for optimized pulses of an isolate qubit. On the other hand, obtaining optimized pulses while including the interaction, would be a potential theoretical work to be done.

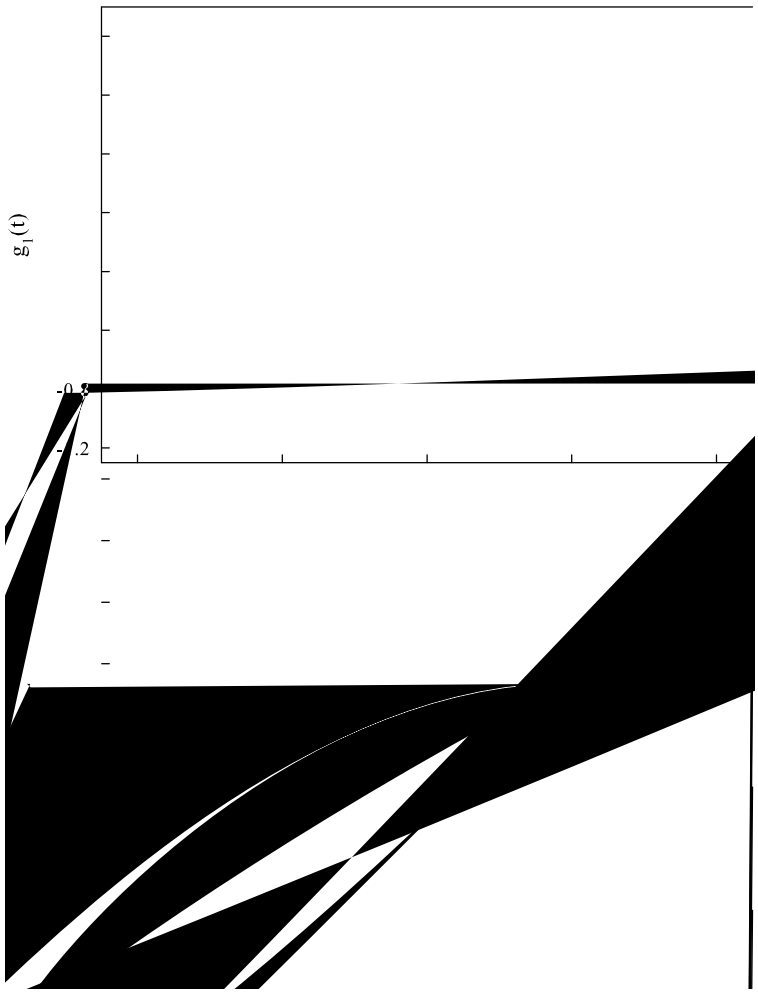
$g_1(t)$
-0.
-.2

Conclusion

The quantum dynamics of superconducting devices is controlled through some applied control parameters such as gate voltages, current or magnetic flux pulses. Typically the operation of such quantum systems can be performed with a reduced fidelity due to superconducting correlations specially for short-time pulses. Since for most of the applications of these kinds of systems, such as quantum computation and metrology, fast and accurate operations are desireable, finding a way to have good control on their dynamics is necessary. A possible strategy to improve the fidelity of the operation of these devices is the optimal control of the applied pulses. In this thesis we employed quantum optimal control theory in order to optimize the operation of two important superconducting devices, Cooper pair pump and Josephson phase qubit. In the case of Cooper pair pumping, the system under consideration was an array of Josephson junctions with biasing gate voltages, which were used as control parameters in the optimization procedure. To optimize the gate voltages, we introduced a new quantum number, the counter, and assumed that the overall superconducting phase accross the array is zero. Numerical results of optimized pumping, in non-adiabatic regime, showed that pumped charge, in each cycle of gating, can achieve very high accuracy and moreover the state of the pump at the end of each cycle is equal to its initial state. Stability of results against $1/f$ noise applied on gate voltages and against uncertainty in charging and Josephson energy was also tested, demonstrating robustness of pumped charge and final state of the system. In the case of phase qubits we considered a current-biased Josephson junction and, motivated by recent experiments, employed optimal control theory to optimize the quantum NOT-gate by searching for optimal modulations of microwave current pulses. Compared to conventional Gaussian pulses, several orders of magnitudes improvement in the fidelity was achieved, even for very short pulses and in presence of levels outside the computational Hilbert space. Effect of off-resonance elements of the Hamiltonian, which are normally ignored, and the effect of possible interaction with another qubit in the experimental setup were also addressed. Although optimized pulses were obtained for a single-qubit setup and by ignoring off-resonance terms, still show orders of magnitude improvement in comparison with Gaussian pulses. The Fourier analysis of the optimal pulses, in both Cooper pair pump and phase qubit cases, shows that the pulse generator bandwidth of few GHz would be sufficient to gain orders of magnitude improvement in fidelity of pumping or NOT-gate.

Furthure developement of the research to be done for this thesis are as follows. According to Fourier analysis in both systems under consideration, implementation of optimized pulses with present technology would still lead to orders of magnitude improvement of fidelity. However, finding optimal pulses with simpler shapes and lower bandwidth would be desireble from the experimental point of view. Moreover, In the case of Cooper pair pumping, finding a method of optimization which does not require a counter and also investigation of the effect of phase on the fidelity would be potential works to be done. In Josephson phase qubit, the considerable increase in the error of NOT-gate, due to off-resonance terms of the Hamiltonian and effect of interaction, clarifies the fact that these effects must be taken into account in optimization,

when very high fidelity of gates are desired. Although, the optimization procedure in laboratory frame and for a two-qubit setup is straightforward, controlling the shape of pulses in this case in order to prevent high-frequency bandwidths needs to be addressed.

Bibliography

[1] M. A. Nielsen and I. L. Chuang, *Quantum Computation and Quantum Information* (CAMBRIDGE UNIVERSITY PRESS, Cambridge, 2000).

[2] Y. Makhlin, G. Schön and A. Shnirman, Rev. Mod. Phys. **73**, 357 (2001).

[3] G. Wendin and V. S. Shumeiko, arXiv:cond-mat/0508729v1.

[4] M. H. Devoret, A. Wallraff, and J. M. Martinis, arXiv:cond-matt/0411174v1.

[5] B. D. Josephson, in *Superconductivity*, R. D. Parks, edition (Marcel Dekker, New Yourk, 1969).

[6] M. Tinkham, *INTRODUCTION TO SUPERCONDUCTIVITY*, 2nd edition (McGraw-Hill, New Yourk, 1996).

[7] A. P. Peirce and M. A. Dahleh, Phys. Rev. A **37**, 4950 (1988).

[8] N. Khaneja, T. Reiss, C. Kehlet, T. Schulte-Herbrüggen, and S. J. Glaser, Journal of Magnetic Resonance **172** (2005) 296-305.

[9] J. Werschnik and E. K. U. Gross, J. Phys. B: At. Mol. Opt. Phys. **40** (2007) R175-R211.

[10] T. Calarco, U. Dorner, P. S. Julienne, C. J. Williams, and P. Zoller, Phys. Rev. A **70**, 012306 (2004).

[11] A. Spörl, T. Schulte-Herbrggen, S. J. Glaser, V. Bergholm, M. J. Storcz, J. Ferber, and F. K. Wilhelm, Phys. Rev. A **75**, 012302 (2007).

[12] S. Montangero, T. Calarco, and R. Fazio, Phys. Rev. Lett. **99**, 170501 (2007).

[13] P. Rebentrost, I. Serban, T. Schulte-Herbrüggen, and F. K. Wilhelm, arXiv:quant-ph/0612165v3.

[14] P. Rebentrost and F. K. Wilhelm, arXiv:0808.2680v1.

[15] F. Motzoi, J. M. Gambetta, P. Rebentrost, and F. K. Wilhelm, arXiv:0901.0534v2.

[16] H. Kamerlingh Onnes, *Leiden Comm.* **120b**, **122b**, **124c** (1911).

[17] G. Bednorz and K. A. Müller, *Z. Phys.* **B64**, 189 (1986).

[18] W. Meissner and R. Ochsenfeld, *Naturwissenschaften* **21**, 787 (1933).

[19] F. London and H. London, *Proc. Roy. Soc.* (London) **A149**, 71 (1935).

[20] A. B. Pippard, *Proc. Roy. Soc.* (London) **A216**, 547 (1953).

[21] J. Bardeen, L. N. Cooper, and J. R. Schrieffer, *Phys. Rev.* **108**, 1175 (1957).

[22] R. E. Glover and M. Tinkham, *Phys. Rev.* **104**, 844 (1956); **108**, 243 (1957).

[23] V. L. Ginzburg and L. D. Landau, *Zh. Eksperim. i Teor. Fiz.* **20**, 1064 (1950).

[24] L. P. Gor'kov, *Zh. Eksperim.i Teor. Fiz.* **36**, 1918 (1959) [*Sov. Phys. JETP* **9**, 1364 (1959)].

[25] A. A. Abrikosov, *Zh. Eksperim.i Teor. Fiz.* **32**, 1442 (1957) [*Sov. Phys. JETP* **5**, 1174 (1957)].

[26] U. Essmann and H. Träuble, *Phys. Lett.* **24A**, 526 (1967).

[27] H. F. Hess et al. Phys. Rev. Lett.**62**, 214 (1989); Phys. Rev. Lett. **64**, 2711 (1990).

[28] J. Bardeen and M. J. Stephen, *Phys. Rev.* **140**, A1197 (1965).

[29] B. D. Josephson, *Phys. Lett.* **1**, 251 (1962); *Adv. Phys.* **14**, 419 (1965).

[30] *Single Charge Tunneling*, edited by H. Grabert and M. H. Devoret (Plenum Press, New Yourk, 1992).

[31] M. Büttiker, Phys. Rev. B **36**,3548 (1987).

[32] V. Bounchiat, D. Vion, P. Joyez, D. Esteve, and M. H. Devoret, Physica Scripta T **76** (1998) p.165-70.

[33] Y. Nakamura, Yu. A Pashkin, and J. S. Tsai, Nature **398**, 786 (1999).

[34] D. J. Thouless, Phys. Rev. B **27**, 6083 (1983).

[35] P. W. Brouwer, Phys. Rev. B **58**, R10 135 (1998).

[36] F. Zhou, B. Spivak, and B. Altshuler, Phys. Rev. Lett. **82**, 608 (1999).

[37] Yu. Makhlin and A.D. Mirlin, Phys. Rev. Lett. **87**, 276803 (2001).

[38] M. Moskalets and M. Buttiker, Phys. Rev. B **66**, 205320 (2002).

[39] M. Moskalets, and M. Büttiker, Phys. Rev. B **66**, 035306 (2002).

[40] O. Entin-Wohlman, A. Aharony, and Y. Levinson, Phys. Rev. B **65**, 195411 (2002).

[41] J. Wang, Y. Wei, B. Wang, and H. Guo, Appl. Phys. Lett. **79**, 3977 (2001).

[42] M. Blaauboer, Phys. Rev. B **65**, 235318 (2002).

[43] F. Taddei, M. Governale, and R. Fazio, Phys. Rev. B **70**, 052510 (2004).

[44] L.P. Kouwenhoven, A.T. Johnson, N.C. van der Vaart, C.J.P.M Harmans, and C.T. Foxon, Phys. Rev. Lett. **67**, 1626 (1991).

[45] H. Pothier, P. Lafarge, C. Urbina, D. Esteve, and M. H. Devoret, Europhys. Lett. **17**, 249 (1992).

[46] M. W. Keller, J.M. Martinis, M.M. Zemmermann, and A.H. Steinbach, Appl. Phys. Lett. **69**, 1804 (1996)

[47] M. W. Keller,J.M. Martinis, and R.L. Kautz, Phys. Rev. Lett. **80**, 4530 (1998)

[48] M. W. Keller, A.L. Eichenberg, J.M. Martinis, and N.M. Zimmerberg, Science **285**, 1716 (1999)

[49] L. J. Geerligs, S. M. Verbrugh, P. Hadley, J. E. Mooij, H. Pothier, P. Lafarge, C. Urbina, D. Esteve, and M. H. Devoret, Z. Phys. B: Condens. Matter **85**, 349 (1991).

[50] A. O. Niskanen, J. M. Kivioja, H. Seppä, and J.P. Pekola, Phys. Rev. B **71**, 012513 (2005).

[51] J. P. Pekola, J.J. Toppari, M. Aunola, M.T. Savolainen, and D.V. Averin, Phys. Rev. B **60**, R9931 (1999).

[52] A. O. Niskanen, J.P. Pekola, and H. Seppa, Phys. Rev. Lett. **91**, 177003 (2003).

[53] M. Aunola and J.J. Toppari, Phys. Rev. B **68**, 020502(R) (2003).

[54] M. Governale, F. Taddei, R. Fazio, and F.W.J. Hekking, Phys. Rev. Lett. **95** 256801 (2005).

[55] M. Möttönen, J.J. Vartieinen, J.P. Pekola, V. Brosco, and F.W. Hekking, Phys. Rev. B **73**, 214523 (2006).

[56] R. Leone, L. Levy, and P. Lafarge Phys. Rev. Lett. **100**, 117001 (2008).

[57] V. Brosco, R. Fazio, F.W.J. Hekking, and A. Joye, Phys. Rev. Lett. **100**, 027002 (2008).

[58] G. Falci, R. Fazio, G. M. Palma, J. Siewert and V. Vedral, Nature (London) **407**, 355 (2000).

[59] M. Möttönen, J. J. Vartieinen and J. P. Pekola, Phys. Rev. Lett. **100**, 177201 (2008).

[60] G. Wendin and V. S. Shumeiko, Fiz. Nizk. Temp. **33**, 957 (2007) [Low Temp. Phys. **33**, 724 (2007)].

[61] J. Q. You and F. Nori, Phys. Today **58**, 42 (2005).

[62] J. Clarke and F. K. Wilhelm, Nature **453**, 1031 (2008).

[63] A. J. Leggett and A. Garg, Phys. Rev. Lett. **54**, 857 (1985).

[64] J. R. Friedman, V. Patel, W. Chen, S. K. Tolpygo and J. E. Lukens, Nature **406**, 43 (2000).

[65] A. E. Bryson and Y. Ho, *Applied Optimal Control* (Hemisphere, Washington, D.C., 1975).

[66] D. G. Luenberger, *Introduction to Dynamics Systems* (Wiley, New Yourk, 1979).

[67] D. J. Tannor and S. A. Rice, J. Chem. Phys. **83**, 5013 (1985).

[68] D. J. Tannor, R. Kosloff, and S. A. Rice, J. Chem. Phys. **85**, 5805 (1986).

[69] S. A. Rice and D. J. Tannor, J. Chem. Soc. Faraday Trans. 2 **82**, 2423 (1985).

[70] S. Conolly, D. Nishimura, and A. Macovski, IEEE Med. Im. **5**, 106 (1986).

[71] A. G. Butkovskii and Y. I. Samoilenko, Autom. Remote Control (USSR) **A**, 485 (1979).

[72] A. G. Butkovskii and Y. I. Samoilenko, Dokl. Akad. Nauk SSSR, **250**, 51 (1980).

[73] G. M. Huang, T. J. Tarn, and J. W. Clark, J. Math. Phys. **24**, 2608 (1983).

[74] V. P. Belavkin, in Proceedings of the 7th All Union Conference on Encoding and Transmission of Information, Vilnius 1978 (in Russian) [Nauchn. Sovet Kompleks. Probl.Kibern. Akad. Nauk SSSR **1**, 23 (1978)].

[75] E. V. Davies, IEEE Trans. Inf. Theory, **IT-23**, 530 (1977).

[76] A. V. Balakrishnan, *Applied Functional Analysis*, 2nd eddotion (Springer-Verlag, New Yourk, 1981).

[77] D. G. Luenberger, *Linear and Nonlinear Programming*, 2nd edition (Addison-Wesley, Reading, MA, 1984).

[78] I. R. Sola, J. Santamaria, and D. J. Tannor, J. Phys. Chem. A **102**, 4301-4309 (1998).

[79] G. D. Smith, *Numerical Solution of Partial Differential Equations: Finite Difference Methods*, 2nd edition (Oxford University Press, Oxford, 1978).

[80] A. Askar and A. S. Cakmak, J. Chem. Phys. **68**, 2794951(.)71n(,)43552]1Ω-96393749(8)0.433749())0319971(s)6(

[97] M. Steffen, J. M. Martinis, and I. L. Chuang, Phys. Rev. B**68**, 224518 (2003).

[98] M. H. S. Amin, Low Temp. Phys. **32**, 198 (2006).

[99] A. Borzi, G. Stadler, and U. Hohenester, Phys. Rev. A**66**, 053811 (2002)

[100] S.E. Sklarz and D.J Tannor, Phys. Rev. A**66**, 053619 (2002)

[101] S. Safaei, S. Montangero, F. Taddei, and R. Fazio, Phys. Rev. B**77**, 144522 (2008).

[102] R. W. Simmondos, K. M. Lang, D. A. Hite, S. Nam, D. P. Pappas, and J. M. Martinis, Phys. Rev. Lett.**93**, 077003 (2004).

[103] R. Fazio, G.M. Palma and J. Siewert, Phys. Rev. Lett.**83** 5385 (1999).